AALBORG UNIVERSITY
DENMARK

Master's Thesis

MSc. Structural and Civil Engineering

Analysis of suction installation of monobucket in cohesionless soil.

Written by
Eric Geraldo De-Lima

Supervised by
Professor Lars Bo Ibsen
Aleksandra Katarzyna Koteras

20^{th} October 2021

School of Engineering and Science
Department of Civil Engineering
Thomas Manns Vej 23
9220 Aalborg Øst
http://www.civil.aau.dk

Title:

Analysis of suction installation of
bucket foundation in cohesionless soil

Project:

Master's Thesis

Period:

September 2020 - October 2021

Author:

Eric Geraldo De-Lima

Supervisor(s):

Lars Bo Ibsen
Aleksandra Katarzyna Koteras

Full document: 89 pages
Main paper: 44pages
Appendix: 35 pages
Finish date: 20/10/2021

Preface

This thesis report reflects the effort directed towards the completion of final project within the master's programme titled *M.Sc. in Structural and Civil Engineering* at Aalborg University, Aalborg, Denmark. It is comprised of the main report and appendices. and provides a record of the research results.

It has been a quiet and humbling experience, with moments of wonder as I discovered new ideas and ways of solving problems. There were moments I was not certain of what I was suppose to do and lost focus, but I have come to appreciate the AAU approach to learning and would like to take the opportunity to thank all my professions who did a great job impacting knowledge. And it is my hope that the reader finds the information contained in this report to be useful and adds to the body of knowledge on the subject.

I would like to express my gratitude to my supervisors, Prof. Lars Bo Ibsen and Aleksandra Katarzyna Koteras, who made available all the resources need for the task. And especially to Lars Bo, for his understanding and patience with me, and to Tomas Sabaliauskas, for the time spent helping to perform the experiments and deliberating ideas. I want to mention the support from my family and their words of encouragement. And to those many individuals who at various stages of my education, advised me to not opt for the easy option but challenge myself to do something different. Their words have been reason enough for me to take responsibilities I initially considered avoiding.

Eric Geraldo De-Lima
15^{th} October, 2021.

For the reader

Sources and external references mentioned are listed according to the Harvard method [Author, Year] and may be found under the section "Biblography". For undated internet sources, a date is stated for the time of the last visit.

Figure and table numbering follows the current chapter number in order. Mathematical equations and expressions may be numbered, and these are referenced in the format: "...Eq.(1.1)", where the parentheses refer to the equation in (chapter, equation number). In general, calculation and example expressions are not assigned an equation number unless special reference is deemed necessary. Table columns will, when necessary, contain the unit(s) of the below indexes in a square bracket [kg]. For appendices, the above are assigned letters instead of chapter numbers, e.g. 'Figure A.1', 'Table C.1' and Eq.'(E.1)'.

Abstract

Offshore wind turbine (OWT) development continuous faces new challenges, with planned future developments aiming for larger turbines with greater energy output located in more hostile environments. Such a trend presents new challenges for existing foundation solutions for the offshore wind turbine, and gives rise to the possibility of deviations for commonly used designs and/or entirely new concepts such as floating OWT platfroms.

An optimized foundation design for the OWT is thus crucial to meet the technical challenges such ventures present, while remaining competitive by providing potential cost savings. The suction bucket foundation offers such a solution and this paper presents an investigation into the soil-structure interaction during suction installation of bucket foundation in dense cohesionless soil, where the technology shows great potential for implementation in OWT foundation.

This study is concerned with the installation of a suction bucket (monobucket) with thickened skirt tips installed in dense cohesionless soil. The mentioned subject is studied to examine how well proposed existing suction installation prediction methods cater for deviations in standard suction bucket design, and identify area of optimization for design parameters.

Data for analysis of the suction installation process is obtained from experimental CPT and monobucket installation in the geotechnical lab of AAU. Also, a numerical model is employed to analyze seepage flow during suction installation. Experimental results are compared to previous test results which employed skirts with uniform thickness, and it is shown that no greater requirement for suction is required for installing buckets with thickened tip. Also, a significant reduction (91.3%) in maximum force required for reaching target depth was achieved for suction installation.

Comparison of results is made with results obtained from prior studies, in order to show how well existing design prediction methods are suited for the case of the suction bucket presented in this report.

Contents

Introduction 1

1.1 Background

Increasing demand for energy, and a common goal to reduce dependence on fossil fuels has driven the development of alternative energy sources. Among such alternatives is the offshore wind turbine (OWT). In recent years, plans for new OWT farm development tend towards developing farms with larger turbines in deeper waters located farther away from shore (Figure 1.1)with the aim of achieving higher energy production capacity [WindEurope, 2020]. Such advancement presents many technical challenges, and providing functional and robust foundations to support these massive structures over a design life of 25 years in the harsh offshore environment is an issue requiring further research.

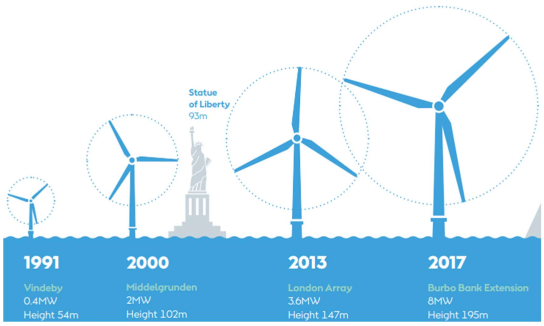

(a) Increasing offshore wind turbine size.[Ørsted, 2019]

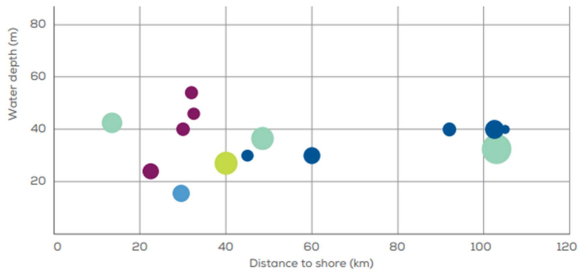

(b) Water depth vs offshore distance for farms under construction in 2019. Bubble size indicates capacity of farm [WindEurope, 2020]

Figure 1.1: Trends in offshore wind turbine installations

So far, the monopile has been the OWT foundation of choice, supporting over 80 %, of all installed foundations, [Ørsted, 2019], see Figure 1.2a. However, the monoplie's economic and environmental feasibility is a concern given the current trend of OWT farm development. Approximately 25 % - 34 % of project costs is attributed to the foundation [EWEA, 2009], with Blanco [2009] noting that the average cost of foundations for the Horns Rev and Nysted projects, founded on monopiles and gravity-based foundations respectively accounted for 21 % of project cost. This can be expected to increase as OWT farm development goes further offshore. As such, alternative solutions that best suit the growing trend for increasing turbine capacity with a potential for reduced Levelized Cost of Electricity (LCOE) is crucial for future advancement and widespread adoption of the OWT as a major renewable energy source of the future.

An adopted solution from Oil and Gas industry is the suction bucket (also referred to as suction anchor, suction cassion). When feasible, this offers the advantage of quick installation time with minimal environmental impact compared to the monopile, complete retrieval of foundation at the end of design life of the OWT and an often reduced LCoE.

The engineering design of the suction bucket for the OWT is a complex process. The foundation needs to be designed carefully to avoid structural and/or geotechnical failure of the foundation during the suction installation process and operation of the OWT. The geotechnical design aspect of the suction installation is generally understood, however, there are still aspects of the design that will benefit from a better understand of the factors affecting the mechanisms taking place and its incorporation in design [Koteras, 2019*b*]. Successful installation of suction bucket prototypes for OWT have already been carried out in Frederikshavn, Denmark [Ibsen, 2008]. However, the first commercial demonstration prototype installation carried out as part of the Deutsche Bucht 252 MW Project, located 95 km offshore, could not be completed as scheduled due to some technical issues [Northland Power Inc., 2020]. This emphasizes that unique challenges face the development of foundation solutions for OWT. Conditions differ from those in the Oil and Gas industry, and any design optimization can have significant impact on cost as OWT farms can have more than 100 OWT units. As such, methods adopted from other industries, though feasible for OWT application, need further optimization in order to be better suited as competitive solutions in the OWT industry.

A lot of research into suction bucket installation has already been undertaken, but further research is still required to better understand and possibly optimize suction bucket foundations as an OWT foundation solution. It is from this background that the problem of this thesis is approached and it is hoped that results obtained may provide insight into the implementation of suction buckets as foundations for OWT. Current implementation of suction buckets for OWT are executed as either a monobucket (also, monopod) with a single suction bucket connected to a pile-like shaft or a tripod/tetrapod with three/four suction buckets attached to the base of a jacket structure as shown in Figure 1.2b.

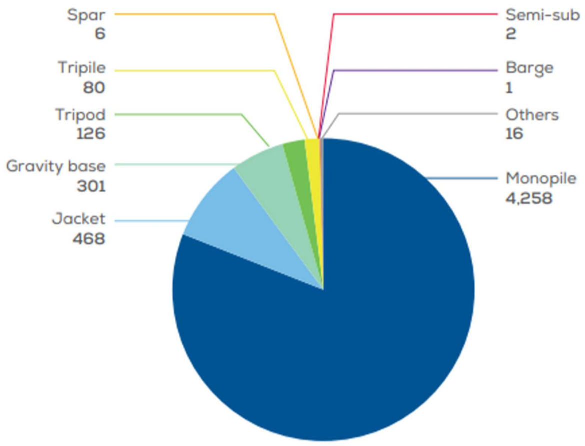

(a) Number of installed foundations, by type, up to 2019.[WindEurope, 2020]

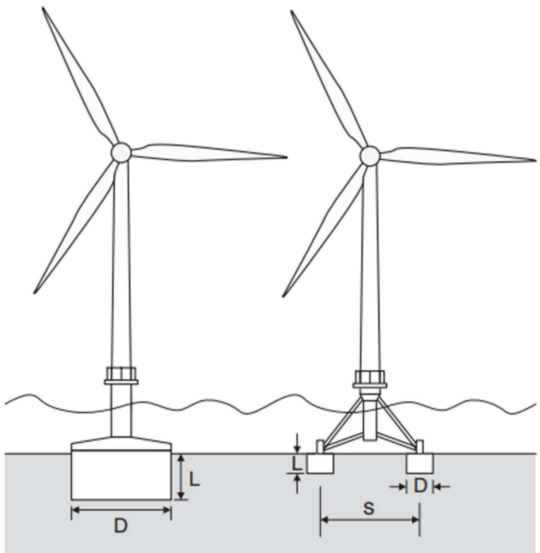

(b) Implementation of suction bucket for OWT. [Houlsby et al., 2005]

Figure 1.2: (a) Share of installed foundations by type and (b) Implementation of suction bucket, monobucket(left) and tripod/tetrapod (right)

1.2 Problem formulation

The installation of a monobucket is achieved through a two-step stage: an initial self-weight embedment stage, which creates a hydraulic seal between the soil and bucket tip and enables suction installation to proceed, followed by a suction-assisted embedment stage. Generally, the suction-assisted installation is considered to be driven by the differential pressure created by the application of suction under the bucket lid. This is the main driving force for suction installation in cohesive soils. For installation in cohensionless soil, significantly greater resistance to penetration is expected, however, the installation driving force is enhanced by a reduction in resistance at the bucket tip and along skirt wall. Initial research into suction-assisted installation in sands recognized that suction-induced seepage flow is responsible for the observed resistance reduction as the flow lowered the soil effective stresses and permeability, and thus influenced the critical suction limit in cohesionless soil [Erbrich and Tjelta, 1999].

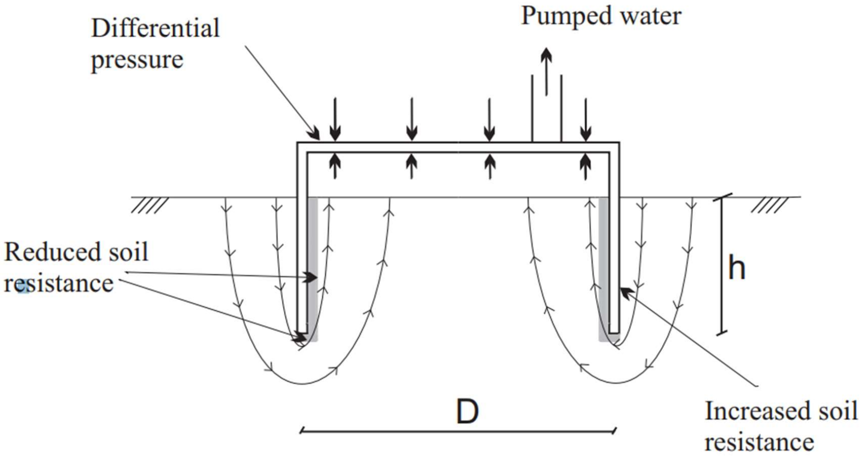

Figure 1.3: Driving force for installation in cohesionless soil: Differential pressure under bucket lid and tip resistance reduction due to seepage flow. [Koteras et al., 2016*a*]

Geotechnical design for suction-assisted installation requires the prediction of the required suction pressure to be applied with respect to the penetration depth during installation. It is expected that suction-assisted installation proceeds as long as a certain critical condition is not encountered. At the critical condition, installation comes to a halt and an increase in the driving force does not produce an further penetration into the soil. Theoretical predictions for this limit, termed the critical suction limit, predicts installation failure caused by the development of piping channels, termed piping failure. In this state, the seepage flow creates channels of least resistance through which water is pumped out of the inner bucket compartment. Manifestation of piping failure may be characterized by a major outflow of water from the suction bucket without further penetration [Houlsby and Byrne, 2005] or a major inflow of soil from outside the bucket into the bucket compartment without further penetration [Houlsby et al., 2005].

Comparison of the calculated critical suction limit to lab and field measurements however shows that the theoretical limit used is exceeded without any piping failure occurring, The results indicate the conventional methods used for predicting suction installation tend to underestimate the critical suction limit. This is most likely due to implementation of governing factors affecting the suction installation, such as the suction-induced seepage flow that drives installation in sand.

Given that design predictions have been observed to deviate model installations with standard geometry and commonly utilized aspect with $L/D \leq 1$, then much more significant deviation could be observed for suction installation with modified buckets where there could be greater soil-bucket skirt interaction. Thus, the problem to be investigated in this report is then presented as:

How will consideration of flow effects affect prediction of suction installation limit of a monobucket with thickened tips and are the factors affecting prediction of critical suction limit in cohensionless soil duly accounted for in design?

1.3 Purpose of the thesis

Factors influencing the installation of suction bucket in dense sand have been identified in previous research efforts by numerous researchers, [Tjelta et al., 1994; Houlsby and Byrne, 2005; Senders and Randolph, 2009]. However, the prediction of the critical suction limit seems to be an element of installation design that can be improved. Researchers in recent years have made attempts to address this and have identified properly accounting for seepage flow effects in design as a means of making better prediction for installation limit. Proposals for methods of incorporating flow effects have been developed in recent years, [Houlsby and Byrne, 2005; Senders and Randolph, 2009; Koteras and Ibsen, 2018], with varying results, and this may be due to the implementation of the flow effects in design.

Deviation in prediction could be amplified when modifications from the commonly adopted design implementation of suction buckets for OWT are used, such as modified bucket geometry with increased friction area and/or aspect ratios L/D≥1 [Rodriguez and Barari, 2020]. One of the aims of this thesis is that the result of the analysis will reflect the extent of such behaviour and identify which factors bear influence on installation design.

Also, a consensus on which of the proposed methods offer the best means for incorporating flow effects in design has not yet been reached. This thesis will therefore also serve as a test for the different proposed design methods.

These goals will be pursued by analyzing the suction installation of a monobucket with $L/D = 1$ and thickened skirt tip installed in uniform cohesionless soil. It is hoped that the tests will highlight how well the identified factors contributing to suction-assisted installation are accounted for and incorporated in design.

State of the art review 2

Papers relevant to suction installation in cohesionless soils were reviewed as a first step in identifying and understanding the state of the art. The findings from recent research effort by leading researchers in bucket foundation installation in sand are presented in this section and will be the basis for further analysis in subsequent chapters of this report.

2.1 Introduction to suction installation in sand.

The process of suction bucket installation can be divided into two main stages; the self-weight installation phase and the suction-assisted installation phase. The self-weight installation stage forms the first part of the installation. In this stage, the bucket is lowered to the surface of the soil deposit where the bucket is driven into the soil by the buoyant weight of the suction bucket. For lightweight structures installed in dense sand deposits, as is the case for OWT in the North Sea , high resistance to self-weight penetration resulting in shallow penetration depth is expected [Senders and Randolph, 2009]. Sufficient penetration of the bucket in this stage is necessary to create a hydraulic seal between the skirt tip and the surrounding soil. Koteras and Ibsen [2019] indicated that a minimum of 50 mm proved sufficient from medium scale testing campaign. The hydraulic seal enables the effective application of suction pressure within the bucket compartment for the subsequent suction-assisted stage. Development of excess pore pressure in the enclosed soil mass is prevented by open valve-controlled vents situated on the lid of the bucket. The self-weight penetration ends when the built up soil resistance balances the weight of the suction bucket. This is then followed by the suction-assisted stage, where the valve-controlled vents on the lid are closed and suction is applied under the bucket lid to drive the skirt to the final target depth.

Applied suction creates a differential pressure under the bucket lid, generates excess pore pressures and a hydraulic gradient which enables seepage flow from the outside to the inner compartment of the bucket skirt. The seepage flow has been identified as the dominanting enhancing factor for penetration in dense sand, as it alters effective stresses and permeability of the soil volume and results in significant reduction in soil penetration resistance [Erbrich and Tjelta, 1999]. The required suction needed to drive the suction-assisted stage is determined through design calculation to ensure that installation proceeds successfully to the target depth. Control of the required suction is necessary to avoid potential geotechnical failure of the installation. Theoretically, exceeding the critical suction is expected to trigger geotechnical installation failure, resulting in development of piping channels within the enclosed soil volume. Piping channels break the hydraulic seal created at the end of the self-weight installation stage and this allow ingress of large quantity of soil from the outside of the bucket or water to be pumped out freely from the bucket chamber, thus reducing the beneficial effect of seepage flow. Also, it is worth mentioning that geotechnical failure can manifest in the form of excessive soil heave development which prevents achieving target penetration depth, and liquefaction due to excessive loosening of the soil volume which can affect performance of the bucket foundation [Tjelta et al., 1994].

Methods utilized in suction installation design calculations seek to determine the feasibility of reaching a target depth at a site. These are adapted from knowledge for pile installation design against soil resistance, and attempt to predict the resistance to penetration at depth in order to determine the required driving force necessary for installation to the target depth. The general expression, which forms the basis for calculation of resistance to installation, is given in Eq. (2.1) and penetration is expected to proceed provided the applied driving force balances the soil resistance to penetration.

$$R_{tot} = F_{in} \; + F_{out} \; + Q_{tip} \tag{2.1}$$

where:

R_{tot}	the total soil penetration resistance
$F_{in}; F_{out}$	the mobilized skirt wall friction, inside and outside
Q_{tip}	the skirt tip resistance

Recommendations specified in reference standards, mainly API [2000] , DNV [1992] and ISO(2000) , for determining the terms in Eq. (2.1), are based on recommendations from design calculations developed by researchers (Erbrich and Tjelta [1999]; Tran et al. [2005]; Houlsby and Byrne [2005]; Senders and Randolph [2009]), with subsequent improvements proposed by researches such as Koteras and Ibsen [2018] and Chen et al. [2016]. A review of the current design calculations, namely the classical bearing capacity theory approach and the CPT design approach. was carried out and is presented to outline the state of art in suction bucket installation design.

2.2 Bearing capacity theory-based resistance prediction

2.2.1 Penetration under self-weigtht / load force.

Design procedure used for skirted offshore foundations in the Oil and Gas industry was adapted from pile installation design and is based on the bearing capacity theory. This is the method prioritized by API [2000] for design. For the self-weight installation stage, the resistance to installation, represented by Eq. (2.1), is given in the form ;

$$R_{tot}^{API} = (A_{s,in} + A_{s,ot}) \cdot min\left[(K_o \, tan\, \delta) \cdot \int_0^h \sigma^{'}(h)\, dh \, , f_{lim}\right] + A_{tip} \cdot min\left[\sigma^{'}(h) N_q \, , Q_{lim}\right] \tag{2.2}$$

where:

$A_{s,in}$	inner skirt perimeter given by (πD_{in})
$A_{s,ot}$	outer skirt perimeter given by (πD_{ot})
A_{tip}	skirt tip area given by $(\frac{\pi}{4}(D_{ot}^2 - D_{in}^2))$
K_o	lateral earth pressure coefficient at rest
δ	interface friction angle given by $(r\varphi)$
$\sigma_v^{'}$	the vertical effective stress given by $(\gamma' h)$
h	penetrated depth
D_{ot}, D_{in}	outer and inner skirt wall diameter
N_q, N_γ	dimensionless bearing capacity factors
f_{lim}, Q_{lim}	limiting unit friction and unit end bearing recommended by API
	API suggests guideline values, however tests results are recommended for use
γ'	the effective soil unit weight
r	the roughness factor between skirt wall and sand
φ	the peak drained friction angle of sand

Houlsby and Byrne [2005] in his analysis proposed a modification to Eq. (2.1) to account for the effect of enhanced stresses due to friction along deep skirts with thin wall. This is expressed in Eq. (2.3), and accounts for friction contributing to increased stresses at the tip (σ_{end}) and the skirt inner and outer walls ($\sigma_{v,in}^{'}$ and $\sigma_{v,ot}^{'}$), respectively.

$$R_{tot}^{Byrne} = A_{s,in}\,(K_o\,tan\,\delta)_{in}\cdot\int_0^h \sigma_{v,in}^{'}(h)\,dh + A_{s,ot}\,(K_o\,tan\,\delta)_{ot}\cdot\int_0^h \sigma_{v,ot}^{'}(h)\,dh + A_{tip}\cdot\sigma_{end} \tag{2.3}$$

with:

$$F_{in} = A_{s,in}\,(K_o\,tan\,\delta)_{in}\cdot\int_0^h \sigma_{v,in}^{'}(h)\,dh \tag{2.4}$$

$$F_{out} = A_{s,ot}\,(K_o\,tan\,\delta)_{ot}\cdot\int_0^h \sigma_{v,ot}^{'}(h)\,dh \tag{2.5}$$

$$Q_{tip} = A_{tip}\cdot\sigma_{end} \tag{2.6}$$

where:

$\sigma_v^{'}$	enhanced vertical effective stress
σ_{end}	end bearing stress given by $((\sigma_{v,in}^{'}\,N_q + \gamma^{'} t N_\gamma)\cdot(\pi D t))$

Andersen et al. [2008] reported that the bearing capacity formulation with the triaxial friction angle produced good agreement with measured penetration resistance in the self-weight installation phase.

2.2.2 Penetration under suction force.

Applied suction generates excess pore pressures and a hydraulic gradient around the bucket skirt causing seepage flow. Outside the bucket, a downward flow increases the effective stresses while an upward flow inside the bucket reduces the effective stresses. The increase/reduction effect of seepage flow on the effective stresses is expressed in Eq. (2.7), and the flow has been observed to alter the relative density, and thus the permeability of the soil plug within the skirt wall. These changes are accounted for in the design calculation proposed by Houlsby and Byrne [2005]. Thus, prediction of the resistance to installation penetration in homogeneous soil is expressed in Eq. (2.8).

$$\sigma_v^{'} = \gamma^{'} z \pm \iota\gamma_w^z \tag{2.7}$$

where: ι is the hydraulic gradient.

$$R_{red}^{Byrne} = A_{s,in}\,(K_o\,tan\,\delta)_{in}\cdot\int_0^h \sigma_{v,in}^{'}(h)\,dh + A_{s,ot}\,(K_o\,tan\,\delta)_{ot}\cdot\int_0^h \sigma_{v,ot}^{'}(h)\,dh + A_{tip}\cdot\sigma_{end} \tag{2.8}$$

where the in-situ effective stresses are substituted with the altered effective stresses due to flow effects.

Based on numerical studies on the influence of generated excess pore pressure on the effective stresses, and on an assumption of linear distribution of pore pressure around the skirt, Houlsby and Byrne [2005] proposed a method for accounting for the reduction in effective stresses in soil of constant permeability during suction-assisted installation. This involved the determination of a certain pore pressure factor, α, described as the ratio between the excess pore pressure at the skirt tip, Δu_{tip}, and the applied suction,s.

$$\alpha = \frac{\Delta u_{tip}}{s} \tag{2.9}$$

with theoretical limit values of : $\alpha = \begin{cases} 0.5, & \text{for } \dfrac{h}{D} \approx 0 \\ 0, & \text{for } h >> D \end{cases}$

From the results of the numerical analysis performed by Houlsby and Byrne [2005], a solution for the pore pressure factor as a function of penetration depth (h/D up to 0.8) in soil of constant permeability was found as given in Eq. (2.10), subject to the specified limit for α. To account for the effect of change in soil permeability during suction installation, a factor, k_{fac}, was introduced and its contribution incorporated into the pore pressure factor expression as given in Eq. (2.11) :

$$\alpha_1^{Bryne} = 0.45 - 0.36\left[1 - exp\left(-\frac{h}{0.48\cdot D}\right)\right] \tag{2.10}$$

$$\alpha^{Bryne} = \frac{\alpha_1\cdot k_{fac}}{(1-\alpha_1) + \alpha_1\cdot k_{fac}} \tag{2.11}$$

where:

α^{Bryne}	pore pressure factor accounting for change in soil permeability
k_{fac}	permeability ratio (k_{in}/k_{ot}) for permeability inside/outside the bucket skirt
α_1^{Bryne}	pore pressure as defined in 2.10

An alternative to the expression in Eq. 2.10 and Eq. 2.11 was proposed by Koteras and Ibsen [2015] and Koteras and Ibsen [2019] from numerical studies, which related the pore pressure factor, α, to the penetration ratio in homogeneous sand as given in Eq. (2.12) for the case of constant permeability and Eq. (2.13) for the case accounting for changing permeability due to seepage flow.

$$\alpha_1^{AAU} = \frac{0.21}{\frac{h}{D} + 0.44} \tag{2.12}$$

$$\alpha^{AAU} = 0.47 - 0.25 \left[1 - exp\left(-\frac{h}{0.32 \cdot D}\right)\right] \tag{2.13}$$

With the determined pore pressure factor, α, the effective soil unit weight is altered and thus , the reduced stresses can be found. The altered soil unit weight is obtained as:

$$\gamma'_{alt} = \begin{cases} \gamma'_{in} = \gamma' - \dfrac{(1-\alpha) \cdot s}{h} \\ \gamma'_{ot} = \gamma' + \dfrac{\alpha \cdot s}{h} \end{cases}$$

Koteras and Ibsen [2019] noted that the method gives a good fit between calculated resistance and measured resistance, however, optimization of key soil parameters and experience with the method was required.

The reduced resistance to penetration is used for predicting the required suction, s_{req}, for installation and is expected to give a safe and less conservative result compared to use of unreduced resistance which does not account for flow effects. This is determined from the equilibrium criteria for installation, given as Eq. (2.14), from which the required suction is determined from the expression in Eq. (2.15) as :

$$W'_{sb} + A_{lid,in} \cdot s_{req} \geq R_{red}^{Bryne} \tag{2.14}$$

$$s_{req} = \frac{R_{red}^{Bryne} - W'_{sb}}{A_{lid,in}} \tag{2.15}$$

where:

R_{red}	the reduced soil resistance with flow effects accounted for
s_{req}	the required suction
W'_{sb}	buoyant self-weight of the suction bucket
$A_{lid,in}$	bottom lid area inside the bucket $\frac{1}{4}\pi D_{in}^2$

Using the pore pressure factor,α, Houlsby and Byrne [2005] presents the critical suction against piping as:

$$s_{cr}^{Byrne} = \frac{\gamma' h}{1-\alpha} \tag{2.16}$$

2.3 CPT-based resistance prediction

2.3.1 Penetration under self-weight / load force.

The CPT-based design directly relates the cone tip resistance, q_c, recorded during CPT testing to the skirt wall friction and skirt tip resistance using coefficients k_f and k_p, respectively. The sleeve friction, if measured from CPT testing, is usually not used in installation design as the measure has been found to be less reliable [Lunne et al., 1997] and the use of sleeve friction in pile design has been proven to be unreliable [Engineers, 2004]. However, it is possible to use a measured sleeve friction for installation design as demonstrated in a paper by Houlsby et al. [2005].

By combining q_c with the coefficients k_f and k_p in calculation, as recommended by DNV [1992],the uncertainty and difficulty in estimation of certain soil parameters, namely the bearing capacity factor,N_q, and the coefficient of lateral earth pressure,K_o, is avoided,[Senders and Randolph, 2009]. Also, Feld [2001] suggested a different correlation for the skirt friction based on the effective stress, σ'_{vo}, and a factor that depends on the roughness of the structure and on the friction angle; the roughness calibrated from field tests and the friction angle derived from CPT results. The basis for such a recommendation being that the coefficient k_f has some level of uncertainty. Senders and Randolph [2009] and Chen et al. [2016] reported that results obtained by using the CPT-based method for determining penetration resistance produced better fit to experimental data for suction bucket installation than was obtained using the bearing capacity theory -based approach. Andersen et al. [2008] in his review of data from full scale and prototype installations showed the variability of k_f and k_p, and suggested that a depth/diameter effect could be influencing k_f and k_p values.

Using the CPT-based approach for calculating penetration resistance in homogeneous soil in the self-weight stage, Eq. (2.1) is given in the form ;

$$R_{tot}^{DNV} = (A_{s,in} + A_{s,ot}) \cdot k_f \int_0^h q_c(h)\, dh \; + A_{tip} \cdot k_p\, q_c(h) \tag{2.17}$$

with:

$$F_{in} = A_{s,in} \cdot k_f \int_0^h q_c(h)\, dh \tag{2.18}$$

$$F_{out} = A_{s,ot} \cdot k_f \int_0^h q_c(h)\, dh \tag{2.19}$$

$$Q_{tip} = A_{tip} \cdot k_p\, q_c(h) \tag{2.20}$$

where:

q_c	measured CPT tip resistance
k_f	coefficient relating tip resistance to skirt wall friction
k_p	coefficient relating tip resistance to skirt tip resistance

DNV [1992] proposed a range of values for coefficients k_f and k_p, for dense sand and stiff clay commonly encountered in the North Sea. Recommended values for sand are given- in Table 2.1. The range proposed by DNV [1992] is somewhat in good agreement with the observations of Andersen et al. [2008]. However, modification to the values of k_f and k_p have been proposed by a number of researchers based on the results of their research. Generally, the coefficients provided by DNV [1992] are very well suited for self-weight penetration phase, and for load force penetration with bucket aspect ratio $L/D < 0.5$, [Rodriguez and Barari, 2020].

Table 2.1: DNV [1992] recommended k_p and k_f values for sand in North Sea conditions

	Most probable		Highest expected	
Soil type	k_p	k_f	k_p	k_f
Sand	0.3	0.001	0.6	0.003

Variations in bucket aspect ratio and geometry, presence of stiffeners in full scale buckets, and the presence of sandwiched soil layers present uncertainties in the use of the k_f and k_p values provided by DNV, and may require some calibration. This was evident in the medium scale experiments of Lian et al. [2014] with $L/D = 1.0$, where the DNV value for $k_p = 0.6$ had to be increased to $k_p = 1.2$ for installation in dense sand and silt. Further discussion on the coefficients k_f and k_p is presented in section (2.4).

2.3.2 Penetration under suction force.

A simple CPT-based method accounting for the reduction in penetration resistance during suction-assisted installation was proposed by Senders and Randolph [2009]. The method relates soil resistance to the applied suction pressure by assuming :

- a linear decrease in internal friction and end bearing as the suction pressure increases from zero up to a critical value to cause internal piping.
- insignificant changes in the outer friction along the skirt due to applied suction.

The assumption for insignificant changes in the outer friction along the skirt is confirmed in studies by Lian et al. [2014]; Chen et al. [2016]. Using the assumption, Senders and Randolph [2009] proposed that the requirement for applied suction can be obtained from the vertical equilibrium of forces (Eq. (2.21)), from which Eq. (2.22) is presented as the required suction for driving suction-assisted installation. This was found to give a good fit to data for installation in centrifuge tests.

$$W'_{sb} + A_{lid,in} \cdot s = F_{ot} + (F_{in} + Q_{tip}) \left(1 - \frac{s}{s_{cr}}\right) \quad \text{for } s \leq s_{cr} \tag{2.21}$$

$$s = min\left[\frac{F_{ot} + F_{in} + Q_{tip} - W'_{sb}}{F_{in} + Q_{tip} + A_{lid,in} \cdot s_{cr}}, \quad 1\right] \cdot s_{cr} \tag{2.22}$$

where:

s	applied suction
s_{cr}	the critical suction
$F_{ot}, F_{in,Q_{tip}}$	same as defined for Eq. (2.16) - Eq. (2.18)

An alternative method, called the AAU CPT-based method, is based on the assumption of a decrease in internal friction and end bearing with increasing suction pressure application. The decrease is not necessarily assumed to be linear in contrast to the assumption presented by Senders and Randolph [2009]. The method predicts the reduced resistance contributions resulting from seepage flow by the introduction of resistance reduction factors, that is β factors, [Koteras and Ibsen, 2018] into Eq. (2.17) - (2.19). These are presented in Eq. (2.23) - (2.25), and discussion on the β factors is presented in section (2.4).

$$R_{red}^{AAU} = F_{in,r} \ + F_{ot,r} \ + Q_{tip,r} \tag{2.23}$$

with

$$F_{in,r} = \beta_{in} \cdot A_{s,in} \cdot k_f \int_0^h q_c(h)\, dh \tag{2.24}$$

$$F_{ot,r} = \beta_{out} A_{s,ot} \cdot k_f \int_0^h q_c(h)\, dh \tag{2.25}$$

$$Q_{tip,r} = \beta_{tip} \cdot A_{tip} \cdot k_p \, q_c(h) \tag{2.26}$$

Then the required suction for driving suction-assisted installation can be determined using a similar relation as Eq. (2.21) to obtain:

$$s = \left[\frac{F_{ot,r} \ + F_{in,r} \ + Q_{tip,r} \ - W_{sb}^{'}}{A_{lid,in}} \right] \tag{2.27}$$

A similar approach to the AAU CPT-based method, developed from a medium scale experimental campaign, was also presented by Chen et al. [2016] and Lian et al. [2014]. Resistance reduction factor, α^{Chen} and β^{Lian}, were introduced respectively to account for the resistance reduction around the skirt due to seepage flow. Then, the required suction was presented as :

$$s = \left[\frac{(1 - \alpha_{ot}^{Chen}) \cdot F_{ot} \ + (1 - \alpha_{in}^{Chen}) \cdot F_{in} \ + (1 - \alpha_{tip}^{Chen}) \cdot Q_{tip} \ - W_{sb}^{'}}{A_{lid,in}} \right] \tag{2.28}$$

$$s = \left[\frac{\beta_{ot}^{Lian} \cdot F_{ot} \ + \beta_{in}^{Lian} \cdot F_{in} \ + \beta_{tip}^{Lian} \cdot Q_{tip} \ - W_{sb}^{'}}{A_{lid,in}} \right] \tag{2.29}$$

2.4 Empirical coeffcients k_p, k_f and resistance reduction factors for CPT-based methods

As mentioned in section (2.3.2), coefficients k_p and k_f are selected for relating the CPT tip resistance to the components contributing to total penetration resistance in Eq. (2.18) - Eq. (2.20) during the self-weight stage, and the β factor introduced to account for reduction due to seepage during suction-assisted installation.

The use of k_p and k_f coefficients is adapted from prediction methods for evaluating pile driving installation. Various methods have been proposed for such purpose, and the UWA-05 design method [Lehane et al., 2005], is considered to have some improvements over other methods , namely Fugro-04 [Fugro Engineers, 2004], ICP-05 [Jardine et al., 2005], and NGI-04 [Clausen et al., 2005]. Given the similarity in construction and installation between open ended pile and suction bucket, reference to this method is presented as it has been shown to produce satisfactory results in centrifuge tests for suction buckets, after some adjustments [Senders and Randolph, 2009]. The coefficient k_f is related to the skirt thickness in the UWA-05 design method and is presented in its simplified form for full scale offshore implementation as shown in Eq. (2.30).

$$k_f = C \cdot \left[1 - \left(\frac{D_{in}}{D_{ot}}\right)^2\right]^{0.3} tan\,\delta \tag{2.30}$$

where δ is the interface friction angle and C is a constant with suggested value of 0.021 and is given by the expression:

$$C = 0.03\left[max\left(\frac{h}{D_{ot}}, 2\right)^{-0.5}\right]$$

Koteras [2019*b*] noted that for typical dimensions of suction buckets, this method produces $k_f = 0.0033 - 0.0046$, which is greater than the DNV [1992] proposed values, and thus, adjustments to the value C is necessary for its implementation in suction bucket installation design.

Andersen et al. [2008] also suggested values for the coefficients k_f and k_p, as presented in Table 2.3, based on data from lab tests and prototypes installation in dense sand. From his investigations, lab test produced higher coefficient values when compared to full scaled tests and field tests results which showed lower values, (see Table 2.2).This indicates that small scale lab results,typically from centrifuge tests and Particle image velocimetry (PIV), may not accurately reflect the factors affecting prototype installation, which are the k_f and k_p coefficients in this case. An example of a case with a medium scale experiment $L/D = 1.0$ is reported by Lian et al. [2014] where $k_p = 0.6$, as suggested by DNV, underestimated measured results and a $k_p = 1.2$ was required for a good fit. The suggested values from DNV [1992], suitable for skirt thickness of 20 mm and 30 mm, are also presented in Table 2.3 for comparison. DNV [1992] notes that the value for k_f be decreased for increased tip area and internal stiffness, if present.

Table 2.2: Range of back-calculated results from installation data for installation in dense sand as investigated by Andersen.

Range of results from installation data		
	k_f	k_p
Field tests	0.0010 - 0.0015	0.08- 0.25
Full scaled tests	0.0010 - 0.0015	0.01 - 0.6
Lab tests	0.0053	0.93 - 1.24

Table 2.3: Suggested values for coefficients k_f and k_p

Suggested values for coefficients k_f and k_p in installation sand			
DNV		Andersen	
k_f	k_p	k_f	k_p
0.0010 - 0.0030	0.3 - 0.6	0.0015	0.01 - 0.55
		0.0010	0.3 - 0.6

From the results presented by various researchers, the coefficients k_f and k_p are found to vary from one installation case to another, however the values suggested by DNV serve as a starting value for estimation. Variability in the values of k_f and k_p for suction bucket design may be influenced by the surface finish as pointed out by Andersen et al. [2008] and the investigation of increasing aspect ratio $0.5 \leq L/D \leq 1$ may reveal greater deviation from suggested values.

k_f and k_p coefficients can be estimated for model buckets, if required, from jacking installation and uninstalation tests on the assumption that there is no contribution to resistance from the skirt tip during uninstallation and friction on the inside and outside of the skirt are equal. Based on such an assumption, the friction contributions are isolated to obtain the k_f coefficient, and then the k_p coefficient can be found from the results of jacking installation for model tests. Using (2.17), the resistance contribution during uninstallation can be isolated for k_f and k_p as given in (2.31) and (2.32) :

$$k_f = \left[\frac{R_{uninstall}}{(A_{s,in} + A_{s,ot}) \cdot \int_0^h q_c(h)\, dh} \right] \tag{2.31}$$

$$k_p = \left[\frac{R_{tot} - F_{in} - F_{ot}}{A_{tip} \cdot q_c(h)} \right] \tag{2.32}$$

β factors, presented in section (2.3.2), are employed in accounting for the reduction in resistance during suction-assisted installation. These are defined in normalized form as a ratio of the applied pressure to the critical pressure. Proposed expressions for the β factors have been developed by Lian et al. [2014] and Koteras and Ibsen [2018] and are presented in the following:

The β factors as proposed by Koteras and Ibsen [2018], based on experiments carried out in AAU laboratory, is defined as:

$$\beta_{in} = 1 - \mathrm{r_{in}} \cdot exp\left(\frac{s}{s_{cr}}\right) \tag{2.33}$$

$$\beta_{tip} = 1 - \mathrm{r_{tip}} \cdot exp\left(\frac{s}{s_{cr}}\right) \tag{2.34}$$

$$\beta_{out} = 1 \tag{2.35}$$

where:

r_{in}, r_{tip}	constants dependent on k_p [Koteras and Ibsen, 2018]
$\beta_{in}, \beta_{tip}, \beta_{out}$	factors for reduction on the inner skirt wall, skirt tip and outer skirt wall

The β factors as proposed by Lian et al. [2014] is defined as:

$$\beta_{in}^{Lian};\ \beta_{tip}^{Lian} = 1 - \left(\frac{s}{s_{cr}}\right) \quad \text{for } s \leq s_{cr} \tag{2.36}$$

$$\beta_{in}^{Lian};\ \beta_{tip}^{Lian} = 0 \quad \text{for } s_{cr} < s \leq 1.5s_{cr} \tag{2.37}$$

$$\beta_{out}^{Lian} = 1 \tag{2.38}$$

The reduction factors as presented by Chen et al. [2016], α^{Chen}, was found to be :

$$\alpha_{in}^{Chen} = 0.865 \cdot \left(\frac{s}{s_{cr}}\right)^{1.03} \tag{2.39}$$

$$\alpha_{tip}^{Chen} = 0.707 \cdot \left(\frac{s}{s_{cr}}\right)^{1.86} \tag{2.40}$$

$$\alpha_{out}^{Chen} = 0 \tag{2.41}$$

In the absence of applied suction, the β factors are considered unity. Based on results from experiments carried out in the AAU lab, these factors are considered to approach the limits $\beta_{in} \approx 0.1$ and $\beta_{tip} \approx 0.2$, when the applied pressure approaches the critical pressure. As such, the β_{in} and β_{out} factors are implemented by setting $r_{in} = 0.9$ and $r_{tip} = 0.8$. These have been found to give good agreement with installation in dense sand.

β_{out} can be set to one as the changes in the excess pore pressure on the outer skirt wall are minimal and assumed to be insignificant compared to the changes on the inner skirt wall. Thus, this results in an assumption of a constant resistance on the outer skirt wall as mentioned before and is also confirmed by [Koteras and Ibsen, 2015] in the assessment of induced excess pore pressures during suction bucket installation tests .

2.5 The normalized seepage length and critical suction (s_{cr}).

For any given penetration depth, a critical suction exists at which a critical hydraulic gradient will develop and piping will be expected to occur [Erbrich and Tjelta, 1999]. It has been found that the critical gradient first develops at the skirt tip, but is constrained by the surrounding soil. The critical gradient proceeds towards the surface of the soil plug with increasing suction, and it has found that the critical gradient at the surface of the soil plug, adjacent to the inner skirt wall (denoted exit gradient, ι_{exit}) controls piping failure, [Senders and Randolph, 2009]. Feld (2001) noted that momentarily exceeding the critical suction does not necessarily cause piping failure as full formation of piping channels requires time. Results from laboratory and field installation have often reveal that the predicted critical suction is exceeded without experiencing installation failure by piping , indicating that current predictions methods used tend to underestimate expectations. Also, it has been found that boundary conditions tend to affect critical suction, [Koteras and Ibsen, 2015; Ibsen and Thilsted, 2010]. A review of the proposed methods for predicting the critical suction is present in the following.

Predictions for the critical suction based on the assumption of steady-state flow calculations from numerical studies have been proposed and these express the critical suction as a function of the penetration ratio (h/D). The proposed formulations generally adopt an approach which makes use of the relation between the critical suction and the normalized seepage length (s_L/h) obtained from the definition of the hydraulic gradient, [Ibsen and Thilsted, 2010; Senders and Randolph, 2009; Feld, 2001].

The hydraulic gradient in a medium is defined as the difference in total head (ΔH) over the seepage length (s_l). At the critical gradient, the soil effective stresses are reduced to zero as the seepage force equals the soil effective weight. The theoretical critical gradient can then be expressed as given in Eq. (2.42).

$$\iota_{cr} = \frac{\gamma^{'}}{\gamma_w} \tag{2.42}$$

Since the applied suction induces the hydraulic gradient during suction installation, the exit hydraulic gradient can be expressed in terms of the applied suction (s) and seepage length (s_L). The critical suction is obtained when the exit gradient is equal to the critical gradient, [Senders and Randolph, 2009]. These are described using the expressions given in Eq. (2.43) and Eq. (2.44)

$$\iota = \frac{s}{\gamma_w s_l} \tag{2.43}$$

$$s_{cr} = \iota_{cr}\gamma_w s_l = \gamma^{'} s_l \tag{2.44}$$

For installation in homogeneous sand with constant permeability, various expressions have been proposed for expressing the normalized seepage length as a function of the penetration ratio (h/D).The expression proposed by Ibsen and Thilsted [2010], developed in a study with penetration depth $0.1 \leq h/D \leq 1.2$, is given in Eq. (2.45). The limits for that expression determined for small h/D ratio approached 2.86, and for large h/D ratio approached unity, The lower limit being equal to the theoretical solution for a sheet-pile wall suggested by Hansen (1978), and the upper limit being a result of all the hydraulic head loss occurring within the skirt wall with evenly spaced horizontal equipotential lines. .

$$\left(\frac{s_l}{h}\right)_{exit}^{Ibsen} = 2.86 - arc\left[4.1\left(\frac{h}{D}\right)^{0.8}\right] \cdot \left(\frac{\pi}{2.62}\right) \tag{2.45}$$

Senders and Randolph [2009] derived a similar expression for the exit gradient and is given in Eq. (2.46), with the limit for small h/D ratio approached π and for large h/D ratio approached unity.

$$\left(\frac{s_l}{h}\right)_{exit}^{Senders} = \pi - arc\left[5\left(\frac{h}{D}\right)^{0.85}\right] \cdot \left(2 - \frac{2}{\pi}\right) \tag{2.46}$$

The expression proposed by Feld (2001) is given in Eq. (2.47) as :

$$\left(\frac{s_l}{h}\right)_{exit}^{Feld} = 1.32\left(\frac{h}{D}\right)^{-0.25} \tag{2.47}$$

These results were obtained from seepage studies using the numerical programs Flac 3D, Plaxis and Seep, respectively , and have been found to predict similar seepage lengths for penetration intervals of practical interests, that is $0.1 \leq h/D \leq 1$. As noted, an assumption of constant permeability was used for the results presented in Eq. (2.45) - Eq. (2.47). However, the critical suction is a function of penetration depth and permeability ratio, k_{fac}, and the above mentioned simplifying assumption excludes the effects of changing permeability between the inner and outer soil volume during suction-assisted installation.

Koteras and Ibsen [2019] indicated that that simplifying assumption could be the reason for the observation of theoretical critical suction being exceeded without triggering failure. A solution which attempts to account for varying permeability was proposed by Koteras and Ibsen [2018] and is given in Eq. (2.48). Eq. (2.48) seemed a more suitable formulation for the seepage length as it appeared to give results for theoretical critical suction which was not exceeded by applied suction in the investigation. It is however noted that this was obtained for penetration depth less than 0.5 m.

$$\left(\frac{s_l}{h}\right)_{exit}^{Koteras} = 1.25\left(\pi - arc\left[2.5\left(\frac{h}{D}\right)^{0.74}\right] \cdot \left(2 - \frac{1.8}{\pi}\right)\right) \tag{2.48}$$

A new formulation that directly takes into account the permeability ratio, (k_{fac}), captures an envelop for varying permeability as presented by Rodriguez and Barari [2020], and is given in (2.49).:

$$\left(\frac{s_l}{h}\right)_{exit}^{Rodriguez} = (0.26 + 1.15 \cdot k_{fac}) \cdot \left(\frac{h}{D}\right)^{0.7 \cdot k_{fac}^{(-0.2)}} \cdot \left(\frac{D}{h}\right) \tag{2.49}$$

By combining the results given in Eq. (2.45) - Eq. (2.49) with Eq. (2.44) , the critical suction can be expressed as :

$$\frac{s_{cr}}{\gamma' D} = \left(\frac{s_l}{h}\right)_{exit} \left(\frac{h}{D}\right) \tag{2.50}$$

with $(s_l/h)_{exit}$ for the respective solution method selected from Eq. (2.45) - Eq. (2.49).

Houlsby and Byrne [2005] also proposed a solution for the normalized critical pressure using the pore pressure factor, α, for the case where the influence of varying permeability is included. This is presented in Eq. (2.51) as:

$$\frac{s_{cr}}{\gamma' D} = \left(1 + \frac{\alpha_1 \cdot k_{fac}}{1 - \alpha_1}\right) (h/D) \tag{2.51}$$

where α_1 is as defined in Eq. (2.10).

2.6 Remarks for state of the art review

Both models discussed in the preceding sections have been shown to produce agreeable results, in varying degree, for predictions of installation resistance of suction buckets.

Andersen et al. [2008] concluded in his work that the bearing capacity model gives more consistent agreement with the measured penetration resistance than the CPT model for self-weight penetration. He noted that this observation may be a result of the bearing capacity model directly accounting for the interaction between the skirt wall and the skirt tip, while the CPT model may fail to properly account for the skirt wall-skirt tip interaction due to differences in geometry and wall roughness between CPT and the bucket skirt. However, use of the CPT model is generally preferred over the bearing capacity model. as parameters required for the bearing capacity model are difficult to accurately estimate (N_q, K_o) [Senders and Randolph, 2009], and require the use of CPT data as input for determining the friction angle and relative density across soil stratigraphy. Hence the CPT model provides a more straightforward and convenient approach for solving the problem with relatively lesser uncertainties compared to the bearing capacity model.

Also, the current formulations for the CPT-based method appear to provide conservative solutions, with proposed improvements developed from specific testing conditions. Thus, it seems that the formulations provide a good starting point for suction bucket installation design, and designers must expect to make adjustments for specific problems. Generally, the available formulations give similar results, and the attempts to directly account for seepage effects, such as changing permeability and resistance reduction [Houlsby and Byrne, 2005; Koteras and Ibsen, 2018; Rodriguez and Barari, 2020], appear to have potential to improve predictions for suction installation design.

Experimentation 3

A prototype model of a suction bucket was prepared for use in testing suction bucket installation in homogeneous sand in the AAU geotechnical laboratory. Testing was carried out in normal ground gravity condition (1-g testing), inside a sand box using a medium scale $1:10$ *model with aspect ratio* $L/D = 1.0$*. Details of the model set up and a brief description of the experimental procedure are outlined in this chapter. Results obtained from the testing campaign are also presented in the final sections of this chapter. Further details concerning the experimental procedure and results are presented in Appendix A.*

3.1 The physical model

Experimental suction bucket installations were performed in the AAU geotechnical laboratory using a scaled model of a suction bucket. The tests were carried out in a large, watertight, steel sand box, Figure A.1. The sand box, with internal diameter 2.5 m and a height 3.52 m, is connected to auxiliary systems, comprising a pressurized water supply and drainage system, hydraulic actuators, pressure sensors and a pumping system for suction installation. Schematics for the test set up is presented in Figure 3.1 (sketch of the test set up can be found in Appendix A.2.1 and shows the internal array of sensors.).

The prototype bucket selected for the investigation is a scaled 1:10 model, constructed as a cylindrical steel bucket with unpolished skirt walls and a thickened tip. The thickened tip extends along the bottom 20 mm of the skirt wall. Aspect ratio of the prototype model is $L/D = 1$, with skirt tip width $(t_{tip}) = 10$ mm, and bucket weight with connection flange attached, $W_{sb} = 255$ kg. Geometric properties of the suction bucket are listed in Table 3.1, with Figure 3.2 showing a diagram of the bucket.

Table 3.1: Geometry and weight of bucket foundation model.

Geometry and weight of bucket foundation model.									
D [m]	L [m]	t_{lid} [m]	t_{skirt} [m]	t_{tip} [m]	h_{tip} [m]	W_{sb} [kg]	A_{lid} [m^2]	A_{tip} [m^2]	A_{side} [m^2]
1	1	2e-2	3e-3	10e-3	2e-2	255	0.776	31.32e3	6.26

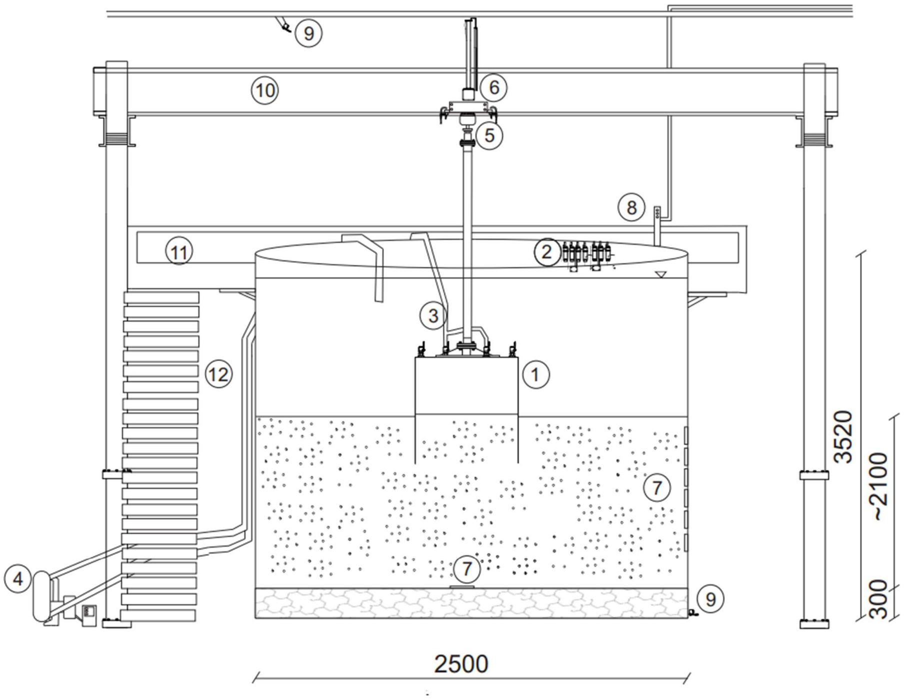

Figure 3.1: Diagram of equipment set up for suction bucket installation, dimensions in mm.
1. bucket foundation
2. pore pressure transducers
3. suction hose
4. suction pump
5. load cell
6. displacement transducer
7. stress sensors and ...
...pore pressure transducers
8. vacuum access point
9. water access points
10. loading frame
11. Working platform
12. Access ladder

[Koteras and Ibsen, 2019]

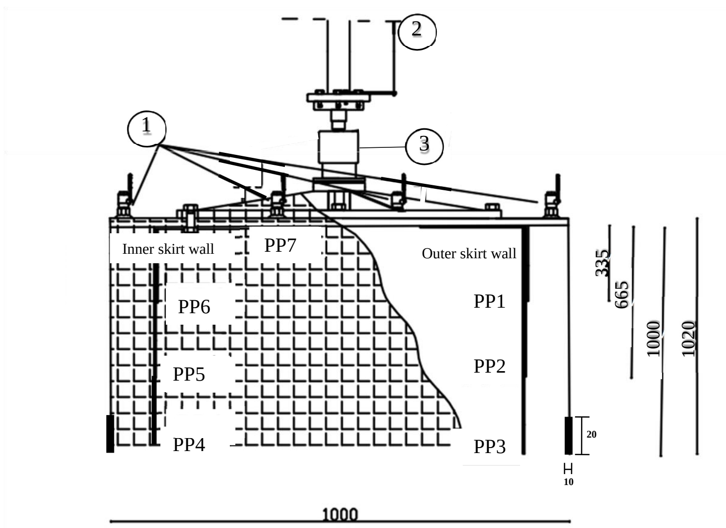

Figure 3.2: Diagram of suction bucket model, dimensions in mm.
1. valves 2. displacement transducer 3. connection flange with load cell

Editted from [Koteras and Ibsen, 2019]

3.2 Test set up and parameter derivation.

The base of the sand box is lined with evenly spaced, perforated pipes, Figure A.1b, which form part of the connected drainage system for the experiment. The perforated pipes are covered with highly permeable gravel, up to 0.3 m high, and a geotextile membrane is on laid on top of the gravel layer. Above this is a 2.65 m layer of homogeneous sand whose properties are presented in Table 3.2. Attached to the loading frame are a load cell and displacement transducer for recording load-displacement measures during bucket installation.

The prototype bucket, as shown in Figure 3.2, is fitted with pore pressure sensors along the skirt wall(PP1-PP6) and beneath the bucket lid (PP7) for measurement of pore pressure variations and applied suction during installation, respectively. These are connected by channels which terminate at distance 1/3 L, 2/3 L and 3/3 L along the outer skirt wall for PP1-PP3, and along the inner skirt wall for PP4-PP6, respectively. Four valves located along the center line on the bucket lid provide connection to a vacuum system for suction application and CPT inside the bucket compartment after installation. All sensors are connected to a data acquisition system for recording data. The mentioned array of sensors in the set up provide continuous data collection for installation analysis.

Prototype bucket installation was performed in laboratory sand referred to as AAU Sand No. 1 (also, Baskarp Sand No. 15). The properties of the sand have been extensively investigated by Borup and Hedegaard [1995] and are presented in Table 3.2. Based on these determined soil properties and results from CPT, important parameters are derived for installation design. Parameter derivation was carried out as described by Ibsen et al. [2009]. Soil parameters of particular interest for installation design include the effective soil unit weight (γ'), relative soil density (I_D), triaxial friction angle (ϕ_{tr}), triaxial dilation angle (ψ_{tr}), in situ void ratio (e_{insitu}) and soil permeability (κ_{perm}).

Data from falling head test performed by Sjelmo [2012] for different relative densities of AAU Sand No. 1 is used as basis for determining soil permeability. Using a quadratic fit to the data, an expression for permeability as a relation with void ratio is obtained, as given in Eq. (3.1). The obtained results allows for determination of the hydraulic conductivity of the material, with temperature effects taken into consideration. Thus, the hydraulic conductivity is correlated to the void ratio, and in effect provides a direct correlation to the soil relative density determined from CPT data. This is expressed by Eq. (3.2) and shown in Figure 3.3.

Table 3.2: Properties of AAU No. 1 Sand

Soil property	Value	Unit
Soil unit weight, (γ)	20	$[kN/m^3]$
50%-quantile, ($d-50$)	0.14	mm
Specific grain density, (d_s)	2640	[-]
Maximum void ratio, (e_{max})	0.854	$[-]$
Maximum void ratio, (e_{max})	0.549	$[-]$
Uniformity coefficient, (C_u)	1.78	$[-]$

$$\kappa_{perm}^{AAUno.1} = 6.8 \cdot 10^{-11} \cdot e^2 - 4.8 \cdot 10^{-11} \cdot e + 1.1 \cdot 10^{-11} \tag{3.1}$$

$$\kappa_{hc}^{AAUno.1} = 7 \cdot 10^{-9} \cdot I_d^2 - 2.3 \cdot 10^{-6} \cdot I_d + 2.2 \cdot 10^{-4} \tag{3.2}$$

where :			
	e	the in situ void ratio	[-]
	κ_{perm}	the soil permeability	[m^2]
	I_d	the density index	[%]
	κ_{hc}	the soil hydraulic conductivity	[m/s]

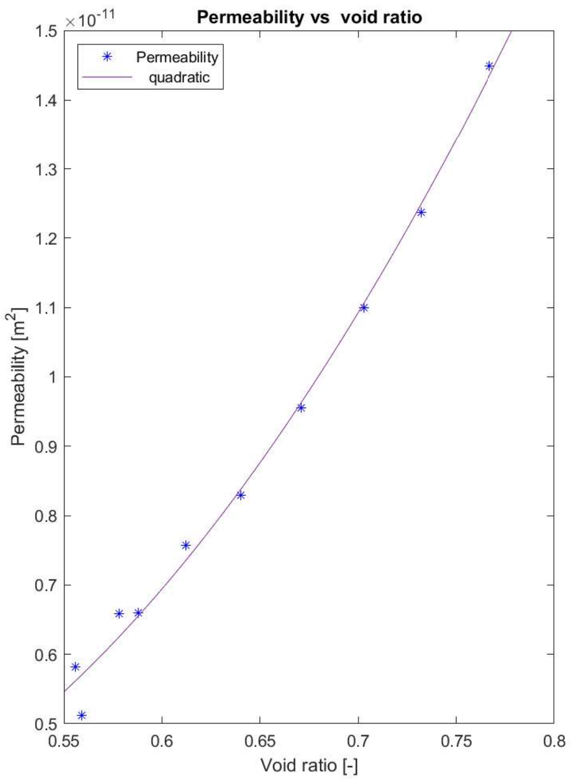

(a) Permeability as a function of void ratio

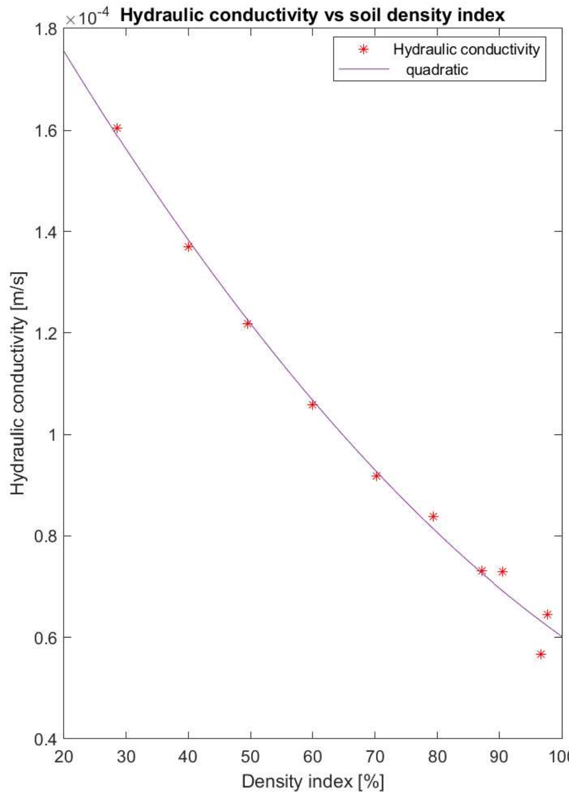

(b) Hydraulic conductivity as a function of density index

Figure 3.3: Relation between (a)permeability and void ratio (b) hydraulic conductivity and density index.[Sjelmo, 2012]

3.3 Brief description of testing procedure

Bucket installation tests- began with the preparation of the soil by filling the sandbox to the desired height, saturating the soil volume, compacting with a shaft vibrator and checking to ensure uniform density is achieved prior to testing. A 2 m long mini-CPT device with diameter 15 mm ($A_{cone} = 176.7\,\text{mm}^2$) and cone angle 30° was used for initial CPT testing in 4 position in the soil volume, Figure 3.4a. This served as a check for soil uniformity prior to installation and obtaining data for subsequent parameter derivation. CPT is performed as a displacement-controlled procedure and measures recorded during the test include time $[s]$, displacement$[mm]$ and cone resistance $[kN]$.

The bucket model was then prepared and connected to the hydraulic actuator on the loading frame for installation. Installation was performed with a partially submerged bucket and saturated pore pressure transducers before start of installation.

Each installation was preceded by a set of CPT's, Figure 3.4a, to obtain data for determining the geotechnical parameter derivation for the sand. This also serves as a check for uniformity of the soil volume. A second set of CPT's was performed immediately at the end of suction installation at 8 locations to identify changes in soil relative density inside and outside the bucket due to the installation process, Figure 3.4b. The bucket was then uninstalled by connecting the bucket to the actuator and pulling out from the soil. Further details on testing procedure is outlined in Appendix B.1. Test run 5 results are presented in section 5.1, with data for other test runs presented in Appendix B.1.

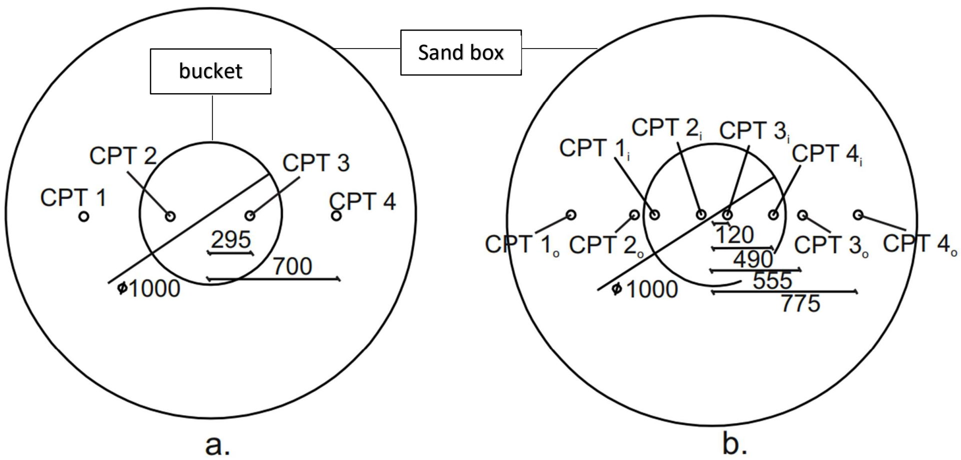

Figure 3.4: Position for CPTs: (a) before installation , (b) after installation. Dimensions in mm. Editted from [Koteras and Ibsen, 2019]

Numerical simulation of the seepage flow 4

Numerical simulation of suction installation was performed to study seepage flow induced pore pressure variations for suction bucket installation in homogeneous sand. This was done using the numerical program Plaxis 2D. It is noted that simulations were performed using the assumptions detailed by Senders and Randolph [2009] specified in section 2.3.2. The procedure employed and the results obtained from numerical modelling are presented in this chapter.

4.1 Model domain

The laboratory model for suction installation was simulated in the finite element program Plaxis 2D in order to investigate the seepage pattern and hydraulic gradients developed during suction installation. Thus, the domain of the finite element model are the same as those used in the laboratory setup, as described in section 3 of this document.

Given the geometry of the installation set up, a domain with 15-node axisymmetric model was selected for the 2D numerical simulation. The symmetry of the installation allowed for a simplification where only half the model was generated in the Plaxis program for the investigation. This approach has been found to produce satisfactory results from 2D simulations. Also, a simplification of the suction bucket was employed where the skirt wall was modelled using plate elements, with ascribed properties that reflect the actual dimension of the skirt wall of the experimental model. Thus, the bottom section of the plate element were modelled to reflect the thickened tip of the skirt wall used in the experimental model (Figure 4.4b). Details on plate element properties are presented in Appendix C.2.

4.2 Material modelling and properties

It was of interest to investigate the hydraulic gradient around the bucket skirt and especially at the skirt tip, and thus seepage flow analysis in permeable soil was executed using steady-state groundwater flow calculations. The linear elastic perfectly plastic model (Mohr-Coulomb model) was adopted for the analysis with its input parameters of interest briefly presented in this section. Details for the selected material model input parameters are presented in Appendix C.1. The input parameters of interest, for this study are listed in Table 4.1 :

Table 4.1: Mohr-Coulomb input parameters of interest

Drainage type	Internal friction angle (ϕ')
Saturated unit weight (γ_{sat})	Dilation angle (ψ')
Unsaturated unit weight (γ_{unsat})	A hydraulic model
Initial void ratio (e_{init})	Soil hydraulic conductivity (κ_x,κ_y)
Young's modulus (E')	Interface strength (R_{inter})
Poisson's ratio (ν')	Interface conductivity
Effective cohesion (c'_{ref})	

Derived geotechnical properties of AAU Sand No. 1, as described in section 3.2, served as basis for soil properties input parameters for the selected Mohr-Coulomb model. An assumption of constant permeability was employed, and the permeability obtained from CPT before bucket installation during lab experiment served as soil hydraulic conductivity. This made it possible to define input parameters for modelling specific experimental test run as required.

For modelling the steady-state groundwater flow, data set for flow parameters was assigned as the USDA series, with the Van Genuchten model selected for as the hydraulic model for groundwater flow in the fully saturated soil. Under such conditions, Darcy's law can be assumed to apply to the groundwater flow.

4.3 Model discretization

A mesh convergence study was performed to determine an appropriate model discretization that offered a balance between computation cost and accuracy of results. This was achieved by varying the local mesh refinement. An area around the skirt, 1 m x 1.5 m, was set to a finer refinement than the rest of the domain as results from the points closest to the skirt structure was of particular interest. To ensure a smooth transitioning between zones of varying mesh density, it was ensured that the local mesh refinement between the area closest to the skirt structure and the rest of the domain had a difference no more than 2 degrees of fineness. The global element size used was set to *Medium* setting. The selected mesh refinement used for simulation is shown in Figure 4.1.

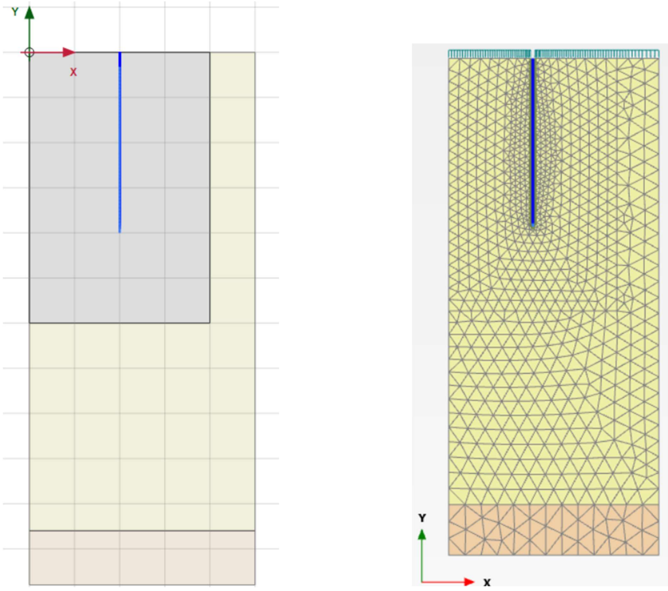

Figure 4.1: (a)Left: Model domain (b) Right: Model meshing .

Results of the convergence study are presented in Figure 4.2 and Figure 4.3. These were selected for the inner exit, ($SP1$), and skirt tip, ($SP2$), to check for variation of excess pore pressure and discharge velocity, as these were the main output of interest. From the results of the simulation, the model with 1,840 elements and 15,314 nodes (E1840-N15314) was selected for the study.

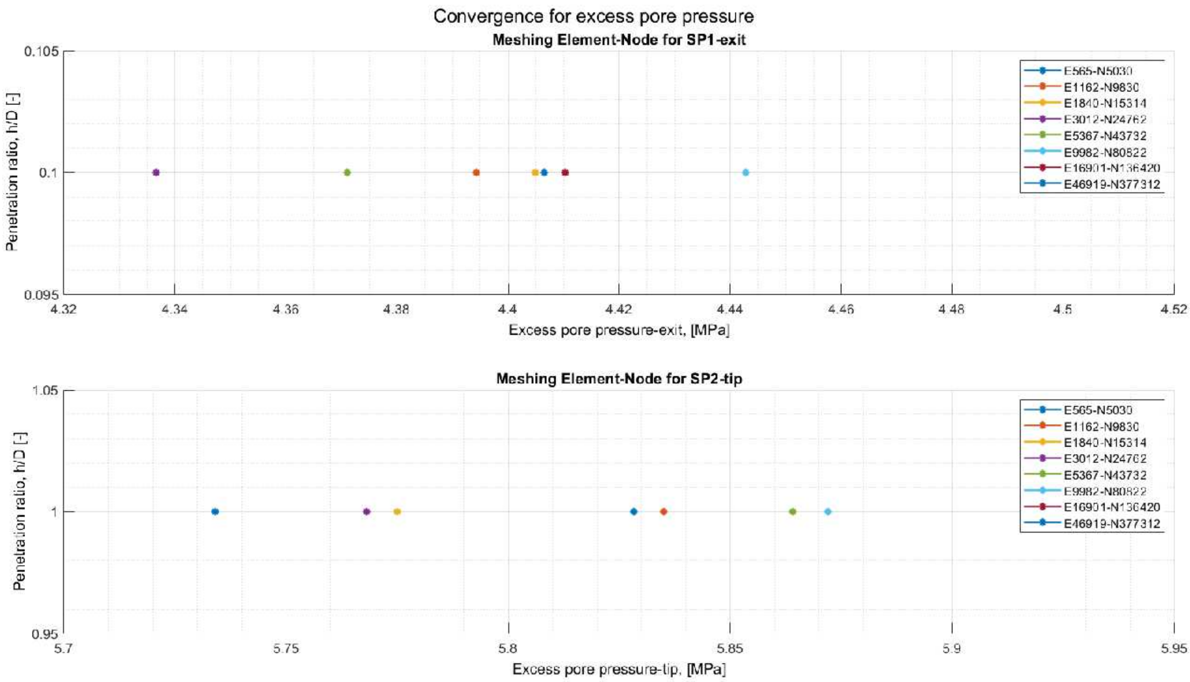

Figure 4.2: Convergence for excess pore water pressure at $SP1$ and $SP2$

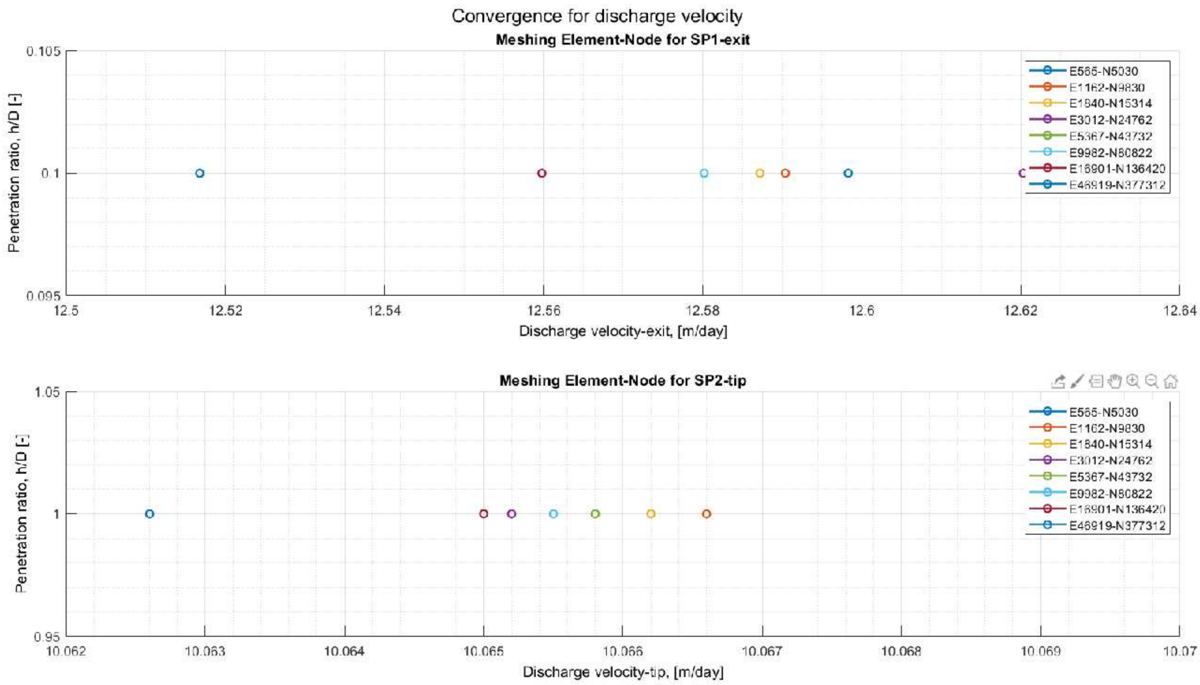

Figure 4.3: Convergence for discharge velocity at $SP1$ and $SP2$

4.4 Flow condition

Model flow conditions need to be specified to reflect conditions of the test set up. Specifically, the boundary flow conditions and the activation of interface along the skirt must be appropriately specified in order for the steady-state groundwater flow calculations to proceed. Failure to activate the required flow conditions for each calculation phase can result in failed execution of a calculation phase. All external boundary conditions were specified as closed flow boundaries. The internal boundaries representing soil polygons were assigned as seepage surfaces and the surface of the soil layers assigned appropriate heads to trigger groundwater flow and simulate applied suction in the model. A head of 3 m was specified for the soil surface outside the area for skirt wall, while reducing head values were specified for the soil surface inside the skirt wall. These were selected in a manner to replicate applied suction at specific penetration depths in lab experiment. It is important to set the head difference in a manner that negative head difference is avoided in the model. Figure 4.4 shows an example of the flow boundary conditions for a selected phase of the calculation with the appropriate interfaces activated and a specified head for inside and outside the skirt wall.

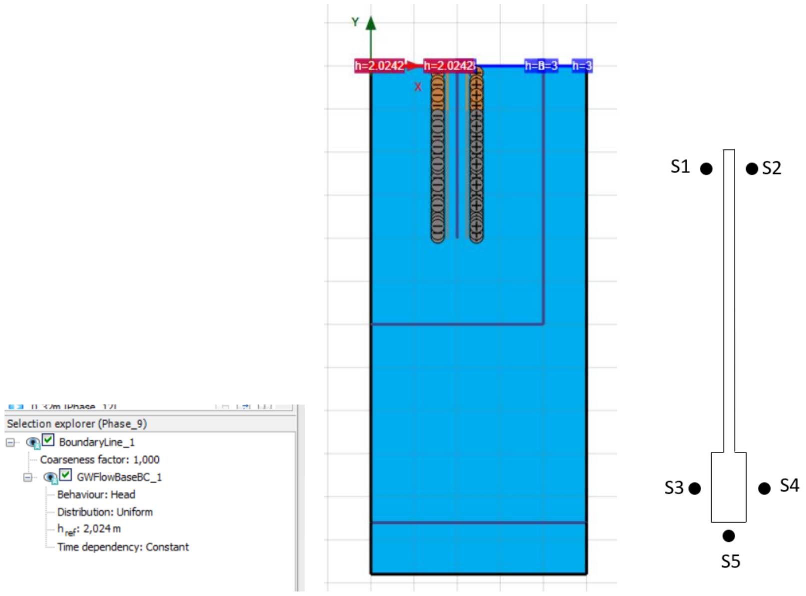

Figure 4.4: (a) Model flow boundary condition. (b) Sketch of stress points for result extraction along skirt

4.5 Calculation phases and results extraction

The continuous process for suction-assisted installation was simplified into discrete phases with increasing penetration depths from 0.1 m - 1 m at intervals of 0.02 m. The calculations proceed as follows:

- Initial phase : Initial soil stresses are generated based on the specified in-situ conditions. Only soil and groundwater flow boundary conditions are active in this phase, and the pore pressure is calculated based on the phreatic level. 'Pore pressure calculation type' in the Phases window was set to 'Steady state groundwater flow'.
- Installation phase (suction phase) : Appropriate interface for each step representing a certain penetration depth was activated.'Pore pressure calculation type' in the Phases window was set to 'Steady state groundwater flow' and pore pressures are calculated for seepage flow generated by the specified head difference.

Calculation results for porewater pressure and discharge velocity were extracted from stress points for each penetration depth, from $0.1\,\text{m} - 1\,\text{m}$. Locations of the stress points are:

- near the surface of the soil,inner exit (S1) and outer exit(S2)
- around the tip of the skirt, mid-height of thickened lips (S3 and S4)
- the tip of the the skirt (S5). (Figure 4.4b)

Also,results for porewater pressure along the boundary of the soil volume were extracted from nodes along the soil volume boundary, in the same position as sensors array locations as shown in Appendix A.1b. The stress points for results extraction were selected within a distance of 1 cm from the skirt wall and tip, within the area representing the interface in the Plaxis Output program.

Results and analysis 5

A previous test campaign (Rodriguez and Barari [2020]) employing a bucket with the same dimensions as that used for this project, but with uniform skirt thickness, provided test results data for comparison with test results obtained from this project's experimental campaign. Observations made are pointed out and comparison of results for proposed formulations for CPT-based suction installation predictions were made. Results realized are presented in the following sections.

5.1 Experiment test results

The experimental campaign comprised of 6 suction tests, out of which 1 was unsuccessful (Test run 3). Also, a jacking test was performed, however an error in data acquisition resulted in failure to capture the installation data. The results from the successful suction installation tests are first presented, and observations on the failed jacking test are presented next.

CPT results for Test run 6 are presented in this section for illustration. Results for the CPT performed before and after installation, progression of suction installation and pullout uninstallation are shown.

Figure 5.1a shows results for CPT performed prior to installation for Test run 6, and Figure 5.1b shows the relative density index prior to installation, determined from the CPT data using parameter derivation methods described by Ibsen et al. [2009] (see Appendix A.5). A comparison of all test run results for suction installation shows a significant reduction in the soil resistance to penetration as indicated by the CPT data for CPT after installation.

Figure 5.2 shows results for CPT performed after installation for Test run 6, and Figure 5.3 shows the relative density index after installation.

The progression of the suction installation for test run 6 is presented in Figure 5.4 and the uninstallation by pull out is also shown in Figure 5.5a. For this installation test, the suction pump was restarted after penetration of the bucket halted. This is reflected in the sudden jump after the initial end of penetration.This was done only for this test with an observation of a minimal increase in the penetration depth. Also, the maximum suction ($20.88[kPa]$) was observed at the point marked 'end of suction installation', after which the suction pressure began to decrease. A similar trend was noted in all tests performed (Appendix B), and an attempt to induce further penetration by restarting suction yielded minimal increased penetration (0.01 m) as shown in Figure 5.4.

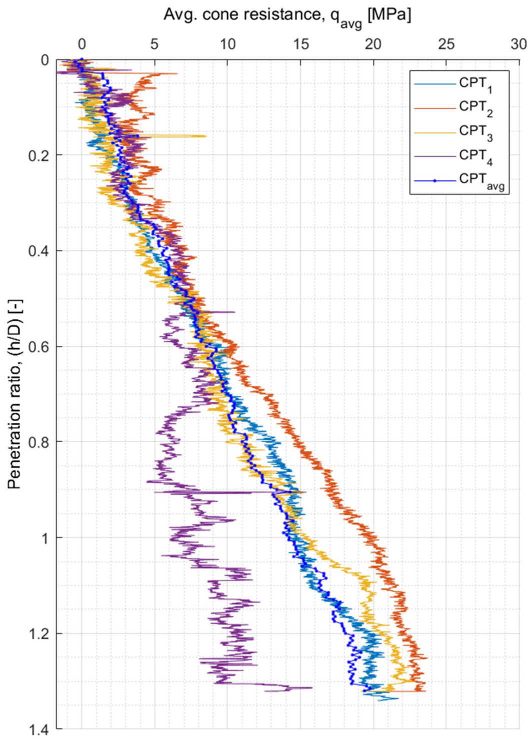

(a) Test run 5 CPT before installation data

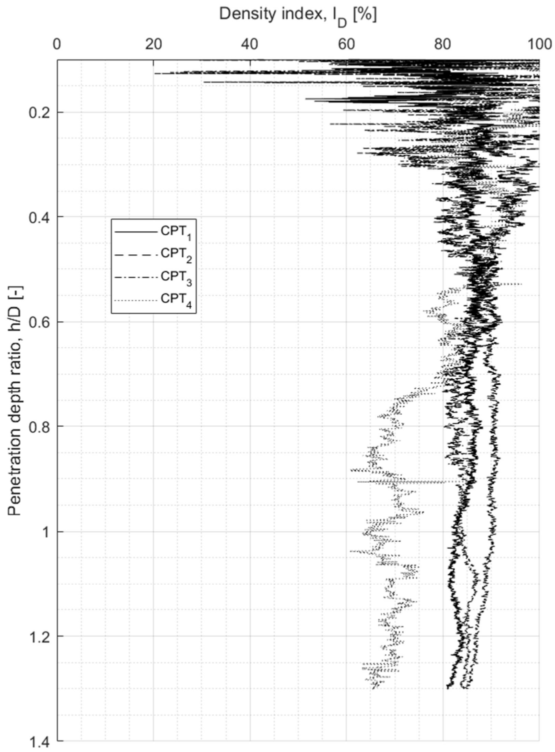

(b) Density index for Test run 5: CPT before installation data

Figure 5.1: (a) CPT before installation and (b) Density index based on CPT data

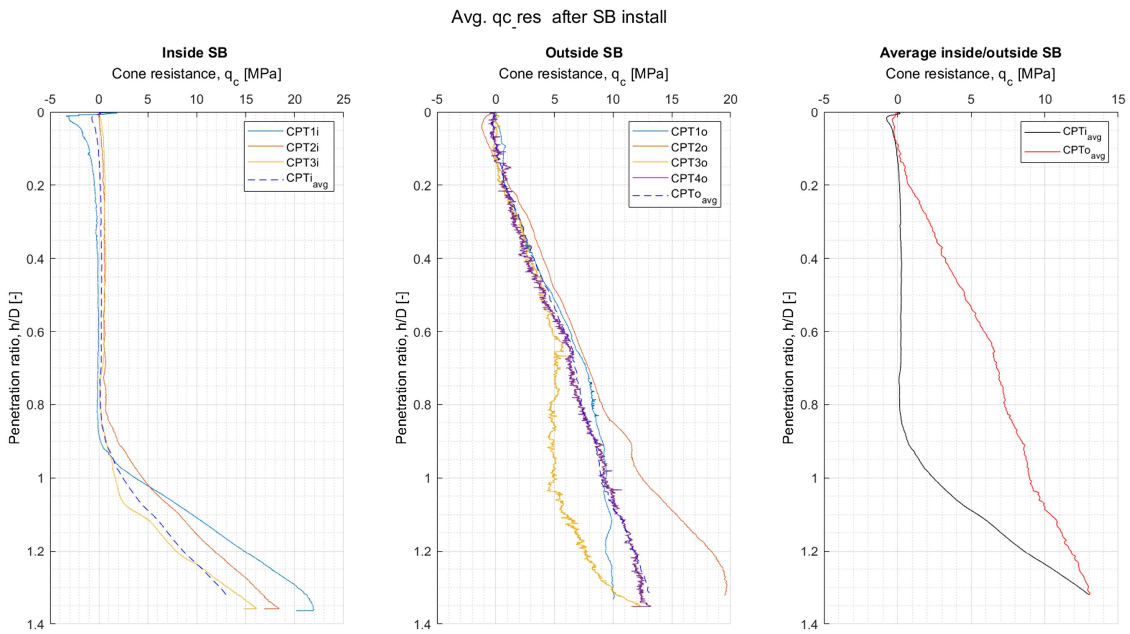

Figure 5.2: Test run 5 CPT after installation data

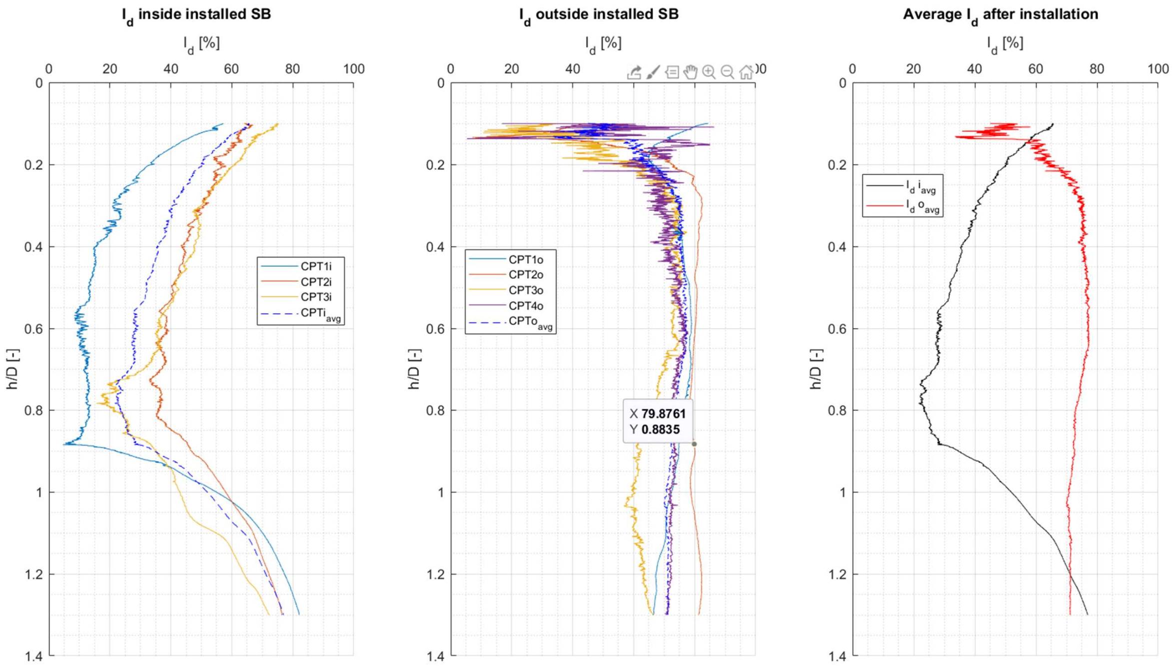

Figure 5.3: Density index for Test run 5: CPT after installation data

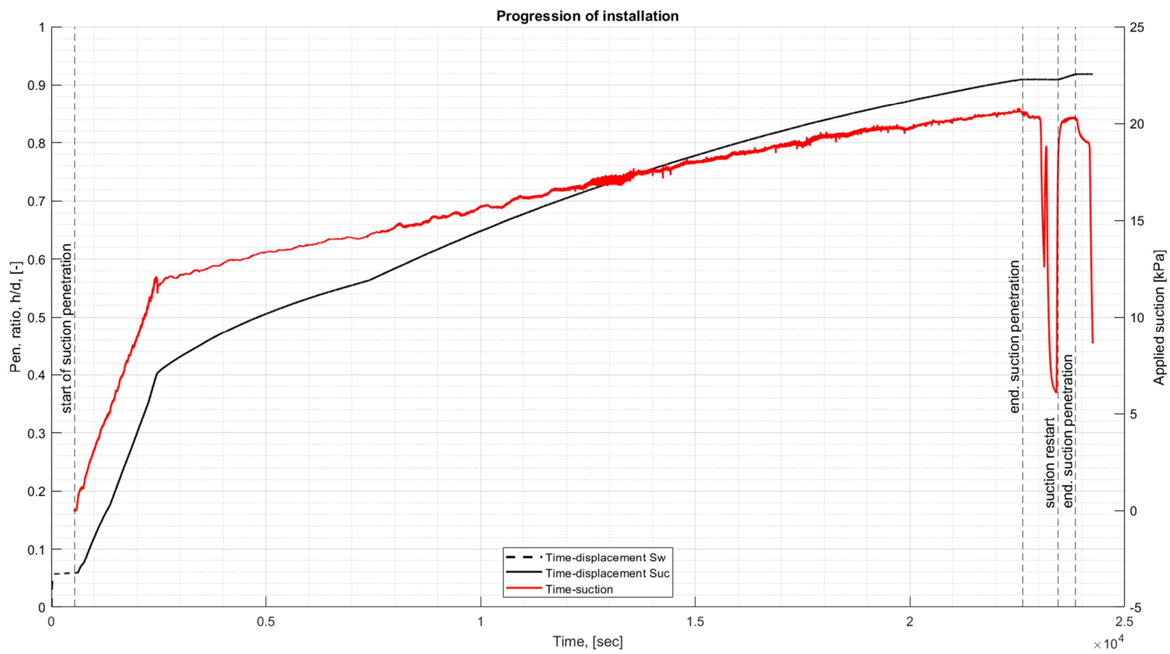

Figure 5.4: Progress of suction installation for test run 5

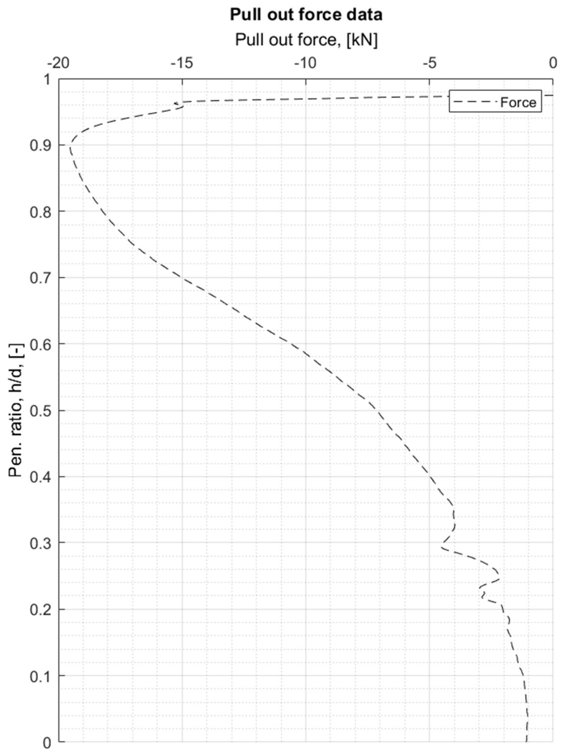

(a) Progress of uninstallation by pull out for test run 5

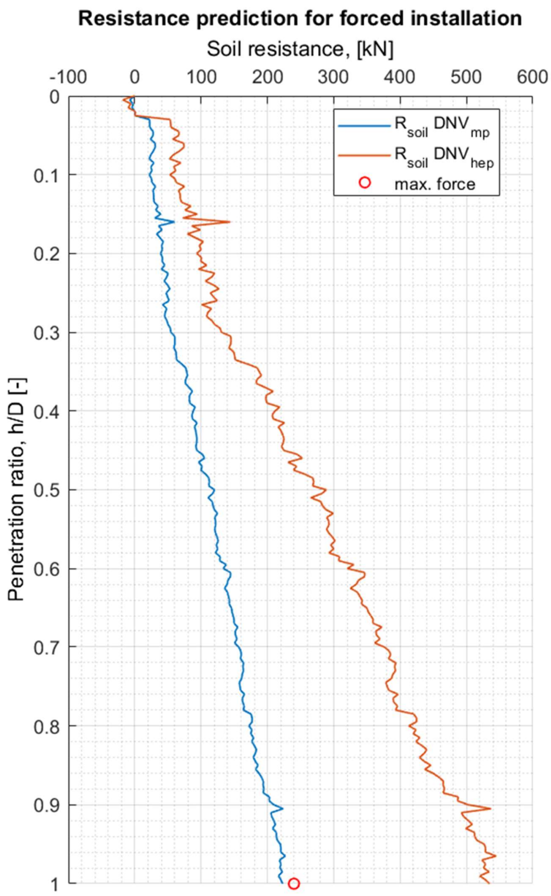

(b) Resistance prediction for jacking installation for test run 5

Figure 5.5: (a) Pull out installation and (b) Resistance prediction

As state earlier, data acquisition for jacking installation failed due to an error and the load-displacement curve could not be captured. However, preliminary resistance predictions using the most probable values of k_p and k_f, as recommended by DNV for bucket installation, indicated close agreement with the value of maximum resistance from the lab experiment. This result is somewhat unexpected, as a bucket with increased tip thickness is expected to offer greater resistance to penetration than a bucket with uniform skirt thickness. Only one test of this kind was performed, however, and it is not possible to say if the observed response occurs along the entire penetrated depth. A comparison with results from a previous test campaign using skirt wall of uniform thickness with a skirt tip 1/3 the size of that used for this project indicated that resistance predictions using the most probable DNV recommended coefficients resulted in a underestimation of the resistance beyond 0.4 m of soil penetration, with the difference increasing with greater penetration depth. More tests need to be executed to conclude on the contradicting observation made for this test.

Though there was an issue with data acquisition with the jacking test, the maximum force for installation and uninstallation were noted and are compared with the maximum obtained from a skirt with uniform thickness as presented in Table 5.1.

Table 5.1: Comparing maximum force for forced installation and uninstallation

	Jacking installation ($I_d \approx 80\%$)		
	Test run 1	Data from previous test	$\Delta\%$
Max. displacementh/D>h/D	$\approx$1.00	0.90	-
Max. force installation [kN]	240	178	34.83
Maximum Pullout force [kN]	32.32	18.5	74.7

5.1.1 Overview of experiment results

An overview of all tests performed is presented in Table 5.2 - Table 5.4. Derived geotechnical parameters and the associated changes before and after suction installation are shown. Changes in soil properties as a result of the installation process, and differences in soil outside and inside the bucket compartment are reflected in changes in hydraulic conductivity of the soil and the soil relative density index. Results for test run 5 (Suc 5) after installation are not exactly accurate as in issues was detected with the CPT probe. Therefore, CPT after installation data for test run 5 was considered as errorneous and not used for analysis.

Seepage effect is most significant in denser soil as shown in Table 5.3, resulting in greater reduction of soil relative density on the inside compartment of the bucket. Also, the hydraulic conductivity of soil trapped within the bucket compartment appear to approach a common value. irrespective of the initial state of the soil prior to installation.

Table 5.2: Parameters derived from CPT data

	Before installation				After installation	
Test	Secant friction angle	Tangent friction angle	Dilation angle	Hydraulic conductivity	Hydraulic conductivity	Hydraulic conductivity
	ϕ_s	ϕ_t	ψ	κ [m/day]	κ_{in} [m/day]	κ_{ot} [m/day]
Suc 1	48.55	38.02	12.09	10.12	11.24	10.25
Suc 2	49.55	38.74	14.17	9.28	10.96	9.77
Suc 4	51.27	39.99	16.39	7.94	11.97	9.05
*Suc 5	51.59	40.22	16.79	7.71	10.06	11.63
Suc 6	53.60	41.68	19.38	6.38	11.23	7.71
Jacking 1	53.57	41.65	19.33	6.40	8.53	6.54
	Issue with cable detected during CPT after installation					

Table 5.3: Density index before and after installation

Test	Before installation	After installation		Percentage change		Heave
	I_d %	$I_{d\,in}$ %	$I_{d\,ot}$ %	$\Delta I_d - I_{d\,in}$ %	$\Delta I_d - I_{d\,ot}$ %	Heave[mm]
Suc 1	52.03	43.89	51.07	18.55	1.8	≈ 50
Suc 2	58.57	45.85	54.72	27.74	7.04	≈ 50
Suc 4	69.92	38.85	60.39	79.97	15.78	≈ 50
*Suc 5	72.01	52.45	41.14	37.29	75.04	≈ 45
Suc 6	85.24	43.94	72.01	93.99	18.37	≈ 45
Jacking 1	85.03	64.73	83.52	31.36	1.81	

Table 5.4: Max. measured force for suction installation and uninstallation by pull out.

Test	Installation	Uninstallation	
	Max. suction [kPa]	Max. force [kN]	Max. h/D
Suc 2	21.5	14.85	0.95
Suc 4	18.35	13.22	0.87
Suc 6	20.79	19.52	0.90 (0.92)
Jacking 1	240 [kN]		≈ 1

Comparing the results for maximum suction applied during the experiments to data from previous test runs not included in this report, it is observed that similar suction requirement exist for a bucket with thickened tips to achieve installation at similar target depth as a bucket with uniform skirt thickness. Similar observations were made in the results of the 2D numerical model where for varying skirt tip thicknesses of 3 mm, 10 mm, 13 mm, 17 mm and 23 mm, similar discharge velocity were obtained. This indicates that the required suction for installation may be indifferent to the skirt tip thickness, as no greater provision for suction is required for full penetration buckets with the same h/D. This is supported by data from experiments, and proves that suction-induced seepage effectively reduces the soil resistance at the tip of the bucket and makes it possible to install suction buckets with varying tip thickness to similar target depths.

Calculation predictions of the critical suction for installation of the suction bucket were performed using the CPT based methods mentioned in section 2.3.2 - 2.5 together with DNV recommended k_p and k_f coefficents and the measured k_{fac} from tests. Predictions performed using the normalized seepage length for critical suction prediction showed somewhat similar results for most of the proposed formulation. The applied suction exceeded the calculated critical suction along most of the penetrated depth, and in the case of test run 6, the applied suction exceed the calculated critical suction by a factor of 1.53, Figure 5.7. It is worth noting that though the mentioned formulations do produce similar results for critical suction (Figure 5.6), and the formulation proposed by Rodriguez and Barari [2020] seems to produce predictions for higher critical suction . This indicates that this implementation of the permeability factor (κ_{fac}) in the formulation for critical suction may be a better solution for accounting for the soil structure interaction that occurs during the suction installation process, even though it underestimates the applied suction in a similar manner as the other formulations.

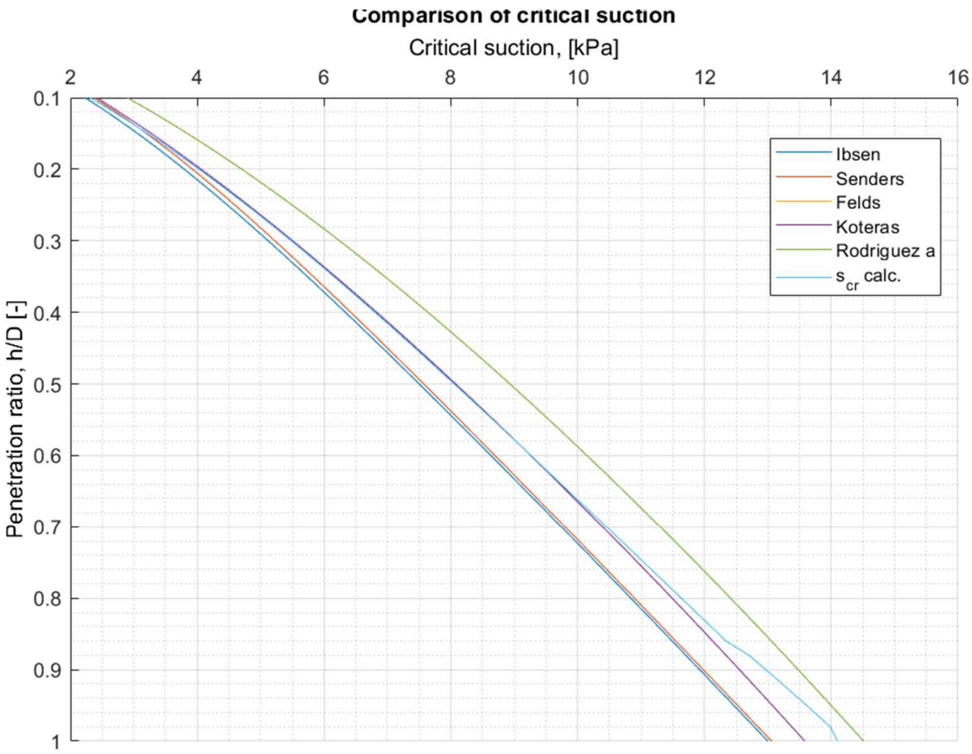

Figure 5.6: Comparing formulations for critical suction

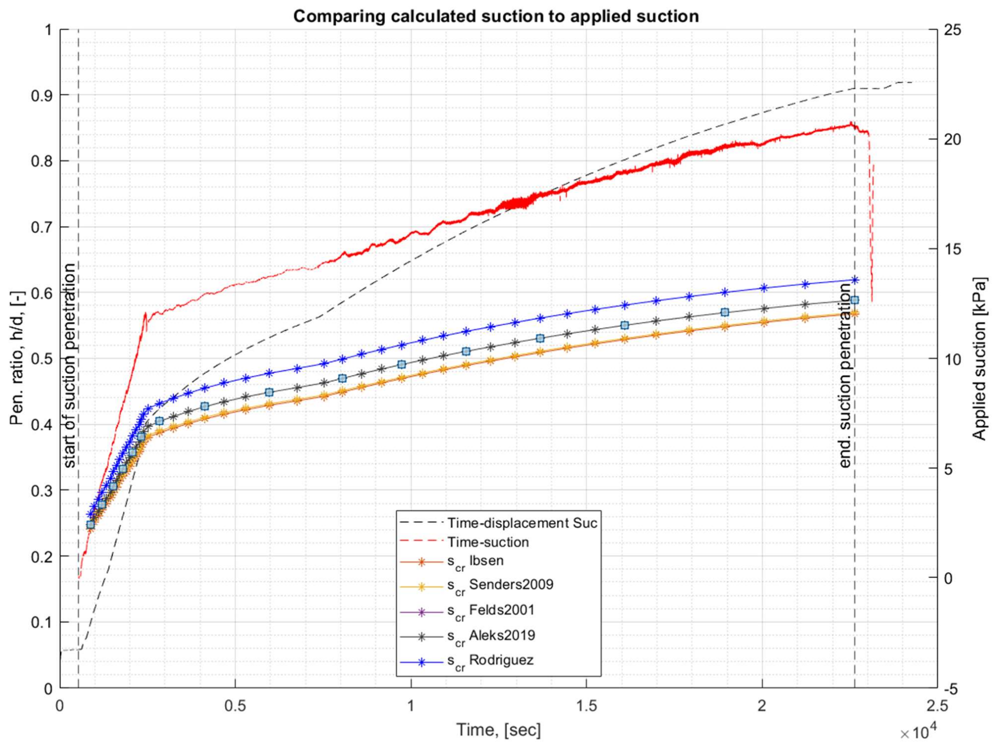

Figure 5.7: Prediction of critical suction vrs applied suction. Prediction formulations employed based on predictions for normalized seepage length

Inconclusive results remain for k_p and k_f coefficients for the skirt used for the experiment, as these factors are calculated from results from jacking test data. It is expected that better results for required suction predictions could be obtained with optimized k_p and k_f coefficients, but further testing would be required for this. However, using the maximum values of the observed uninstallation data and CPT before installation average cone tip resistance in (2.31), a value of $k_f = 0.0002$ is obtained.

Though not in agreement with the DNV recommendation range of values for standard design at first glance, $k_f = 0.0002$ does show an indicative agreement with the DNV recommendation for decreased k_f coefficient for increased tip area as noted in section 2.4. This result should only be considered as an indicative value since more data is required for a proper assessment to obtain k_p and k_f coefficients for the bucket model used in the experiment.

Conclusion and further work 6

A series of experiments were carried out in the geotechnical laboratory of Aalborg University to investigate the installation of a modified suction bucket with thickened lips and a $L/D = 1$. Experiments were performed in sand of varying density, with relative density index ranging from 52 % - 85 %. 5 suction installation tests and an attempt for a jacking installation test were completed for the test campaign.

In all suction tests, it was observed that no greater requirement for suction is required for the installation of the modified bucket when compared to installation with a uniform thickness bucket. This indicates that buckets with such modification can be designed with current design methods for uniform thickness bucket skirts, though the results may be very conservative. Though current design methods have their shortcomings, they have been used for the design of suction bucket foundations with success. Formulation for optimizing design proposed by various researchers in an attempt to properly incorporate the identified factors influencing the suction installation process into design were tested as well for comparing appropriateness for general situations.

Preliminary calculations for critical suction were performed and this highlighted the shortfall of commonly used prediction methods. However, it worth mentioning that proposal have been made for solutions that seem to work for specific conditions, such as small scale test and medium scale test. So far, they all seem to produce conservative design. In this paper, preliminary design was carried out with formulations that did not implement reduction factors. Calculations with reduction factor were inconclusive. More testing is required to build on the results gathered for this report. It is noted, however, that the formulation for critical suction by Rodriguez and Barari [2020] proves to produce slightly better results for critical suction prediction due to the direct incorporation of the pore pressure ratio. Better results for required suction could be obtained after some parameter optimization, but more testing is required to build on the results gathered for this report.

That said, results from the experiments have promising implications. This gives rise to the possibility of designing buckets with thicker, stiffer tips and higher resistance to buckling at the tip without the need to increase the requirement for suction installation to reach target depth.

Further work: Since no conclusive result has been arrived at yet for the ¿p and ¿p coefficients, an appropriate solution for accounting for the effect of increasing tip thickness and increased penetration depth for the case study cannot be decisively given. Thus, there are still areas about the subject of this project that can yield results with interesting implications for the future of suction bucket installation design.

It is encouraged that further jacking tests are undertaken to investigate the inconclusive results observed. Though not yet proven, conclusive results from such work could open new possibilities for modular suction bucket design in which skirt wall could be composed of vertically stacked shells for ease of transportation and assembly. This possibility is just an idea raised in discussion with Tomas Sabaliauskas, but conclusive results are needed in this preliminary stage to serve as a foundation for building upon such possibilities.

Bibliography

Andersen, K. H., Jostad, H. P. and Dyvik, R. [2008], 'Penetration resistance of offshore skirted foundations and anchors in dense sand', *Journal of geotechnical and geoenvironmental engineering* 134(1), 106–116.

API [2000], 'Api recommended practice for planning, designing, and constructing fixed offshore platforms american petroleum institute'.

Blanco, M. I. [2009], 'The economics of wind energy', *Renewable and Sustainable Energy Reviews* 13(6), 1372–1382.
URL: *https://www.sciencedirect.com/science/article/pii/S1364032108001299*

Borup, M. and Hedegaard, J. [1995], 'Baskarp sand no. 15: data report 9403'.

Chen, F., Lian, J., Wang, H., Liu, F., Wang, H. and Zhao, Y. [2016], 'Large-scale experimental investigation of the installation of suction caissons in silt sand', *Applied Ocean Research* 60, 109–120.

Clausen, C., Aas, P. and Karlsrud, K. [2005], Bearing capacity of driven piles in sand, the ngi approach, 1st International Symposium Frontiers in Offshore Geotechnics: ISFOG.

DNV [1992], *DNV-1992 Classification Notes no 30.4. Foundations.*, february 1992 edn, DNV GL A/S.

Engineers, F. [2004], 'Axial pile capacity design method for offshore driven piles in sand', *Furgo Rep* .

Erbrich, C. and Tjelta, T. [1999], Installation of bucket foundations and suction caissons in sand-geotechnical performance, *in* 'Offshore technology conference'.

EWEA [2009], 'Oceans of opportunity. harnessing europe's largest domestic energy resource'. accessed: 11.02.2021.
URL: *http://www.ewea.org/fileadmin/files/library/publications/reports/Offshore$_R$eport$_2$009.pdf* 2009

Feld, T. [2001], 'Suction buckets: a new innovation foundation concept, applied to offshore wind turbines'.

Fugro Engineers, B. [2004], 'Axial pile capacity design method for offshore driven piles in sand', *Report P1003 presented to the American petroleum Institute* (3).

Houlsby, G., Ibsen, L. and Byrne, B. [2005], Suction caissons for wind turbines, *in* S. Gourvenec and M. Cassidy, eds, 'Frontiers in Offshore Geotechnics ISFOG 2005', Marcel Dekker, United States, pp. 75–93. null ; Conference date: 19-09-2005 Through 21-09-2005.

Houlsby, G. T. and Byrne, B. W. [2005], 'Design procedures for installation of suction caissons in sand', *Proceedings of the Institution of Civil Engineers-Geotechnical Engineering* 158(3), 135–144.

Ibsen, L. [2008], Implementation of a new foundations concept for offshore wind farms, *in* 'Proceedings Nordisk Geoteknikermøte nr. 15', Norsk Geoteknisk Forening, pp. 19–33. Keynote: NGM 2008; null ; Conference date: 03-09-2008 Through 06-09-2008.

Ibsen, L. B. and Thilsted, C. [2010], 'Numerical study of piping limits for suction installation of offshore skirted foundations an anchors in layered sand', *Frontiers in Offshore Geotechnics, II* pp. 421–426.

Ibsen, L., Hanson, M., Hjort, T. and Thaarup, M. [2009], *MC-Parameter Calibration of Baskarp Sand No. 15*, number 62 *in* 'DCE Technical reports', Department of Civil Engineering, Aalborg University, Denmark.

Jardine, R., Chow, F., Overy, R. and Standing, J. [2005], *ICP design methods for driven piles in sands and clays*, Vol. 112, Thomas Telford London.

Koteras, A. [2017], *Set-up and Test Procedure for Suction Installation and Uninstallation of Bucket Foundation*, number 63 *in* 'DCE Technical Memorandum', Department of Civil Engineering, Aalborg University, Denmark.

Koteras, A. [2019*a*], *Suction and jacking installation of bucket foundation models: laboratory manual*, number 74 *in* 'DCE Technical Memorandum', Department of Civil Engineering, Aalborg University, Denmark.

Koteras, A. and Ibsen, L. [2019], 'Medium-scale laboratory model of mono-bucket foundation for installation tests in sand', *Canadian Geotechnical Journal* 56(8), 1142–1153.

Koteras, A., Ibsen, L. and Clausen, J. [2016*a*], Seepage study for suction installation of bucket foundation in different soil combinations, *in* J. Chung and H. Wang, eds, 'The Proceedings of the Twenty-sixth (2016) International Ocean and Polar Engineering Conference', Vol. 2 of *Proceedings of the International Offshore and Polar Engineering Conference*, International Society of Offshore Polar Engineers, pp. 697–704. ISOPE: The 26th International Ocean and Polar Engineering Conference, ISOPE 2016 ; Conference date: 25-06-2016 Through 01-07-2016.

Koteras, A., Ibsen, L. and Clausen, J. [2016*b*], Seepage study for suction installation of bucket foundation in different soil combinations, *in* J. Chung and H. Wang, eds, 'The Proceedings of the Twenty-sixth (2016) International Ocean and Polar Engineering Conference', Vol. 2 of *Proceedings of the International Offshore and Polar Engineering Conference*, International Society of Offshore Polar Engineers, pp. 697–704. ISOPE: The 26th International Ocean and Polar Engineering Conference, ISOPE 2016 ; Conference date: 25-06-2016 Through 01-07-2016.

Koteras, A. K. [2019*b*], Jacking and suction installation of bucket foundation for offshore wind turbines, PhD thesis.

Koteras, A. K. and Ibsen, L. B. [2015], Investigation of seepage around the bucket skirt during installation in sand, Technical report, DCE Technical Memorandum.

Koteras, A. K. and Ibsen, L. B. [2018], Reduction in soil penetration resistance for suction-assisted installation of bucket foundation in sand, *in* 'International Conference on Physical Modelling in Geotechnics', CRC Press/Balkema, pp. 623–628.

Lehane, B., Schneider, J. and Xu, X. [2005], 'The uwa-05 method for prediction of axial capacity of driven piles in sand', *Frontiers in offshore geotechnics: ISFOG* pp. 683–689.

Lian, J., Chen, F. and Wang, H. [2014], ‘Laboratory tests on soil–skirt interaction and penetration resistance of suction caissons during installation in sand’, *Ocean Engineering* 84, 1–13.

Lunne, T., Powell, J. J. and Robertson, P. K. [1997], *Cone penetration testing in geotechnical practice*, CRC Press.

Material$_{m}odel_{m}anual$[2021], $PLAXISCONNECTEditionV21.01MaterialModelsManual, march2021edn$

Northland Power Inc. [2020], ‘Northland power provides an update on deutsche bucht offshore wind project’.
URL: *https://www.wind-energy-the-facts.org/development-and-investment-costs-of-offshore-wind-power.html*

Reference$_{m}anual$[2021], $PLAXISCONNECTEditionV21.01PLAXIS2D - ReferenceManual, march2021e$

Rodriguez, Lars Bo, K. A. and Barari, A. [2020], ‘Physical modeling-based investigation of the penetration resistance coefficients in cpt-based method for suction bucket foundations installation’, *Internal manuscript , Department of Civil Engineering, Aalborg University* .

Senders, M. and Randolph, M. [2009], ‘Cpt-based method for the installation of suction caissons in sand’, *Journal of Geotechnical and Geoenvironmental Engineering - J GEOTECH GEOENVIRON ENG* 135.

Sjelmo, A. [2012], ‘Soil-structure interaction in cohesionless soils due to monotonic loading’, *MSc. Student Report, Department of Civil Engineering, Aalborg University* .

Tjelta, T.-l. et al. [1994], Geotechnical aspects of bucket foundations replacing piles for the europipe 16/11-e jacket, *in* ‘Offshore technology conference’.

Tran, M. N., Airey, D. W., Randolph, M. F. et al. [2005], Study of seepage flow and sand plug loosening in installation of suction caissons in sand, *in* ‘The fifteenth international offshore and polar engineering conference’.

Tran, M. and Randolph, M. [2008], ‘Variation of suction pressure during caisson installation in sand’, *Geotechnique* 58(1), 1–11.

van der Sloot, M. [n.d.], ‘Incorrect interface pore pressures after groundwater flow’.
URL: *https://communities.bentley.com/products/geotech-analysis/w/plaxis-soilvision-wiki/45669/incorrect-interface-pore-pressures-after-groundwater-flow*

WindEurope [2020], ‘Offshore wind in europe: Key trends and statistics 2019’.
URL: *https://windeurope.org/wp-content/uploads/files/about-wind/statistics/WindEurope-Annual-Offshore-Statistics-2019.pdf*

Ørsted [2019], ‘Making green energy affordable’. accessed: 11.02.2021.
URL: *https://orsted.com/-/media/WWW/Docs/Corp/COM/explore/Making-green-energy-affordable-June-2019.pdf*

Part I

Appendix

Experimentation A

This section of the appendix provides details of the experimental method employed for suction bucket installation in the AAU geotechnical lab. It is also written in a manner so as to serve as a guide for carrying out experiments on the same set up and thus includes warnings about operations in the lab.

A.1 Introduction to lab experimentation

The sections that follow outline details for performing suction bucket installation in the lab. As the experiments involve working at height and with some heavy machinery, procedures and guidelines have been established with the aim of preventing injury to persons, reducing risk of damage to lab equipment and avoiding excessive delay in completing experiments within the given time frame. Thus, the experimenter is advised to observed the following whenever he/she starts working in the lab or performing the suction bucket installation experiment:

- Always use the provided protective gear (safety gloves, helmet, earmuffs, harness and boots) when starting work in the lab.
- Do not connect/disconnect any cable in the lab.
- Do not try to fix unresponsive/broken equipment by oneself. Ask for help from any of the lab technicians.
- Do not zero down stress transducers H0-H7 and pore pressure sensors P0-P7. They can only be calibrated when the sandbox is empty. Always ask before zeroing down any sensor parameter.
- Do not leave both the water supply settings and the vacuum settings activated simultaneously on the settings control panel.
- Always have a hand ready on an emergency stop button when a Test Run (CPT, suction/jacking installation) is in progress.
- Always turn off pressure supply for actuators off when leaving the lab.

With the above precautions in mind and other guidelines observed, experimenters can safely complete experiments with the set up:

The steps involved in completing the suction bucket installation in the lab can broadly be summarized into the following, and are elaborated on in the sections that follow:

- Set up preparation
- Test procedure and data acquisition

A.2 Set up preparation

Preparations for the experiment involved getting the sandbox, sand and bucket models ready for the Test run. In this section, further details are presented for the physical model used for the experiment, which has been briefly described in section 3.1 of the main report. Also, the experiment procedure is elaborated on in detail, and preparations carried out prior to Test runs are described in detail.

A.2.1 The sandbox, bucket model and sand preparation

.

The sandbox.

As noted in section 3.1, the experiment was performed in a sandbox,Figure A.1a, which is connected to auxiliary systems; a pressurized water/vacuum supply and drainage system, hydraulic actuators, pressure sensors and a hydraulic pump system.

The position of the sensors array located on the wall of the sandbox are as shown in Figure A.1b. The sandbox was filled with sand up to a height of 3 m for the series of tests performed for this project (an alternative height can be chosen if desired). With the sand filled to the desired height, preparation of the soil prior to Test run can be carried out .

(a) The sandbox (yellow box) used for testing

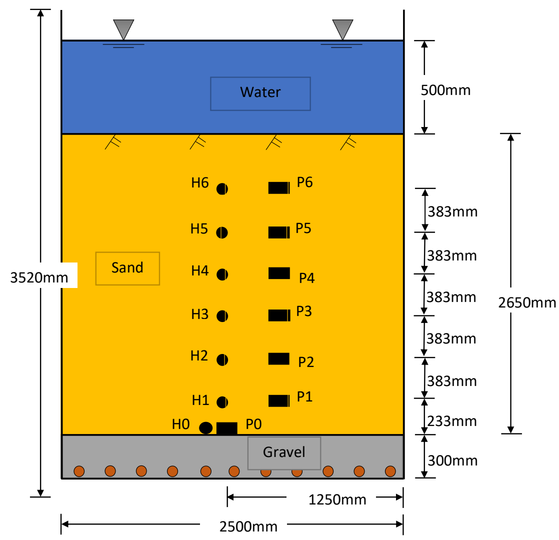

(b) Sensor array position on inner wall of sandbox

Figure A.1: The sandbox

Sand preparation:

. **Saturation and gradient application**

Sand in the sandbox was prepared before each test run as it was desired to have uniform soil characteristics through a horizontal section of the soil volume. Sand preparation commenced with saturating the soil volume by applying an upward hydraulic gradient through pipes at the base of the sandbox. This disturbs the soil volume and 'resets' it to a loose state. Areas on the surface of the soil volume showing signs of piping development during saturation were noted and given attention during the vibration stage.

Water for the saturation process is supplied by the pressurized water/vacuum supply system, which comprises overhead water tanks, vacuum tanks and a series of valves and connecting pipes. A gradient of 90 % is recommended [Koteras, 2019*a*], and is calculated from the existing head. This criterion is satisfied by applying the definition of a hydraulic gradient (ι) expressed as :

$$\iota = \frac{\Delta h}{H} \tag{A.1}$$

where :

ι	desired gradient; in this case 90 %	[-]
Δh	difference between desired head and existing head	[-]
H	height of dry soil volume / existing water head above soil volume surface	[m]

Then the pressure to be applied is given by:

$$\text{applied pressure} = (H + \Delta h) \cdot \gamma_w \quad \text{Or} \quad \text{applied pressure} = 1.9 \cdot H \cdot \gamma_w \tag{A.2}$$

Settings for the water/vacuum supply system is accessed through the settings panel and switches, Figure A.2, next to the data acquisition station. The settings panel regulates switching between access for the water supply system and vacuum system. It is advised that both systems should not be left activated simultaneously. The active setting is displayed on the screen of the panel, and it is advised to set 'Deoxygenation' for the water supply to 'Auto' mode most of the time unless access for the vacuum system is required, Figure A.3. Schematics for the connecting pipes and valves is provided next to the switches for guidance; switches 4 and 5 are used for accessing vacuum when carrying out suction installation.

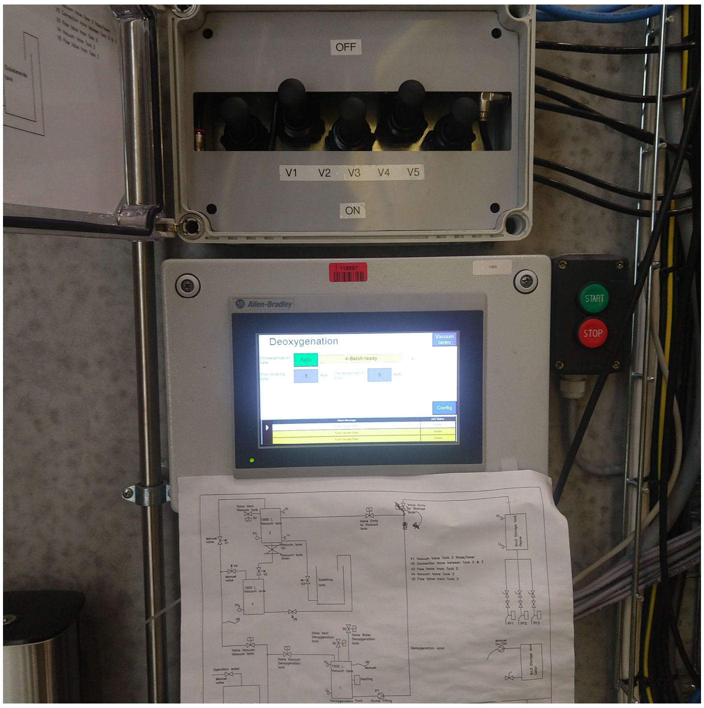

Figure A.2: Vacuum system settings panel

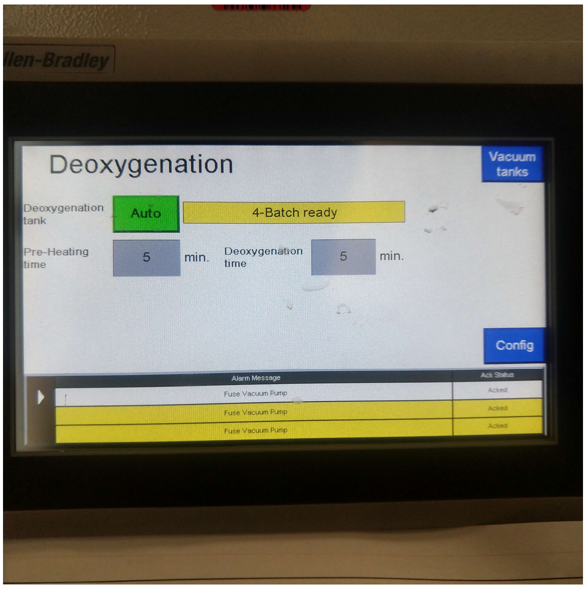

(a) Settings for controlling water access

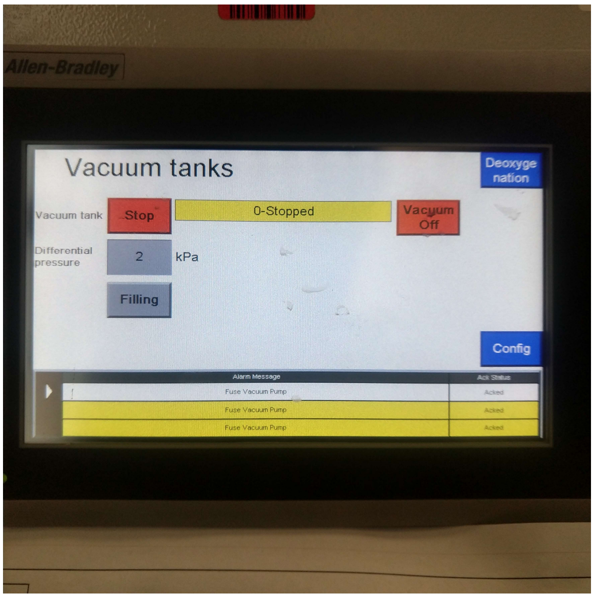

(b) Settings for controlling vacuum access

Figure A.3: Settings window for controlling water and vacuum system

Access valves for controlling water flow into/out of are connected to the sandbox at its base, as shown in Figure A.4, with labels describing the function of each value.

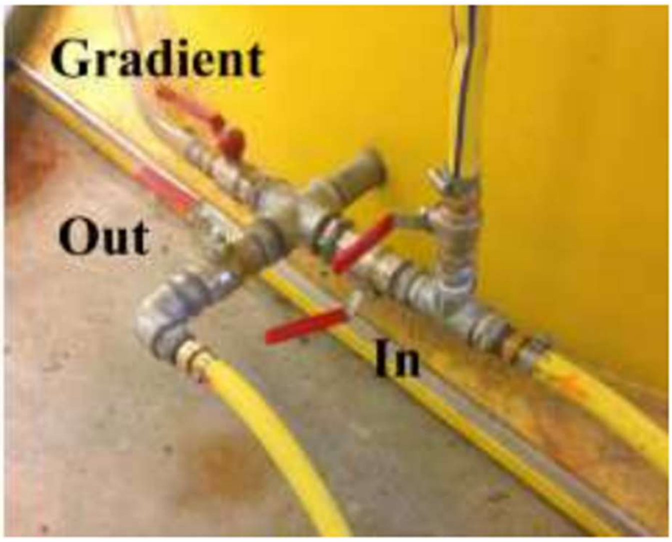

Figure A.4: Valvues for controlling flow of water in/out of the sandbox. Koteras [2017]

Compaction by vibration

With the water level approximately 20 cm above the soil surface, the gradient was cut off and vibration of the soil volume followed. A wooden platform, Figure A.5a, was placed on beams across the top of the sandbox to form a working platform for vibration. When placed on the beams, the platform was checked to ensure that no holes were blocked by the beam beneath as the holes serve as a template for vibration of the soil volume. Vibration was performed by attaching a 3 m long vibrator device to the overhead crane and vibrating every second hole, Figure A.5b. It is important to avoid vibrating too close to the section of side wall where the stress and pore pressure sensors are attached to the sandbox. Depending on the soil density desired, a second or third pass of the vibration can be repeated by vibrating the holes that were skipped during the previous pass (Figure A.5b). Increasing resistance to penetration of the vibrator at depth upon repeated passes serves as an indicator of soil densification. When vibration was completed, the set up was left overnight to allow settlement of the soil volume.

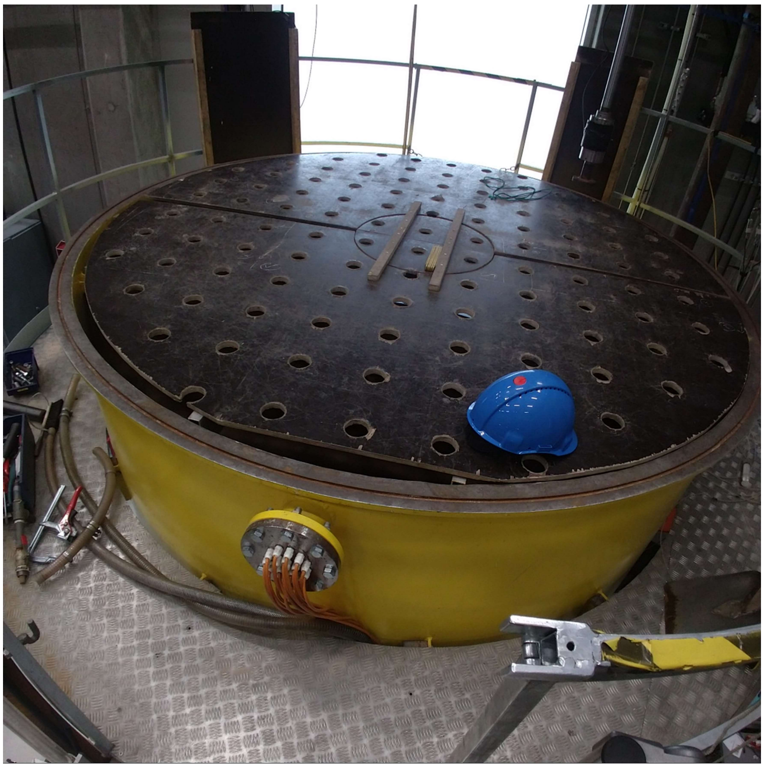

(a) Working platform used as guide for performing compaction of soil volume.

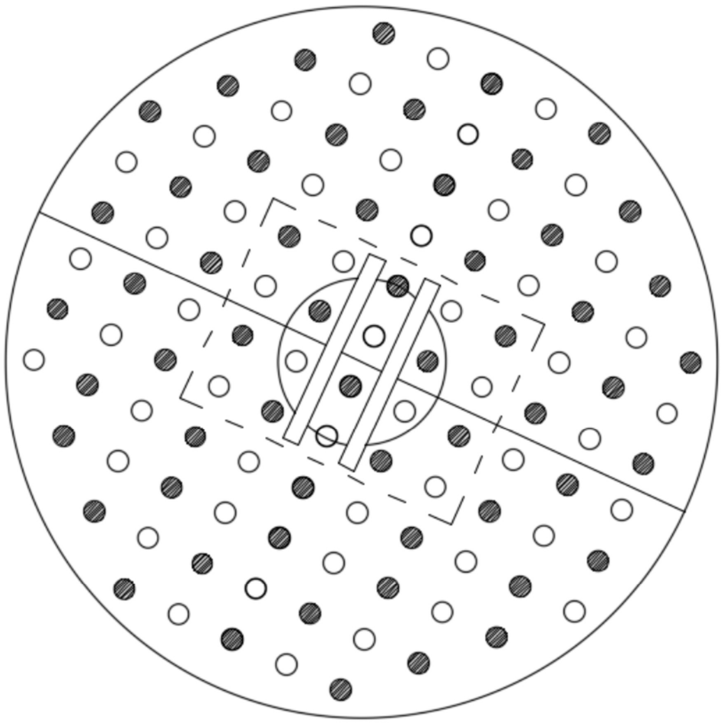

(b) Schematic for order of inserting of vibrator for compaction of soil volume: 1st pass dark holes; next pass blank holes.

Figure A.5: Perforated wooden frame that forms a working platform for performing compaction with the vibrator

A.3 Test procedure and data acquisition

Tests for the suction bucket installation were carried out in the following steps:

1. **CPT before installation:** A 2 m long mini-CPT device was attached to the actuator (the smaller of the two hydraulic actuators fixed to the loading frame) and moved into position for CPT testing. The position for CPT testing are marked on the adjustable frame for moving the actuators over the working platform. Once in position, the actuator was clamped to the loading frame together with the CPT device. The distances between the soil surface and CPT tip were noted prior to each CPT test run. A stabilizing device, Figure A.6, was positioned in place to help prevent bending of the CPT when performing CPT in dense soil. CPT is performed as a displacement-controlled procedure and is controlled using the MTS station manager and data acquistion system. Data from CPT before testing was analyzed to check for the general uniformity across the soil volume. CPT before installation was performed for 4 different locations along the centre line of the sandbox.

2. **Filling the sandbox with water:** After CPT was completed, the water level in the sandbox was increased up to a level approximately 50 mm from the tip of sandbox. This was done to ensure that there was enough water to saturate the pore pressures channels on the skirt of the bucket prior to installation. Filling of the sandbox was carried out by letting in water from a hose located above the loading frame. Water was filled into the sandbox from the surface to ensure that the soil volume is not disturbed by a gradient from the bottom which would otherwise alter the properties of the sand and void parameter derivation for measurements taken from CPT before installation. A metal plate was placed on the surface of the sand next to the side wall of the sandbox and away from the centreline along which CPT measures were recorded.

3. **Assembling the bucket for testing:** The suction bucket model was lifted into position onto the wooden frame using the overhead crane and then attached connected to the actuator piston. Tubes connected to pore pressure transducers on the working platform were connected to the respective channels on the suction bucket for measuring pore pressure values. Also, suction hose were connected to the respective valves on the lid of the bucket. These are as shown in Figure A.7.

4. **Saturation of pore pressure transducers:** The vibration platform was removed and the bucket lowered down slowly into the water to a level approximately 5 cm above the soil surface. The pore pressure transducers were then saturated by passing water through the tubes connecting the pore pressure transducer to the pore pressure channels until the tubes were fully filled with water. This measure also ensures that any blocked channels are identified and remedial measures can be taken to ensure the channels are clear and in a good state for recording pore pressure readings.

5. **Installation test:** The prepared bucket was gently lowered unto the surface of the soil. Testing was controlled and monitored using visual observation from the working platform and also from the MTS station. A self weight installation was first carried out, with ventilation valves (Figure A.7) located on the bucket lid kept opened. The self weight installation was observed to be completed when no further displacement was observed from the measuring station. At this point, the actuator piston was disconnected so an extension

piece could be connected. The extension piece attached to the actuator piston ensures that installation proceeds to the target depth without being limited by the limit of range of motion of the actuator piston. In the case of suction installation, the ventilation valves closed and the suction pumps were then started to proceed with the suction installation process. In the case of jacking installation, the ventilation valves were kept opened and a jacking force was applied to start the process of installation. Installation was monitored and controlled from the measuring station which serves as the data acquisition system.

6. **CPT after installation:** At the end of installation, the water level in the sandbox was lowered to approximately 20 cm above the sand surface. A second CPT test was performed to record changes in the soil volume resulting from the effect of the installation process on the soil. These were carried out are for 4 locations inside the bucket and 4 locations outside the bucket to take note of any differences between the soil outside the suction bucket and soil trapped within the suction bucket. An extension piece for CPT attachment (Figure A.6) was used to help position the CPT through the valve holes (Figure A.8a) in the lid of the bucket.

7. **Uninstallation:** The bucket was then uninstalled from the soil by pulling out from the sand using the actuator Figure A.8b. Water was once more passed through the tubes connected to the pore pressure channels on the bucket. This action ensures that the channels get cleared of any sand lodged in the channels and reduces the risk of blocked channels prior to the next test run.

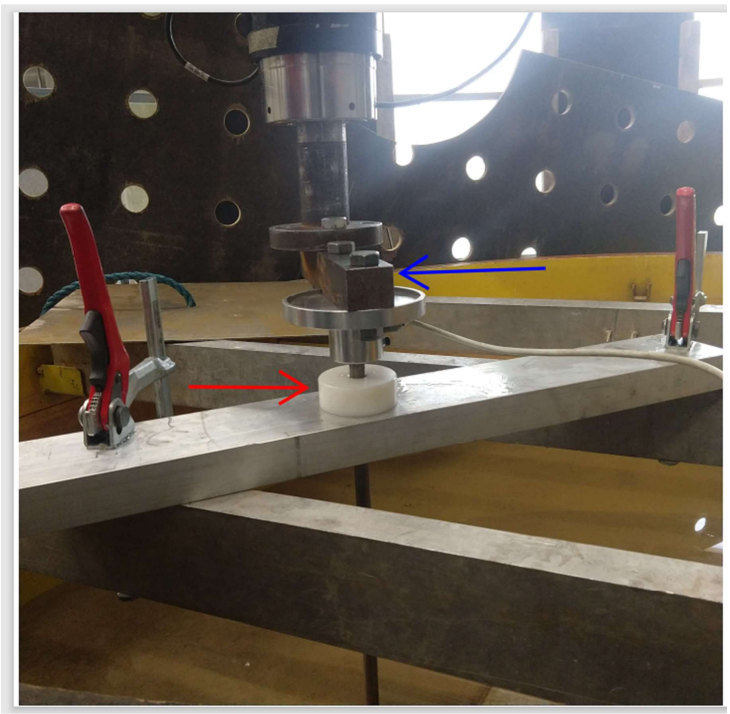

Figure A.6: CPT extension piece (blue arrow) and stabilizer (red arrow)

(a) Bucket used for the experiments. Arrows in red pointing to the location of pore pressure measuring channels PP1-PP3 located on the outside on the bucket.

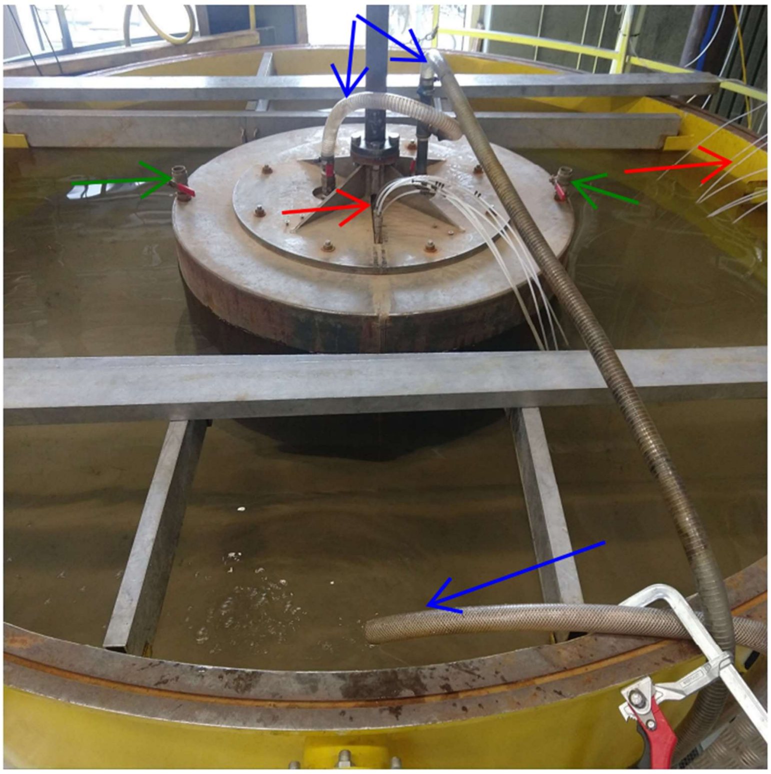

(b) Fixtures to the bucket prior to for testing: blue arrows indicate the suction hoses for drawing water from within the inner bucket compartment and filling back into the tank; red arrows indicating the tubes connecting the pore pressure measuring valves to the pore pressure transducers fixed on the working platform; green arrows indicate the ventilation valves.

Figure A.7: Positioning the bucket on the working platform and connecting fixtures prior to testing.

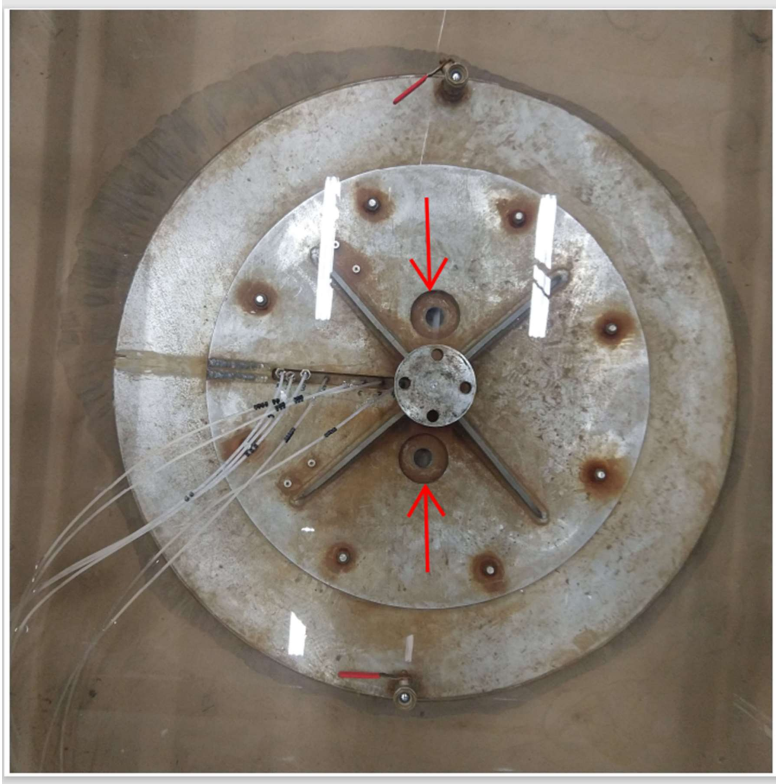

(a) Bucket after installation with scouring around the edges. Red arrows indicate valve holes for CPT inside installed bucket.

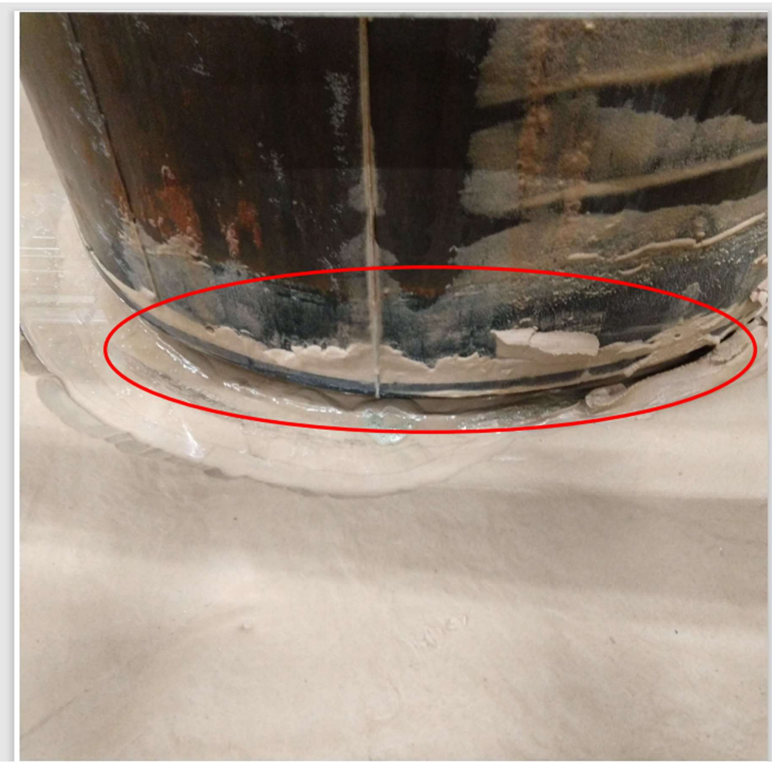

(b) Fully uninstalled bucket with sand attached to thickened edge.

Figure A.8: Positioning the bucket on the working platform and connecting fixtures prior to testing.

A.4 CPT interpretation: MC-paramter derivation from lab mini-CPT

A.5 CPT interpretation: MC-parameter derivation from lab mini-CPT

The following expressions, developed based on previous experiment on Aalborg University Sand No. 1 for parameters for the Mohr Coulomb constitutive model, were used for parameter derivation from CPT data. The parameters were developed on the basis of dependency on confining pressure and density index, using a combination of results for CPT's and drained triaxial tests. Reference for the information presented are taken from Ibsen et al. [2009].

The density index was determined from measured cone resistance from CPT data using the relation:

$$I_d = 5.14 \left(\frac{\sigma'_{\nu o}}{q_c^{0.75}} \right)^{0.42} \tag{A.3}$$

where:

$\sigma'_{\nu o}$	vertical effective stress	$[MPa]$
q_c	cone resistance	$[MPa]$

For the strength parameters, friction angle, dilation angle and cohesion, the secant friction angle and tangent friction angle were both determined using the modified Schmertmann expression for secant friction angle, (A.4) and the Linear Coulomb Criterion expression for tangent friction angle and cohesion, (A.5)-(A.6) were selected for use as given by:

$$I_d = 5.14 \left(\frac{\sigma'_{\nu o}}{q_c^{0.75}} \right)^{0.42} \qquad [^\circ] \tag{A.4}$$

$$\phi_t = 0.11 \cdot I_d + 32.3 \qquad [^\circ] \tag{A.5}$$

$$c' = 0.032 \cdot I_d + 3.25 \qquad [kPa] \tag{A.6}$$

The dilatancy angle as a function of both the friction (Schmertmann) and the density index. It is noted, the the given expression tends towards infinity for very small confining pressures.

$$\psi = 0.195 \cdot I_d + 14.9 \cdot (\sigma'_3)^{-0.0976} - 9.95 \tag{A.7}$$

where:

ψ	dilatancy angle	$[^\circ]$
σ'_3	confining pressure	$[kPa]$

The elastic parameters, Young's modulus and Poisson's ratio, are given as :

$$E_{50} = E_{50}^{ref} \cdot \left(\frac{c \cdot cos(\phi_t) \; + \; sigma'_3 \cdot sin(\phi_t)}{c \cdot cos(\phi_t) \; + \; sigma'^{ref}_3 \cdot sin(\phi_t)} \right)^m \tag{A.8}$$

where:

ϕ_t	tangent friction angle	$[°]$
σ'_3	confining pressure	$[kPa]$
$\sigma'^{\,ref}_3$	reference confining pressure (100kPa)	$[kPa]$
m	amount of stress dependency	$[-]$
E_{50}^{ref}	reference secant modulus corresponding to p_{ref}	$[-kPa]$

E_{50}^{ref} is expressed as :

$$E_{50}^{ref} = 0.06322 \cdot I_d^{2.507} \; + \; 10920 \qquad [kPa] \tag{A.9}$$

Test run results B

B.1 Test run results

CPT data before and after installation, and data for bucket installation are presented in Figure B.1 - Figure 5.5a.

Results for derived geotechnical parameters obtained from CPT before installation are also presented in Table B.1, with the results obtained from CPT after installation presented in Table B.2 and maximum load-displacements observed are presented in Table B.3.

Suction installation Test run 1:

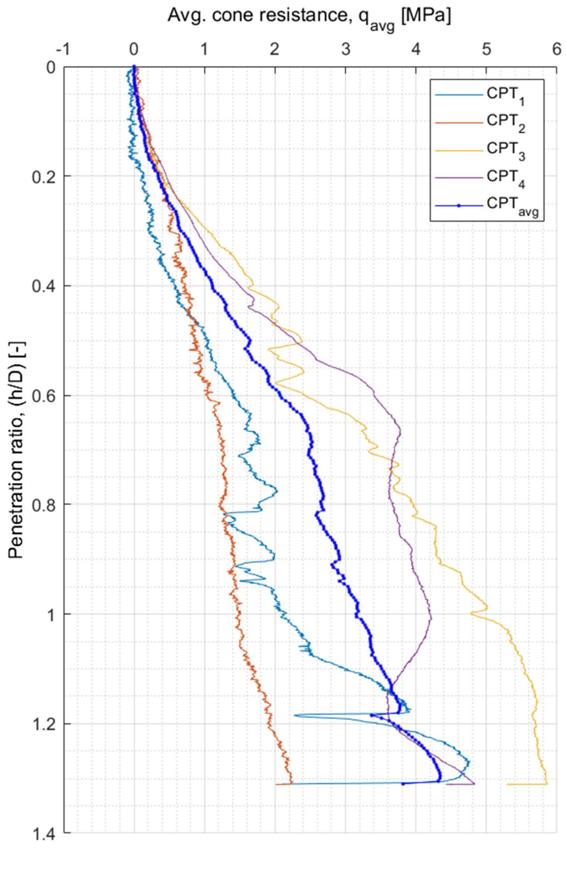

(a) Test run 1: CPT before installation data

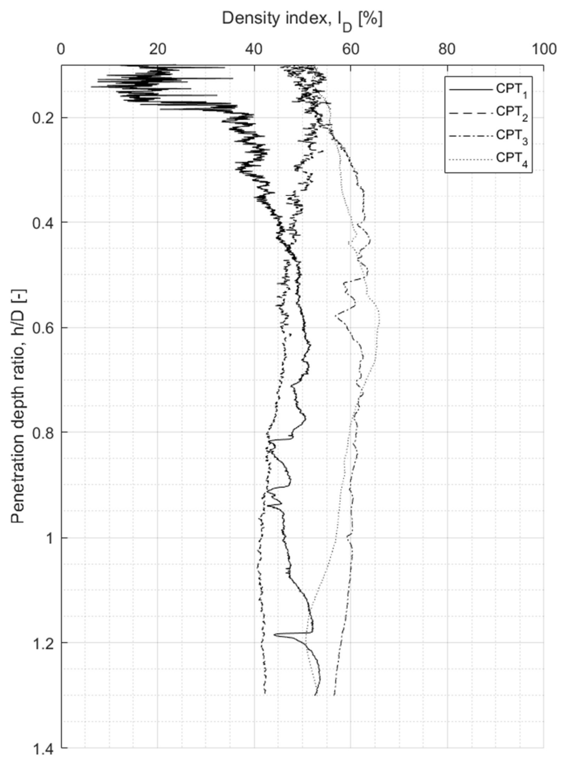

(b) Density index for Test run 1: CPT before installation data

Figure B.1: (a) CPT before installation and (b) Density index based on CPT data

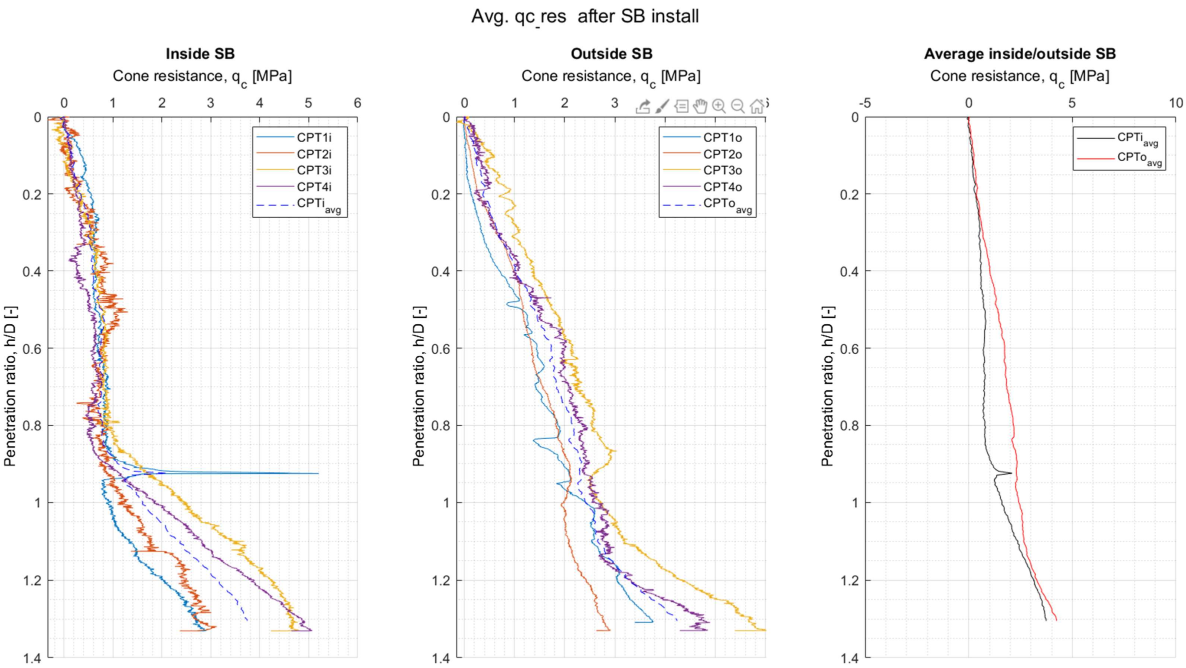

Figure B.2: Test run 1: CPT after installation data

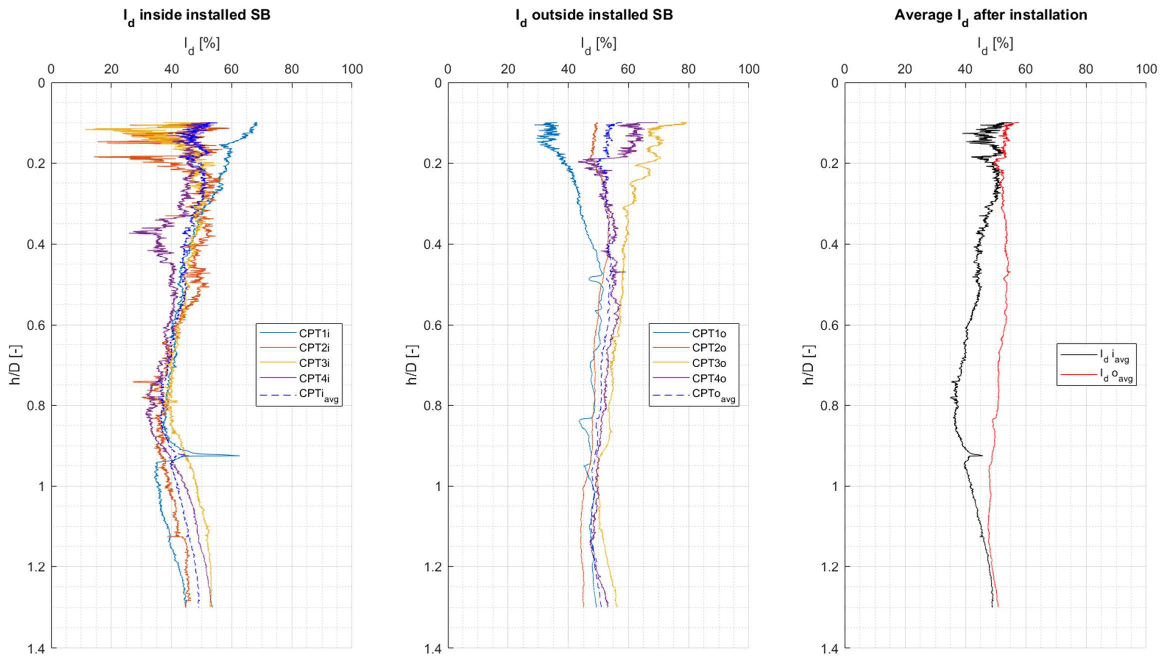

Figure B.3: Density index for Test run 1: CPT after installation data

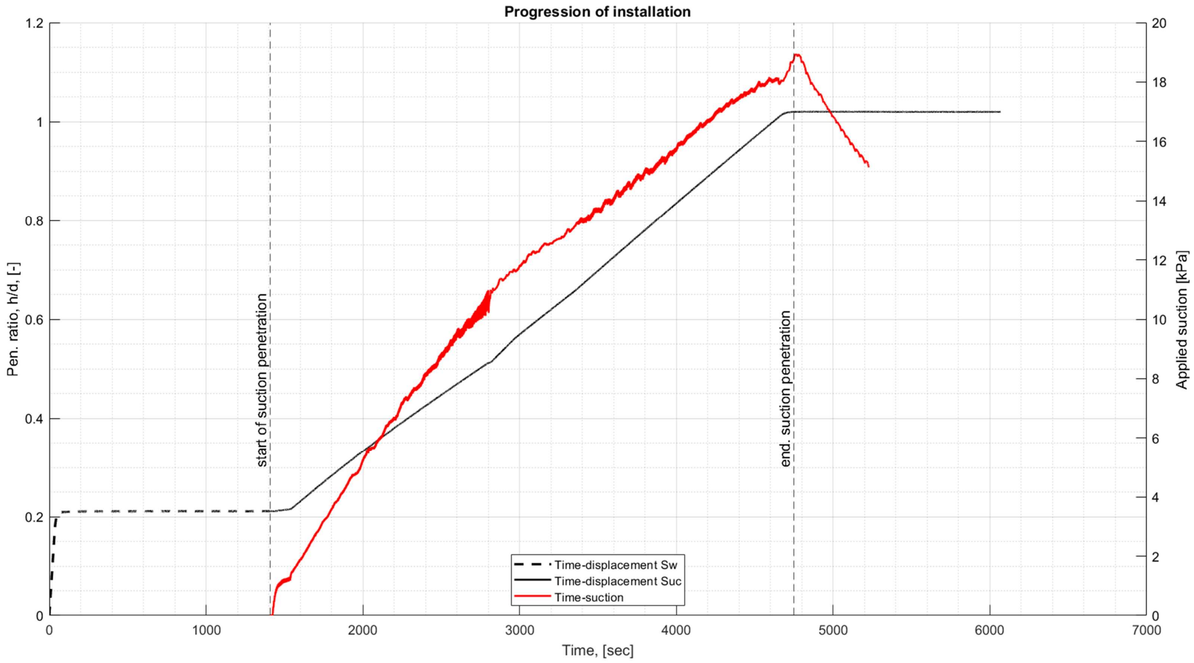

Figure B.4: Progress of suction installation for test run 1

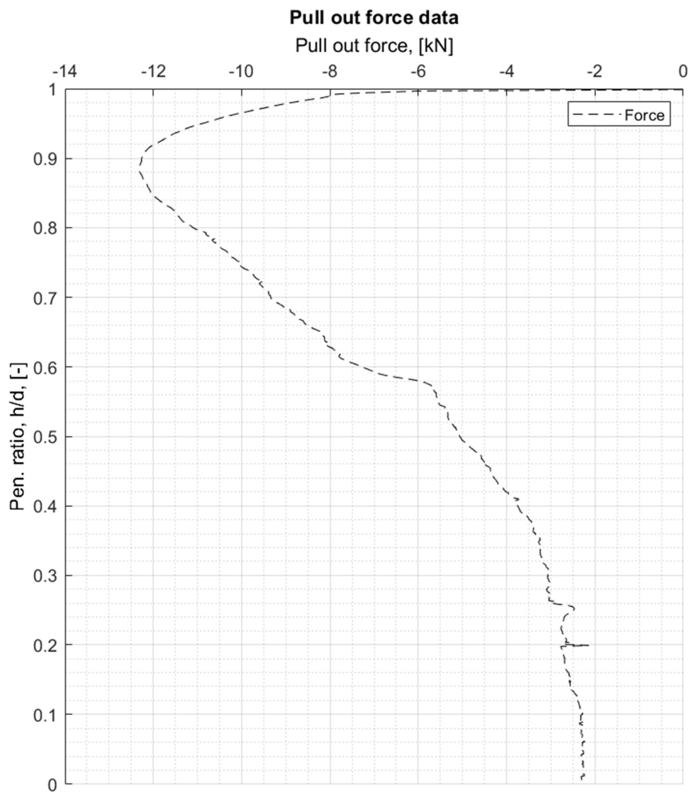

Figure B.5: Progress of uninstallation by pull out for test run 1

Suction installation Test run 2:

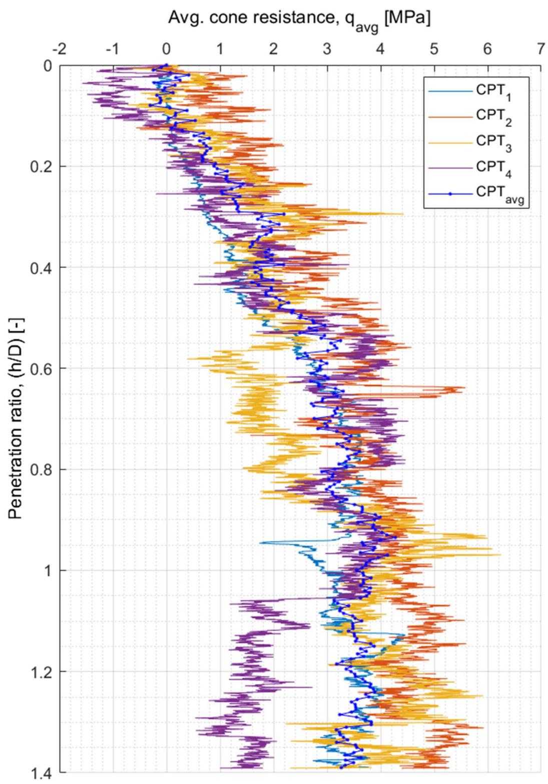

(a) Test run 2: CPT before installation data

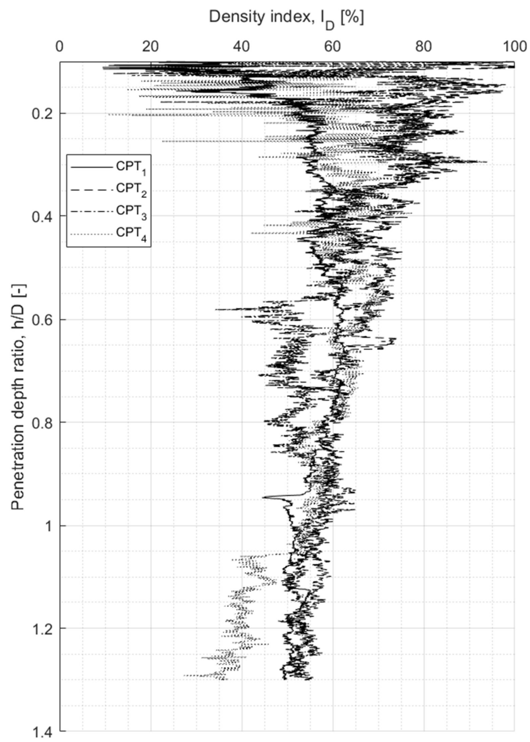

(b) Density index for Test run 2: CPT before installation data

Figure B.6: (a) CPT before installation and (b) Density index based on CPT data

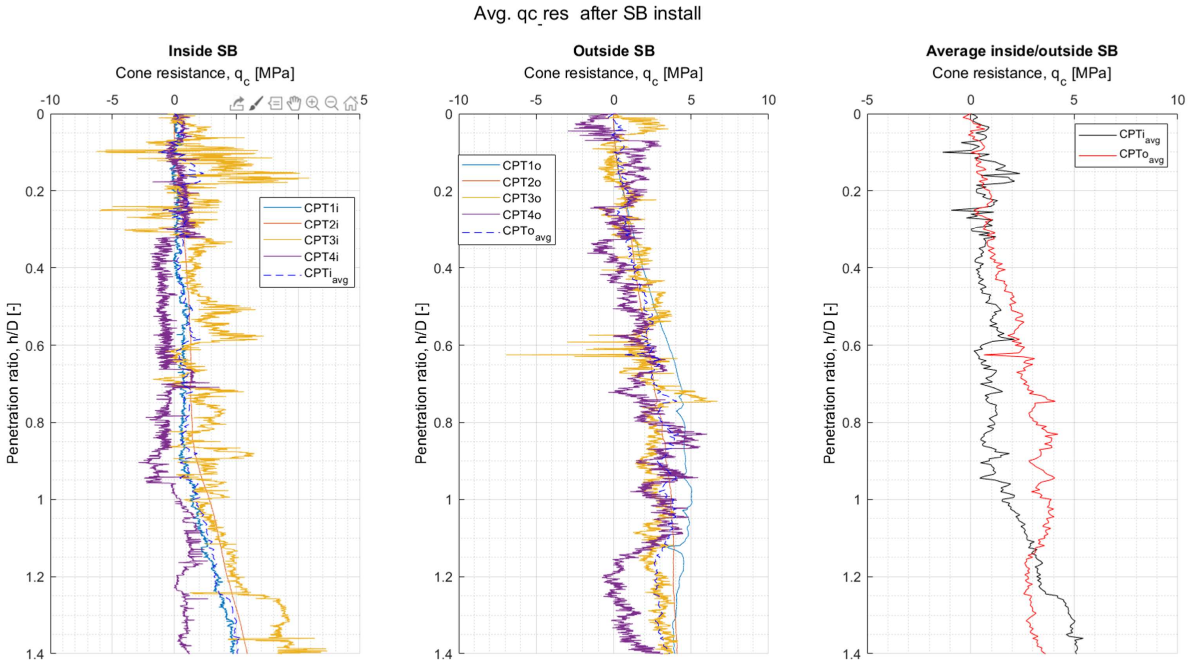

Figure B.7: Test run 2: CPT after installation data

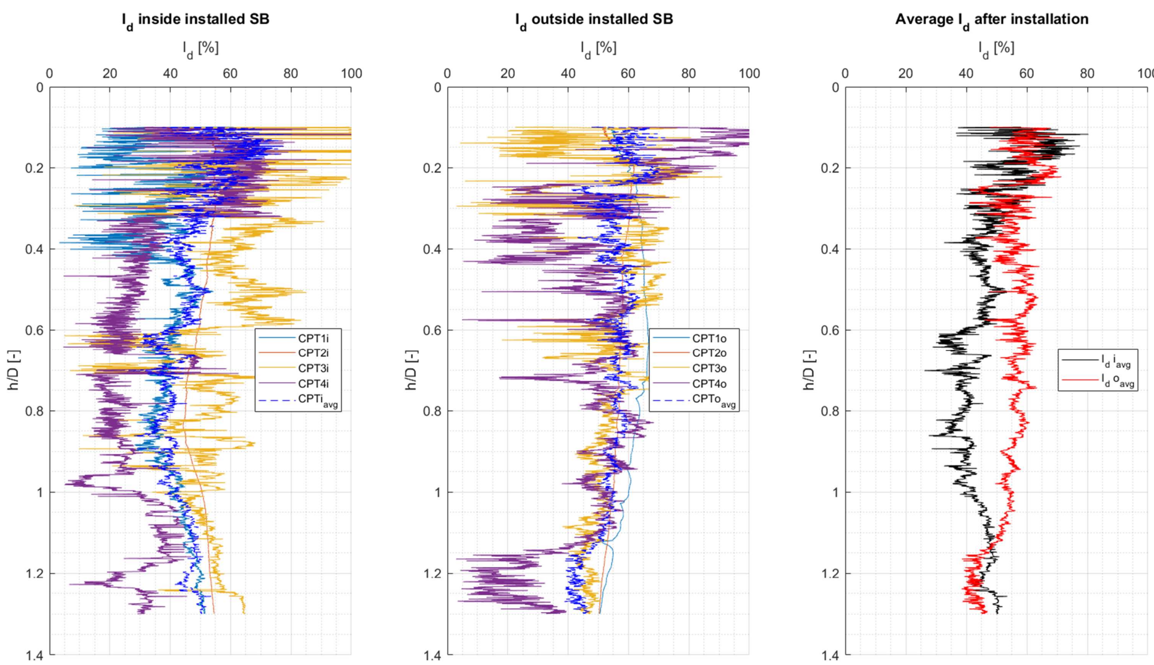

Figure B.8: Density index for Test run 2: CPT after installation data

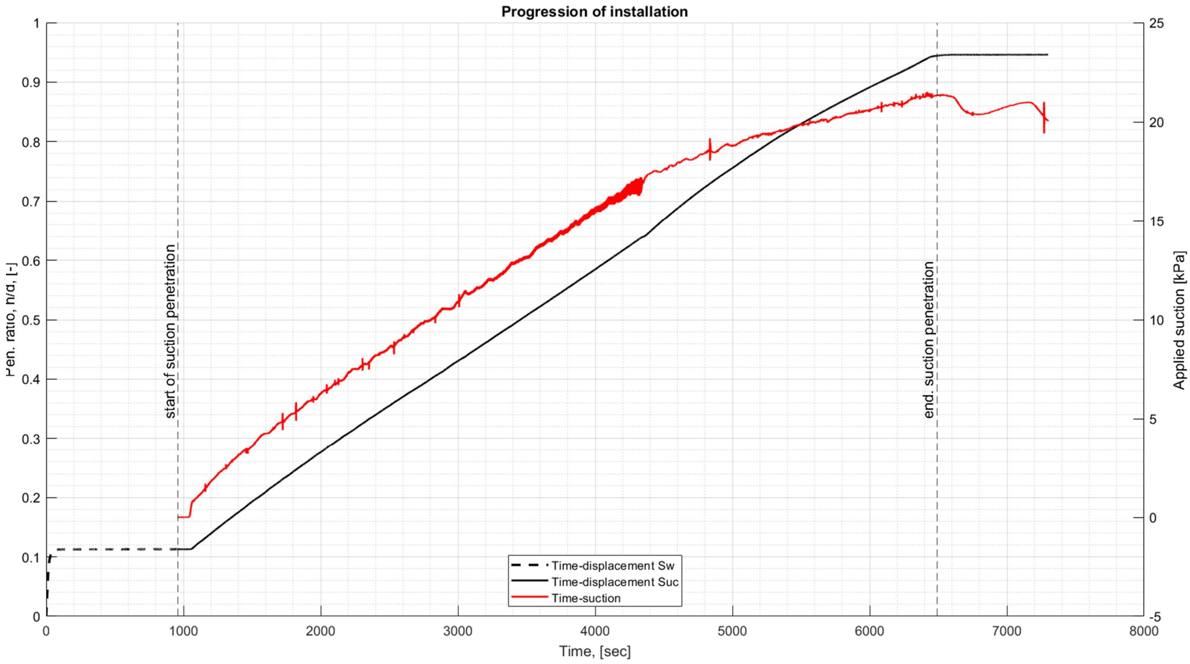

Figure B.9: Progress of suction installation for test run 2

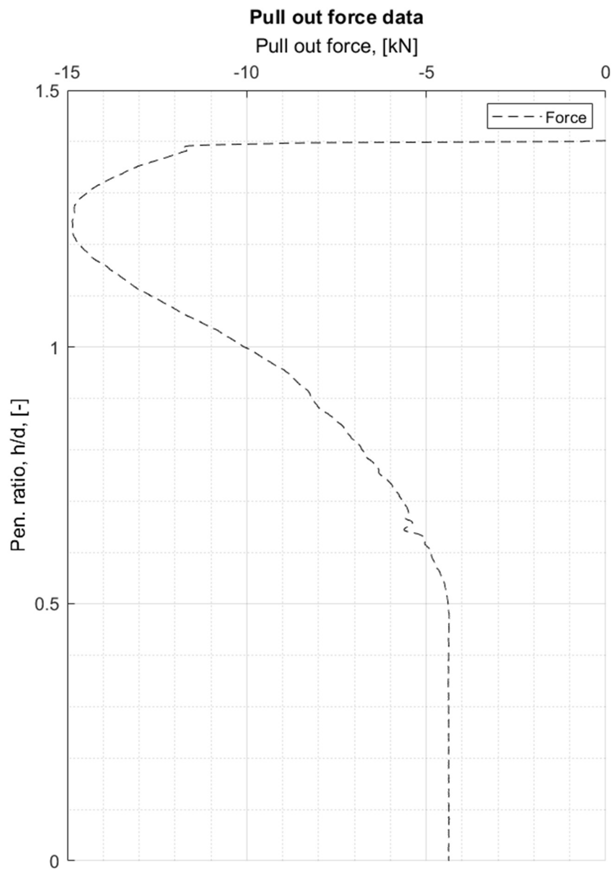

Figure B.10: Progress of uninstallation by pull out for test run 2

Suction installation Test run 4:

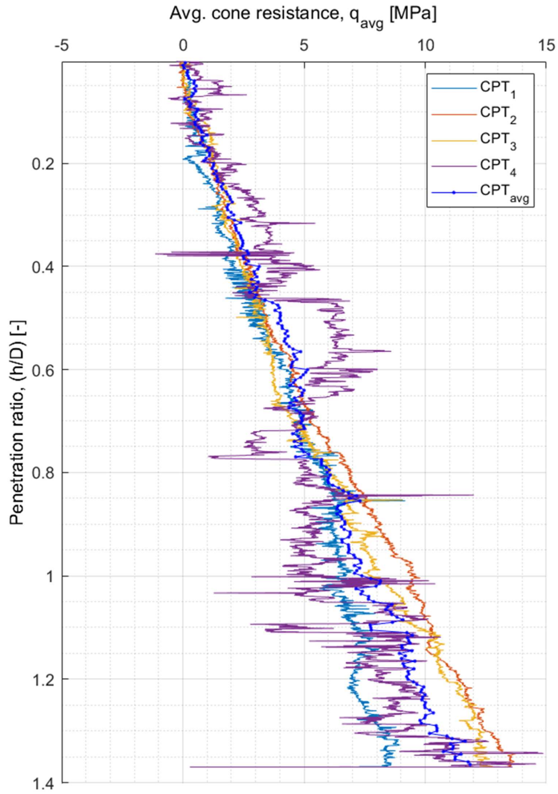

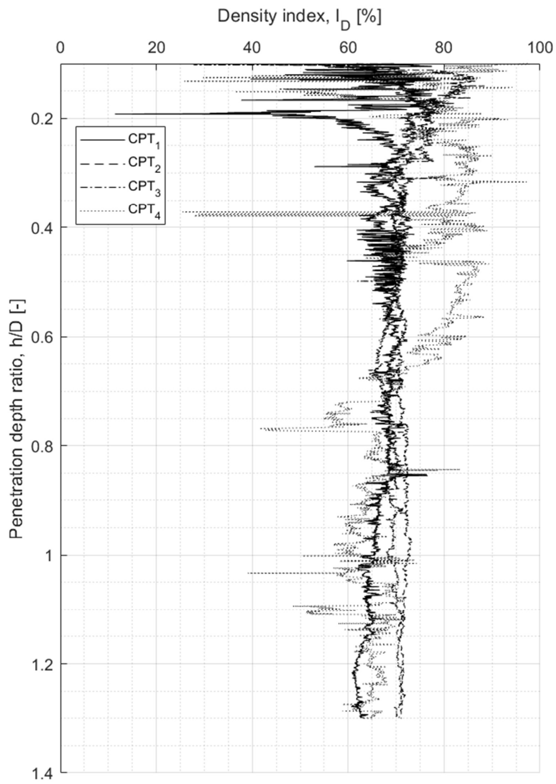

(a) Test run 4: CPT before installation data

(b) Density index for Test run 4: CPT before installation data

Figure B.11: (a) CPT before installation and (b) Density index based on CPT data

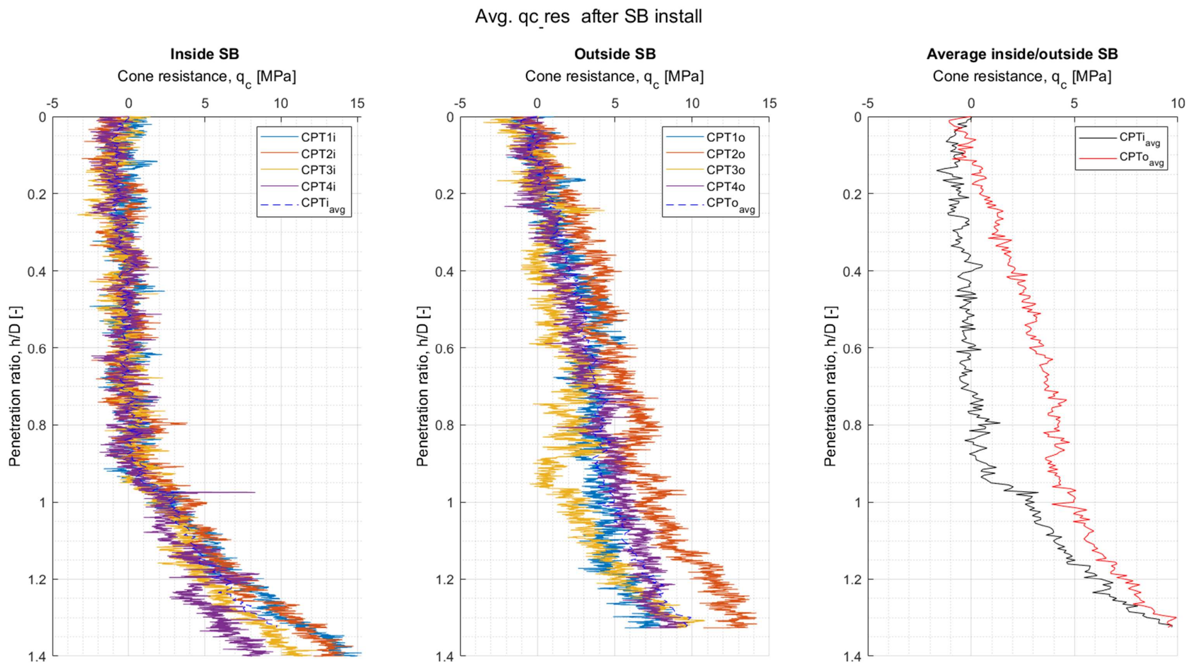

Figure B.12: Test run 4: CPT after installation data

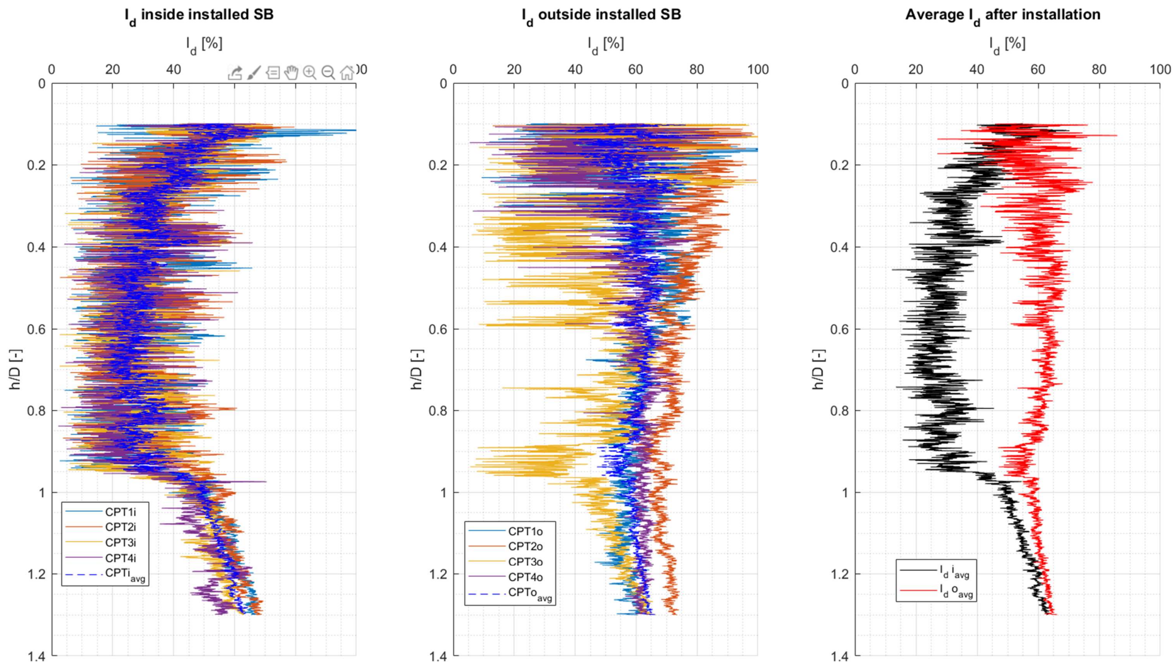

Figure B.13: Density index for Test run 4: CPT after installation data

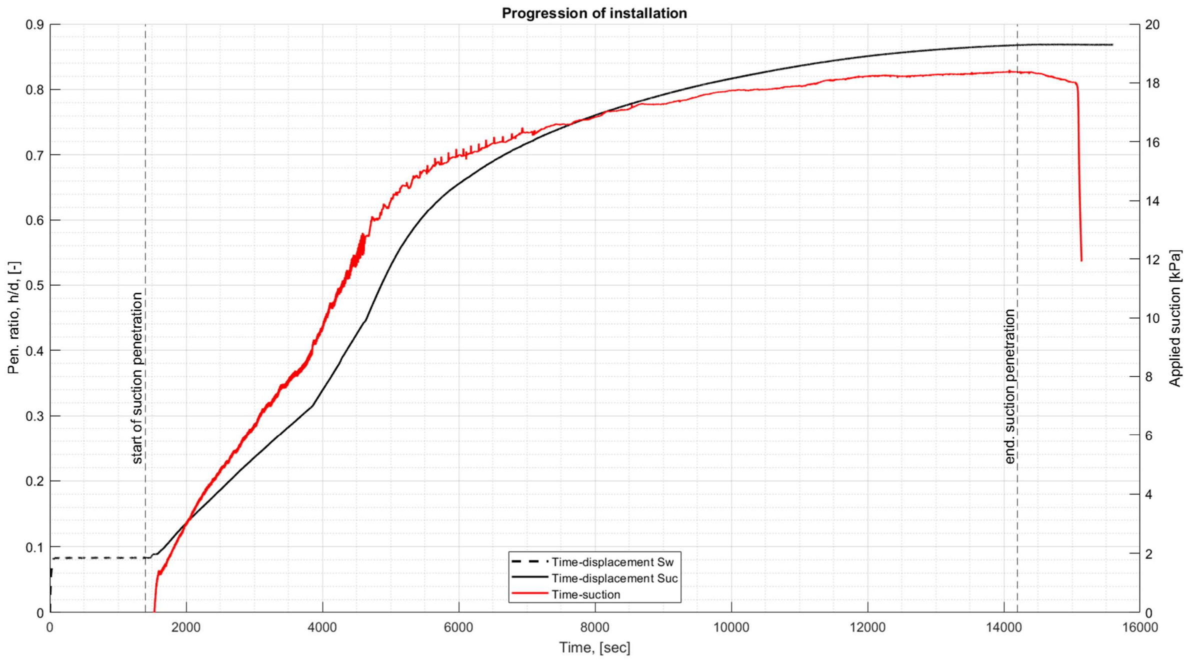

Figure B.14: Progress of suction installation for test run 4

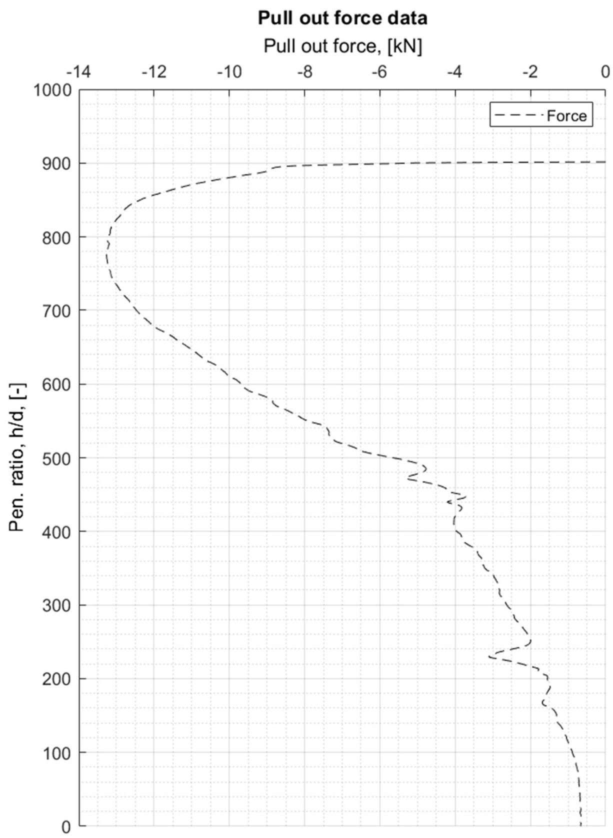

Figure B.15: Progress of uninstallation by pull out for test run 4

Suction installation Test run 5:

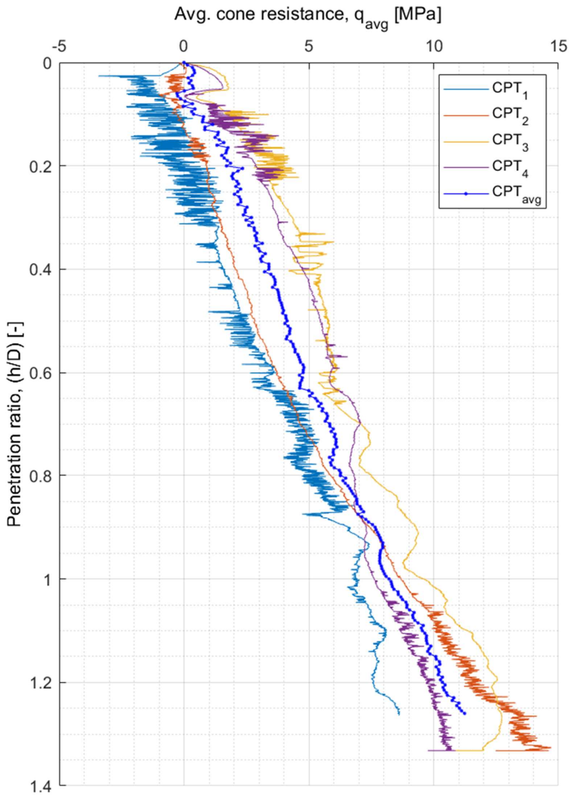

(a) Test run 5: CPT before installation data

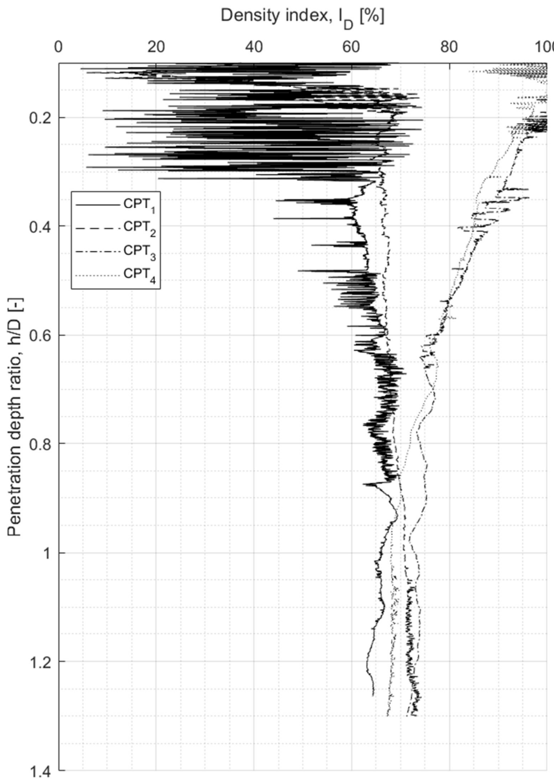

(b) Density index for Test run 5: CPT before installation data

Figure B.16: (a) CPT before installation and (b) Density index based on CPT data

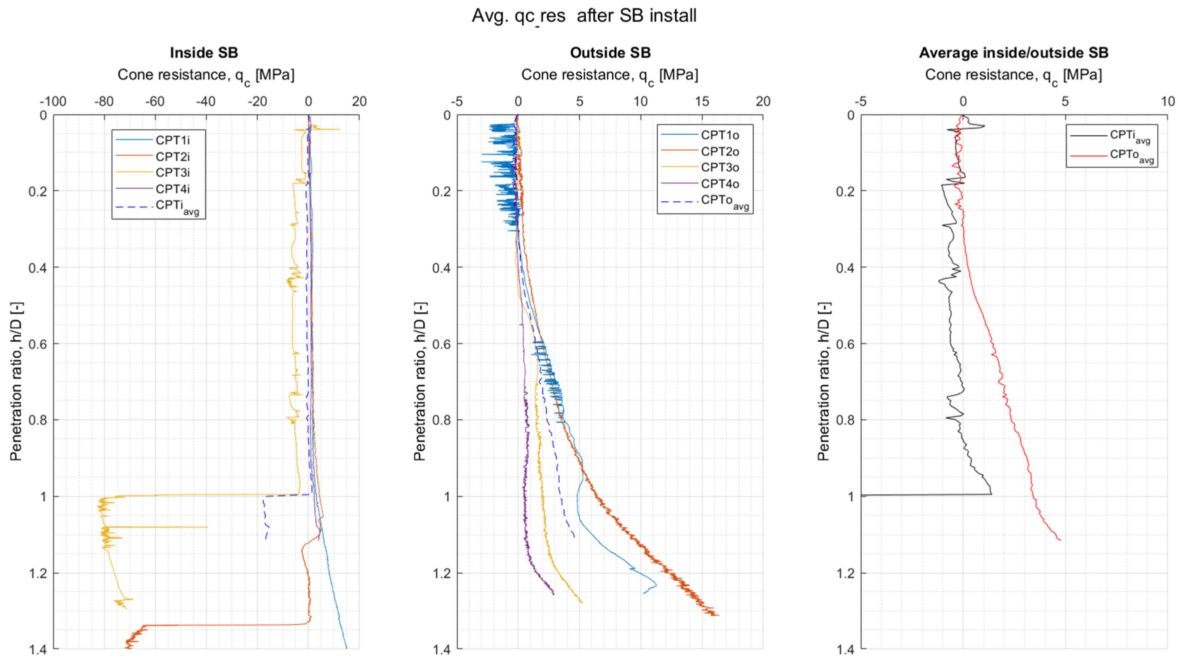

Figure B.17: Test run 5: CPT after installation data

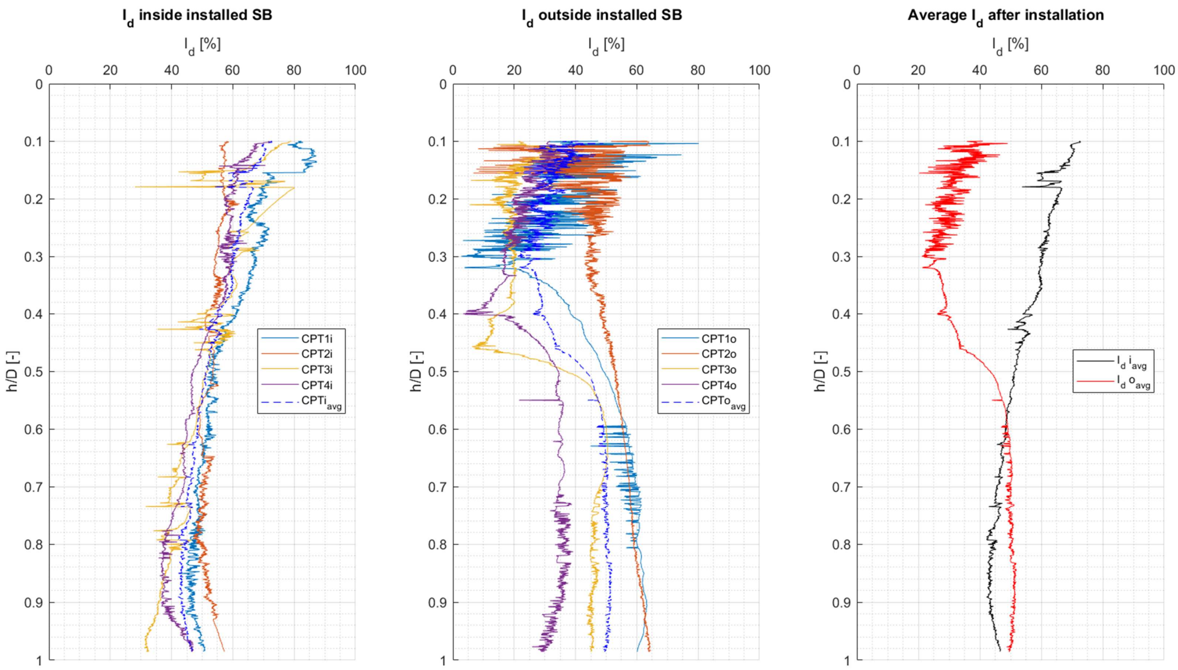

Figure B.18: Density index for Test run 5: CPT after installation data

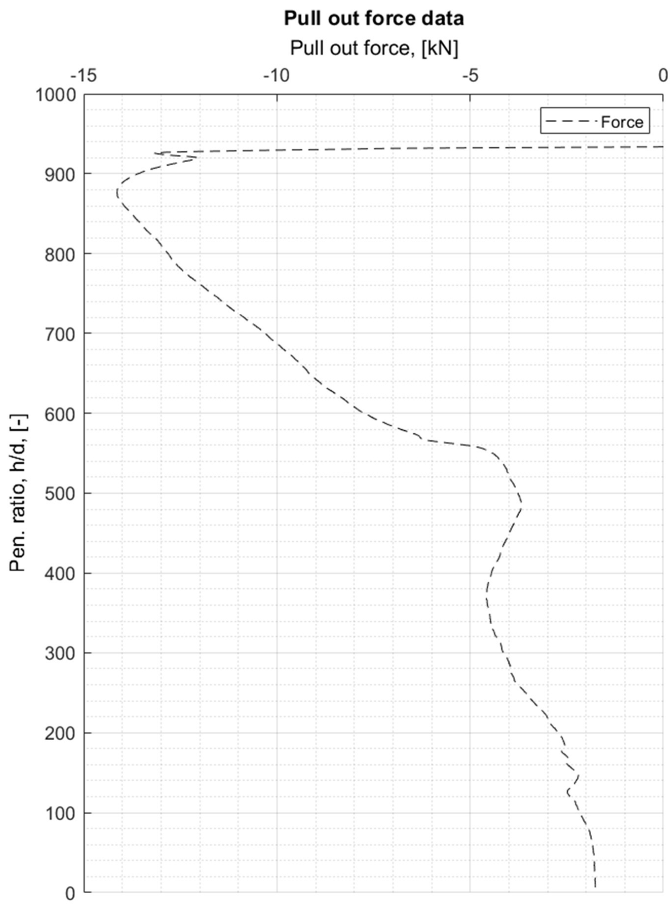

Figure B.19: Progress of uninstallation by pull out for test run 5

Suction installation Test run 6:

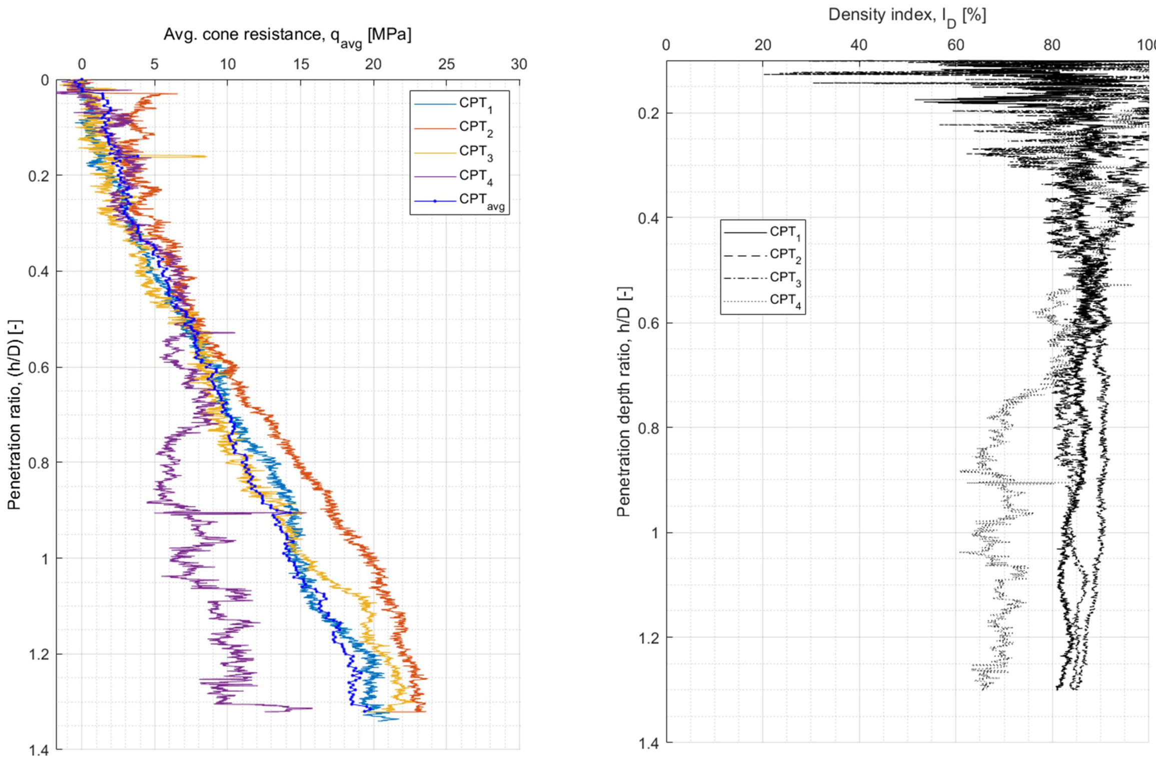

(a) Test run 6: CPT before installation data

(b) Density index for Test run 6: CPT before installation data

Figure B.20: (a) CPT before installation and (b) Density index based on CPT data

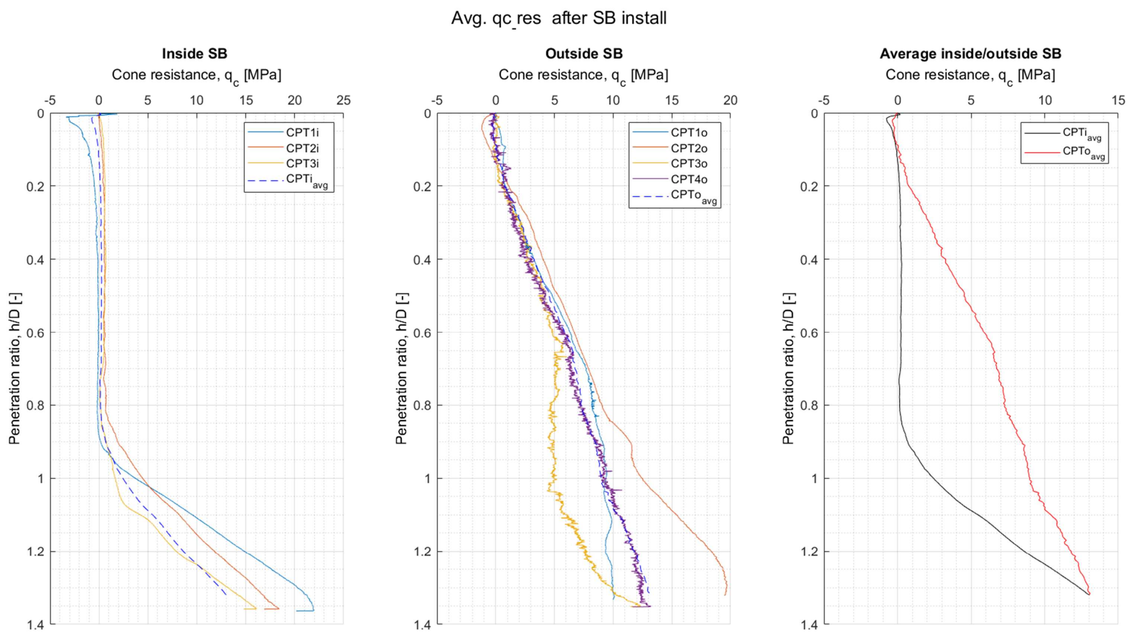

Figure B.21: Test run 6: CPT after installation data

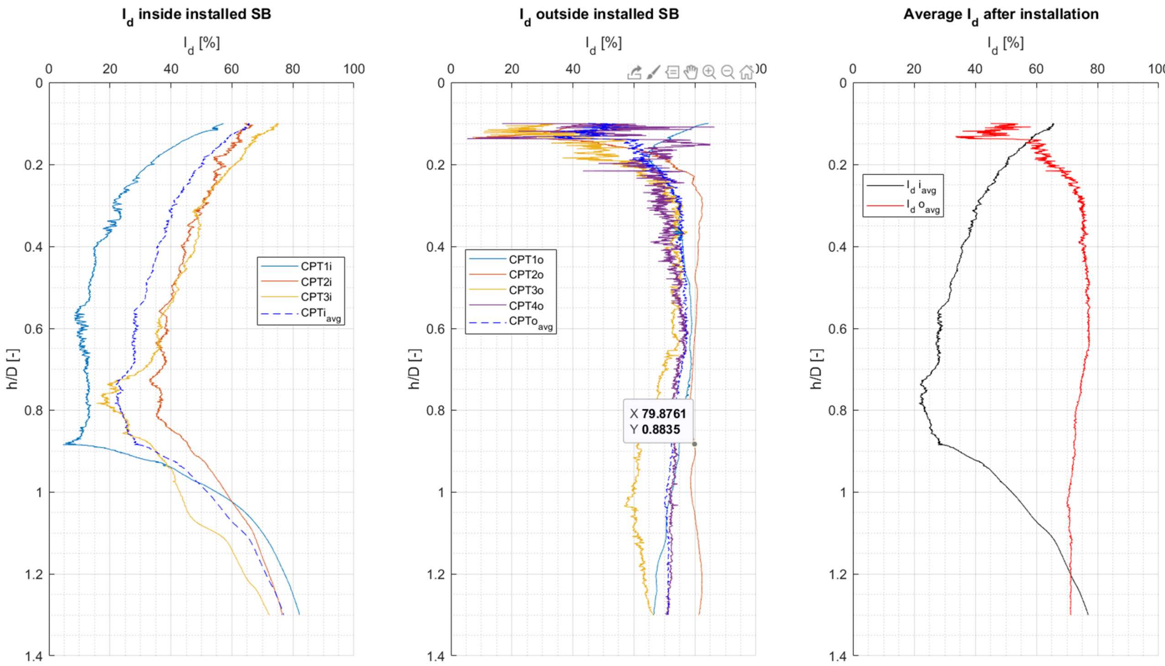

Figure B.22: Density index for Test run 6: CPT after installation data

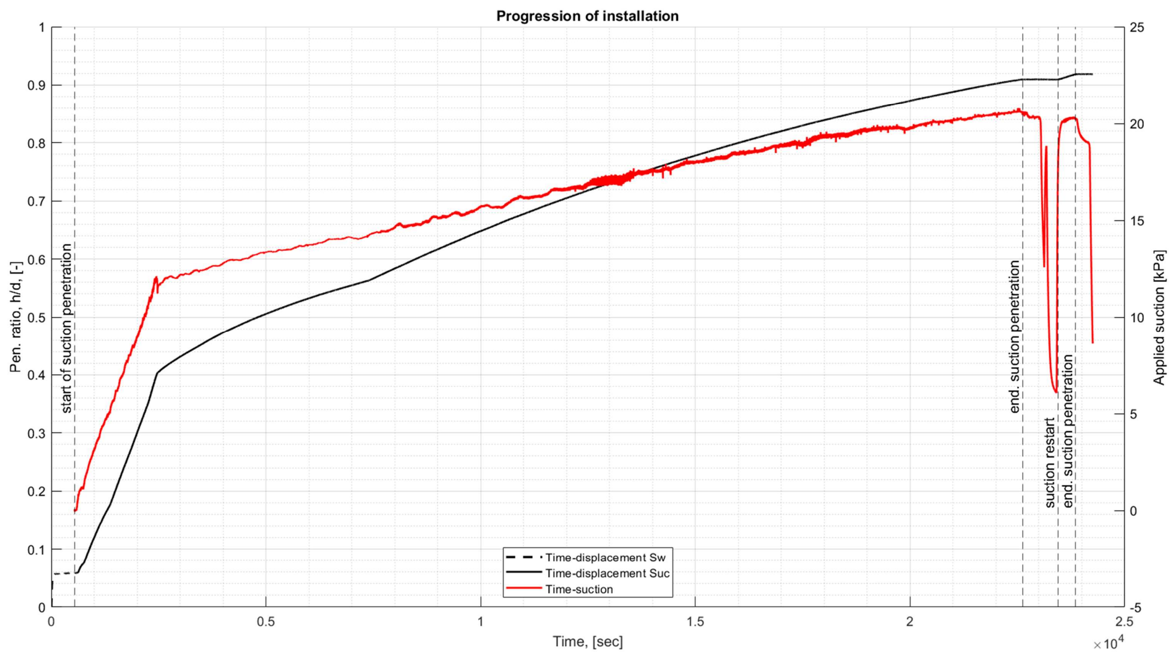

Figure B.23: Progress of suction installation for test run 6

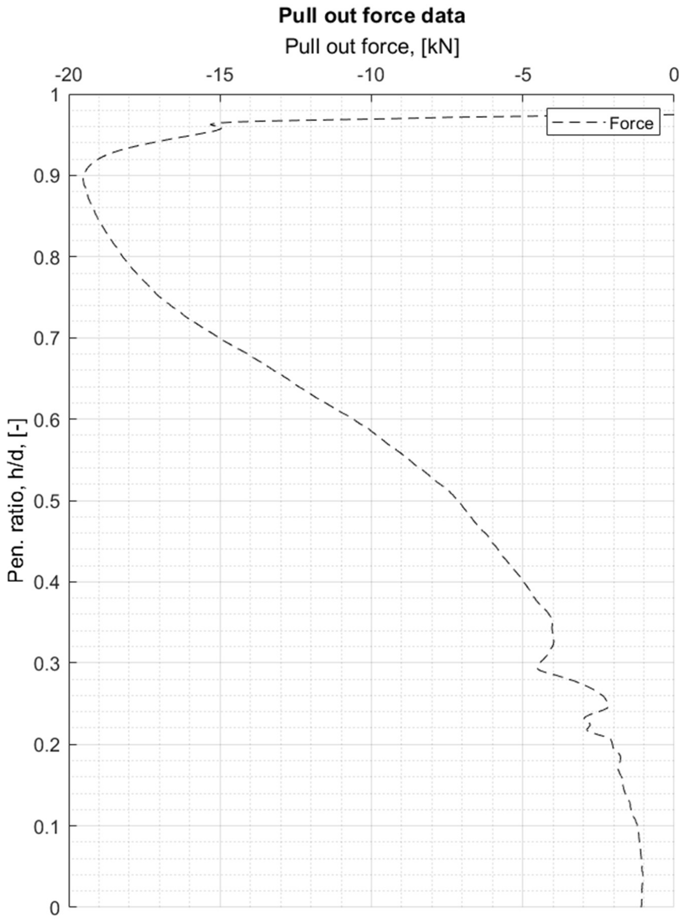

Figure B.24: Progress of uninstallation by pull out for test run 6

Table B.1: Derived geotechnical parameters from CPT before installation.

	Suction installation test					Jacking Test
Derived parameter	Test run 1	Test run 2	Test run 4	Test run 5	Test run 6	Test run 1
Density index ($I_{d\,mean}$), [%]	52.03	58.57	69.92	72.01	85.24	85.03
Tangent friction angle (ϕ_t), [°]	38.02	38.74	39.99	40.22	41.68	41.65
Secant friction angle (ϕ_s), [°]	48.55	49.55	51.27	51.59	53.60	53.57
Dilation angle (ψ), [°]	12.90	14.17	16.39	16.79	19.38	19.33
In situ void ratio (e), [-]	0.70	0.68	0.64	0.63	0.59	0.59
Young's modulus, E [kPa]	24002.49	28145.37	37587.32	40256.32	54939.07	54444.75
Effective cohesion, c' [kPa]	5.18	5.39	5.76	5.82	6.25	6.24
Saturated unit weight (γ_{sat}), [kN/m^3]	19.67	19.79	20.00	20.03	20.29	20.28
Unsaturated unit weight (γ_{unsat}) [kN/m^3]	15.57	15.76	16.09	16.15	16.56	16.56
Effective unit weight (γ') [kN/m^3]	9.67	9.79	10.00	10.03	10.29	10.28
Hydraulic conductivity, $k_{x,y}$ [m/day]	10.12	9.28	7.94	7.71	6.38	6.40

Table B.2: Derived geotechnical parameters from CPT after installation.

	Suction installation test									
Derived parameter	Test run 1		Test run 2		Test run 4		*Test run 5		Test run 6	
	in	out	in	out	in	out	in	out	in	out
Density index ($I_{d\,mean}$), [%]	43.89	51.07	45.85	54.72	38.85	60.39	52.45	41.14	43.94	72.01
Tangent friction angle (ϕ_t), [°]	37.13	37.92	37.34	38.32	36.57	38.94	38.07	36.83	37.13	40.22
Secant friction angle (ϕ_s), [°]	37.40	38.49	37.70	39.05	36.63	39.91	38.70	36.98	37.41	41.68
Dilation angle (ψ), [°]	8.09	9.49	8.47	10.20	7.11	11.31	9.76	7.56	8.10	13.57
In situ void ratio (e), [-]	0.72	0.70	0.71	0.69	0.74	0.67	0.69	0.73	0.72	0.63
Hydraulic conductivity, $k_{x,y}$ [m/day]	11.24	10.25	10.96	9.77	11.97	9.05	10.06	11.63	11.23	7.71

*Not accurate due to issue with cable connection.

Table B.3: Maximum load-displacement for installation

	Suction installation				Jacking
	Test run 1	Test run 2	Test run 4	Test run 6	Test run 1
Sw- displacement max. [h/D]	0.21	0.11	0.08	0.06	N.A
Suc-displacement max. [h/D]	1.00	0.95	0.87	0.91 (0.92)	≈ 1
Suc-suction max. [kPa]	18.88	21.5	18.33	20.80	N.A
Maximum Pullout force [kN]	12.32	14.84	13.22	19.52	32.32

PLAXIS 2D setup C

A few notes are included in this section to elaborate on the parameter selection for the 2D numerical model used for analysis of the problem. Reference for the content in this section is taken mainly from Reference$_m$anual [2021]; Material$_m$odel$_m$anual [2021]

C.1 Soil model parameters

C.1.1 Soil model

Mohr-Coulomb model (MC): The Mohr-Coulomb soil model is a linear elastic perfectly-plastic model generally used for approximation of soil behaviour. A constant average stiffness is estimated for the soil layer in the model.Due to this constant stiffness, computations tend to be relatively fast and a first estimate of deformations can be obtained. Generally, 5 basic input parameters (two stiffness parameters and three strength parameters) are required for using the model, and these are readily obtained from basic tests on soil samples.

The model was selected for use as the derived geotechnical parameters from CPT data provided direct input for the model. Also, the output of interest were the discharge and porewater pressures, and it was deemed sufficient for the case of this project.

C.1.2 Drainage type

Bucket installation results in generation of excess porewater pressures within the soil volume, which due the short-term period of installation, do not have enough time dissipate. Thus, drainage condition for bucket installation can be considered as an undrained type behaviour.

It was desired to develop a model that can appropriately simulate the short term development of excess pore pressure in the undrained soil volume, as was carried out in the physical model. A convenient feature in Plaxis is the acceptance of effective material parameter input for modelling undrained material behaviour. Effective stiffness parameter input for the model are thus selected as effective material parameters, which were determined from parameter derivation for CPT data. A downside of modelling the undrained material behaviour using the effective material parameter is that the output for undrained shear strength is often inaccurate, (Reference$_{m}anual$ [2021], section $2.4 - 2.7$). However, the output of concern for this project does not involve the undrained shear strength. Therefore, drainage type Method A was selected for use with the MC model, as it satisfied the requirement for the simulating the physical model used in the experiment. Drainage type method A is an undrained effective stress analysis with effective stiffness as well as effective strength parameters. This method gives a prediction of the pore pressures. Details on this drainage type can be found in Reference$_{m}anual$ [2021] section 6.1.1.

C.1.3 Stiffness parameters E' and v'

Stiffness parameters for the MC model, Young's Modulus (E') and Poisson's ratio (v'), were determined as effective parameters from CPT data using the methods described in Ibsen et al. [2009]. Thus, the Young's Modulus, based on the triaxial tests on Baskarp Sand No. 15, was selected as the secant modulus at 50 % strength, while Poisson's ratio is given as 0.25.

C.1.4 Strength parameters ϕ, ψ and c' for MC model

Same as the case in the previous section, the strength parameters for the MC model,ϕ, ψ and c' , were determined as effective parameters from CPT data using the methods described in Ibsen et al. [2009]. Reference for implementation in the Plaxis 2D can be found in Reference$_{m}anual$ [2021] section 6.1.2

C.1.5 Groundwater flow

The seepage flow problem associated with bucket installation is a continuous, time-dependent phenomenon, which would require a transient analysis calculation type. However, it has been found that an approximation of the time-dependent seepage problem to a simplified discrete, steady-state groundwater flow calculation type provides satisfactory results for suction bucket installation analysis ([Tran and Randolph, 2008; Koteras et al., 2016*b*; Koteras and Ibsen, 2019].). Such a procedure offers the advantage of reduced computational cost (number of input parameters to be determined, time for calculation) involved in the numerical analysis.

As such, a steady-state groundwater flow calculation type was selected for the model, where the parameter of significance in such a model is the soil permeability. In Plaxis, groundwater flow parameters are provided in the Groundwater tabsheet (Reference$_{m}anual$ [2021], sec. 6.1.5). Hydraulic data set and models for modelling flow in the soil saturated zone are available for selection and the definition of the soil's permeability is provided through input for the hydraulic conductivity of the soil as shown in Figure C.2a.

C.1.6 Interface

The soil-structure interaction in the numerical model was accounted for by applying interface elements. The interface allows for proper representation of realistic soil behaviour in close proximity to the structure, where soil strength may experience a reduction, and/or in the case of this project, where the pore pressure distribution can be influence by such an interaction. Thus, a reduction factor of 2/3 the internal soil friction angle is set as the interface friction angle. The interface strength is defined by the parameter R_{inter}, with flow through the interface defined by 'Groundwater' in the Plaxis Interface tabsheet. Details regarding Interfaces in Plaxis 2D can be referenced from Reference$_{m}anual$ [2021] sections 5.7.6 and 6.1.7.

C.1.7 Initial

Parameters for the initial stress generation for the soil model can be specified from the Initial tabsheet. For this project, the values are set to the default conditions. Reference for the definitions of the parameters in the Initial tabsheet are presented in Reference$_{m}anual$ [2021] section 6.1.8.

C.2 Structure parameters

C.2.1 Plates

For the purpose of this project, the steady state flow across the tip of the bucket skirt is of interest, and deformation of the skirt wall during installation is neglected. Therefore, the embedment of the bucket skirt is simulated such that it is whished in position at discrete depths and the analysis is carried out for the flow simulation. This is achieved by modelling the skirt wall as plate elements whose mechanical properties are assigned through the material data set in the Structures menu in Plaxis 2D. Reference for specifying material data set for plates is provided in Reference$_{m}anual$ [2021] sec. 6.4.2.

C.2.2 Interface

Interfaces in the 2D model were added to properly model the soil-structure interaction between the plate element and the soil volume around the plate. For simulations involving groundwater flow, activating of the the interfaces in a Phase results in the assigned properties of the interface being active, in this case, an impermeable interface is activated for the Phase calculation. The assigned interface properties used are as shown in Figure C.2b. Nodes and stress points selected for result extraction of soil-structure interaction need to be appropriately selected for accurate representation of results. Figure C.3 shows the correct selection of results extraction points within the interface zone of a model. Results for porewater pressures and discharge were taken from the model interface zone as depicted in Figure C.4. Details on Plaxis 2D interface elements are provided in Reference$_{m}anual$ [2021] section 5.7.6 and 6.1.7.

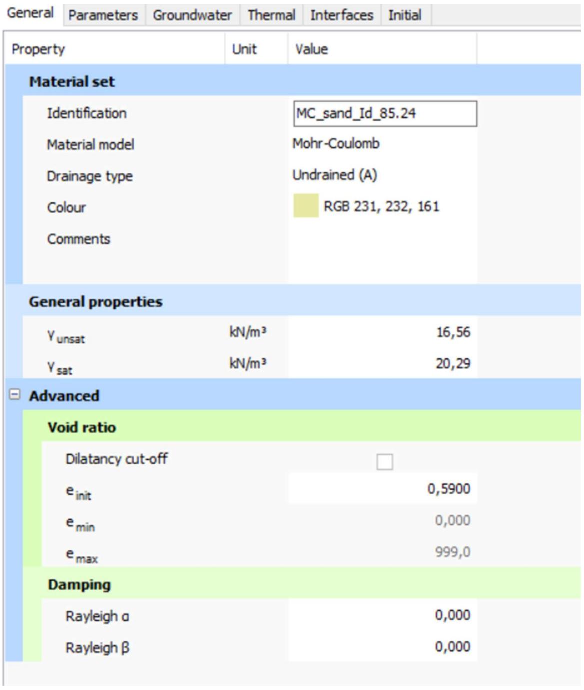

(a) Specifying soil model and drainage type in General tabsheet

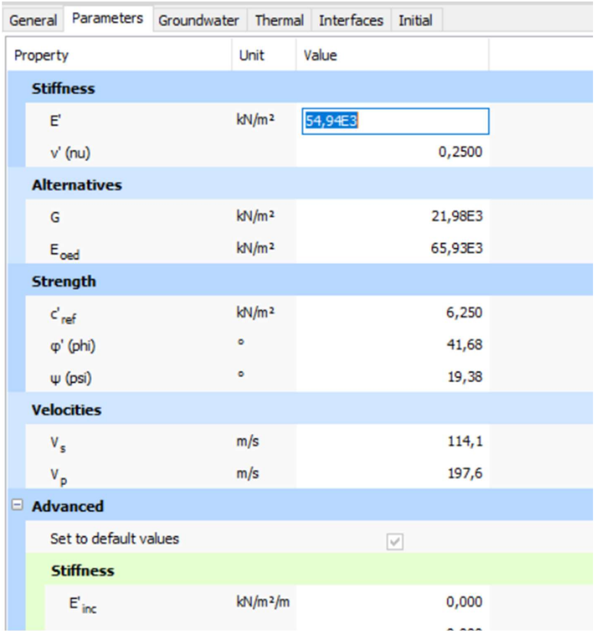

(b) Specifying stiffness and strength type in Parameters tabsheet

Figure C.1

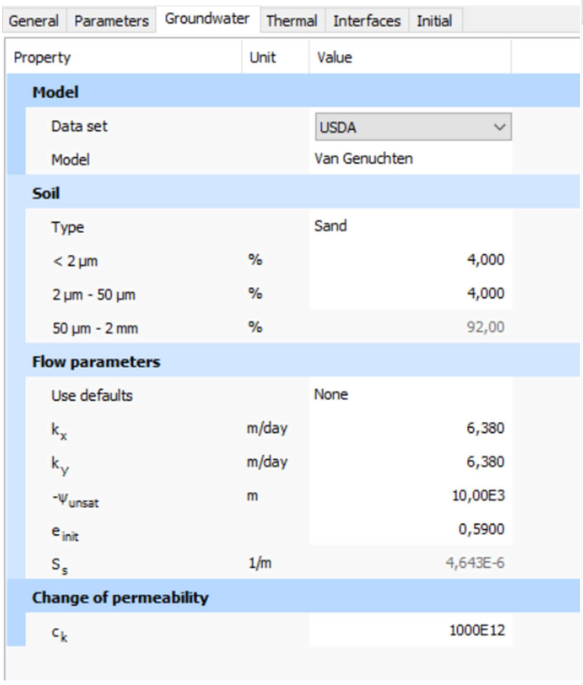

(a) Specifying groundwater flow conditions in Groundwater tabsheet

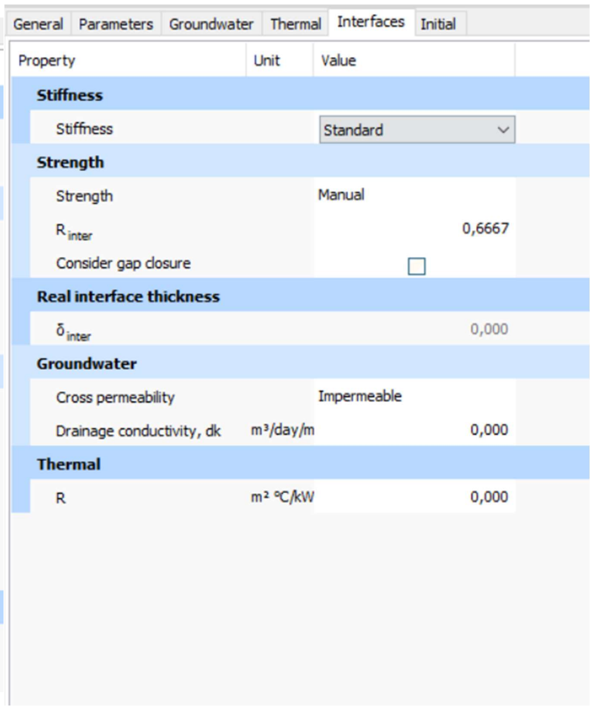

(b) Specifying interface properties in Interfaces tabsheet

Figure C.2

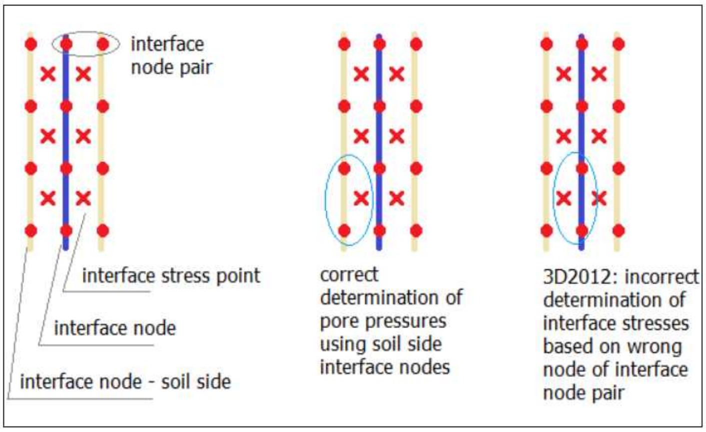

Figure C.3: Extraction of results from interface elements [van der Sloot, n.d.]

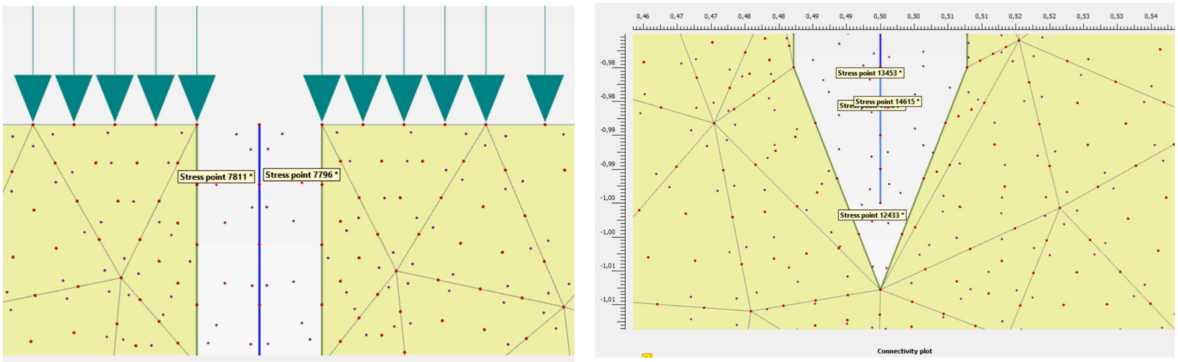

(a) Result extraction point for exit inside suction bucket model

(b) Result extraction point for plate tip of suction bucket model

Figure C.4

Attached documents D

The following document were submitted together with the report:

- Report - PDF file
- Bibliography
- Experiment data
- Numerical calculations - Matlab files
- Numerical simulations - Plaxis 2D files